Dissertation

submitted to the
Combined Faculty of Natural Science and Mathematics
of the Ruperto Carola University Heidelberg, Germany

for the degree of
Doctor of Natural Science

Presented by

M.Sc. Malin Insa Jansen

Born in Achim, Germany

Oral examination:

Phenotyping the potential antagonistic knock-out of the chromatin remodeler EZH2 and CHD7 in neural stem cells and the adult brain

1. Referee Prof. Dr. Frank Lyko

2. Referee Dr. Hai-Kun Liu

Abstract

CHARGE syndrome describes a combination of severe developmental defects including, among other things, a delayed or retarded mental development, sometimes combined with a variety of psychological symptoms. Especially the molecular mechanisms behind this brain phenotype is little understood, and cannot be treated effectively up to now.

This syndrome is caused by a heterozygous mutation in the *Chromodomain helicase protein 7* (*chd7*) gene, which encodes an epigenetically active protein (CHD7) mediating nucleosome sliding, and associated with open and active chromatin (H3K27ac, Feng et al., 2017).

Another epigenetically active protein fulfilling an opposite task is EZH2 (the catalytic part of the *polycomb repressive complex 2* (PRC2)) which silences gene expression by methylating histon 3 lysin 27. Both EZH2 and CHD7 are expressed in overlapping brain regions, and a knock-out of the respective protein has opposing effects on neuronal branching (Feng et al., 2013 and Liu, Y.). With these hints it was hypothesized that EZH2 might counteract CHD7 deficiency and could be beneficial for the CHARGE condition.

In the frame of this thesis I was able to generate and analyze a CHARGE mouse (CMVCre;CHD7$^{+/fl}$) that displayed a variety of CHARGE related symptoms. Heterozygous *chd7* mutant mice had a reduced body weight, were significantly more active, developed sever eye malformations with narrowed palpebral fissures, significantly smaller eye diameter, a thinner retina and inner nuclear layer, and partially completely dysfunctional eyes. Furthermore, the cerebellum of CHARGE mice showed a missing anterior lobe, and a disorganized purkinje cell layer with less primary branches. Also CHARGE mice have less neurogenesis ind the hippocampus.

Following the main hypothesis a genetic rescue (CMVCre;CHD7$^{+/fl}$;EZH2$^{+/fl}$) could restore; body and brain size, the strong eye malformations observed under CHARGE conditions, the amount of neural stem cells in the dentate gyrus, and the cerebella purkinje cell layer. Moreover, an RNA sequencing of the cerebellum tissue revealed that the gene expression of many genes in the double knock-out was indeed rescued. Furthermore, a homozygous inducible double knock-out of *chd7* and *ezh2* (NesCreERT2;CHD7$^{fl/fl}$;EZH2$^{fl/fl}$) rescued the neural stem cell pool in comparison to a *chd7* single knock-out.

Finally, these findings encourage me to use a very potent EZH2 inhibitor to treat neural stem cells *in vitro* and *in vivo*, thus attempting a novel CHD7 deficient treatment.

Zusammenfassung

Das CHARGE Syndrom besteht aus einer Kombination schwerer Entwicklungsdefekte. Insbesondere die molekularen Hintergründe des Gehirns Phänotyps die in teilweise schweren psychischen St^rungen und sogar geistigen Behinderungen resultieren können, sind wenig untersucht und können derzeit nicht behandelt werden. Diese Krankheit wird von einer heterozygoten Mutation im *Chromatin DNA Helicase 7* (*chd7*) Gen verursacht, das ein Protein kodiert das Nukleosomen verschiebt und mit offenem, aktivem Chromatin assoziiert ist (H3K27ac) (Feng et al., 2017).

Eine funktional gegenteilige Chromatinmarkierung, nämlich die einfach- zweifach und dreifach Methylierung von Histon 3 Lysin 27 wird von EZH2 umgesetzt, welches der katalytische Teil des *polycomb repressive complex 2* (PRC2) ist. CHD7 und EZH2 werden in ähnlichen Hirnregionen exprimiert und es konnte gezeigt werden, dass ein knock-out des jeweiligen Proteins gegenteilige Effekte auf die Ausbildung neuronaler Dendriten hat (Feng et al., 2013 and Li, Y). All diese Hinweise führten zu der Hypothese, dass EZH2 in der Lage sein könnte einen Teil des CHD7 Phänotyps auszugleichen.

Im Rahmen dieser Arbeit konnte ich eine CHARGE Maus (CMVCre;CHD7$^{+/fl}$) kreuzen und analysieren, die viele CHARGE-ähnliche Symptome zeigte. Diese heterozygoten *chd7* knock-out Mäuse waren signifikant kleiner und aktiver als die Kontrolltiere, sie zeigten schwerwiegende Fehlentwicklungen der Augen, die ein geringeren Augendurchmesser, einen dünnere innere Körnerschicht der Retina, sowie komplette Fehlbildungen der Augen ohne Pupille und mit geschlossenen Augenlidern beinhalten. Weiterhin zeigte das Kleinhirn einen fehlenden anterioren Lobus und eine unorganisierte Purkinjezellschicht mit reduzierter Dendritenbildung. Weiterhin konnte ich in CHARGE Mäusen signifikant weniger BrdU und Nestin positive Stammzellen im Gyrus Dentatus nachweisen.

Unserer Haupthypothese folgend, generierte ich einen genetischen Rescue der CHARGE Maus (CMVCre;CHD7$^{+/fl}$;EZH2$^{+/fl}$), diese Mäuse hatten ein normales Gewicht, normal entwickelte Augen, ein unauffälliges Kleinhirn mit intakter Purkinjezellschicht und eine normale Menge and BrdU und Nestin positiven Stammzellen im Gyrus Dentatus. Darüber hinaus zeigte eine RNA Sequenzierung des Kleinhirngewebes, dass die Expression vieler Gene im Doppel-Knockout normalisiert waren. Außerdem konnte ein homozygoter Knockout von *chd7* und *ezh2* (NesCreERT2;CHD7$^{fl/fl}$; EZH2$^{fl/fl}$) den neuralen Stammzellpool des Gyrus Dentatus, in Vergleich zu einen *chd7* Einzel-Knockout, retten.

Diese Ergebnisse führten zu ersten Behandlungsversuchen CHD7 defizienter Stammzellen *in vitro* und *in vivo* mit einem sehr potenten EZH2 Inhibitor.

Acknowledgement

First, I would like to express my sincere gratitude to my advisor Dr. Hai-Kun Liu for this challenging project, continuous support of my Ph.D study and related research. His guidance helped me through all the time of research.

Besides my advisor, I would like to thank Prof. Frank Lyko and Prof. Georg Köhr for supervising my research work, their insightful comments and encouragement, but also for their critical questions which widen and also sharpen my scientific views.

My sincere thanks also goes to Prof. Augustin for providing me with the Cre deleter mouse strain which has been crucial for crossing some of my experimental lines.

For teaching me the main technics, project supervision and challenging me and my work in every aspect and being a great scientific role model, I have to thank Dr. Weijun Feng.

Dr. C. Shao I like to thank a lot for providing me with the analysis of my RNA sequencing data. This was a great help and I really appreciate it!

Further, I would like to thank the complete team for their support and stimulating discussions.

Last but not least I would like to thank my family, especially my mum, my sister and my husband for their invaluable great support, patience and understanding throughout my research time. I could not have done this without you! Also, I am very grateful for our healthy little daughter. You are the best distraction there is.

Preface Foreword

A project based onto two other projects is always challenging in giving consideration to two main focussing fields. Both *chd7* and *ezh2* where analyzed respectively in a different scope, before and alongside this project.

In a CHD7 single knock-out Dr. Weijun Feng generated and analyzed a lot of data and also published two papers (W. Feng et al., 2013, and W. Feng et al., 2017). In the second paper I could participated.

The second project closely related to this thesis was the work of Dr. Yuting Li. She worked on an EZH2 single knock-out in the dentate gyrus neural stem cells and synapse formation.

Relevant data pieces of these two projects can be found in the supplement and named as such.

Further Dr. C. Shao kindly provided his professional analysis of my RNA sequencing data. His graphs are declared as such in the figure legends.

Herewith I declare that the data shown in the results section was created by myself and all other original sources are stated.

Contents

List of Figures

1 Introduction

1.1 Epigenetic active Proteins and their Modifications

Pluripotent stem cells develop into various cell types and tissues during the embryonic development. Gene expression patterns between different cells types containing the same DNA, are established through a coordinated process of transcriptional components and changes in the chromatin structure. To mediate these changes, chromatin remodeling enzymes interact with the assembly and compaction of chromatin.

Chromatin is formed by DNA and protein nucleosomes consisting of eight histone proteins, wherein each histone is surrounded by 147 base pairs of DNA. A nucleosome contains two copies of each core histone H2A, H2B, H3, H4 and a variable amounts of biochemical variants, which differ only in a few amino acids. The DNA/ histone interaction is stabilized by about 142 hydrogen bonds, hydrophobic interactions and charging differences between the positive charged lysins and arginines of the histone, and the negative charged phosphodiester backbone of the DNA. The nucleosome complex, when further stabilized by the linker histone H1, condensates the linear DNA molecule around 30 to 40-fold (Luger et al., 1997).

As a part of the nucleosome, N-terminal histone residues protrude out of the histone/DNA structure and are thus accessible to chemical modifications like acetylation, methylation, phosphorylation, sumoylation, ubiquitylation, ribosylation and glycosylation (Zink and Paro 1989) (Fig. 1). These modifications are mediated by enzymes which have been conceptualized by their biochemical task as *reader*, *writer* and *eraser*. Readers are distinct effector proteins which recognize for example specific methylated lysines depending on the neighboring amino-acid sequence and methylation state (Hyun et al., 2017). Enzymes categorized as writers, set chemical histone marks such as acetyltransferases (HATs), lysine methyltransferases (KMTs), and ubiquitylation enzymes (E1, E2 and E3 enzymes), or phosphokinases while erasers work primarily as lysine demetylases (KDMs), deubiquitinases (DUBs), histone deacetylases (HDACs), or phosphatases (Chen and Dent, 2014; Kolybaba and Classen 2014, Valencia and Kadoch, 2019).

The functions of these histone modifications are thought to be predetermined by the structural effect to the histone/DNA structure. Covalent histone modifications can change the charge and structural properties of the nucleosome and therefore open or restrict the access to the DNA (Wood and Shilatifard 2004). As a consequence, genes of the before blocked DNA

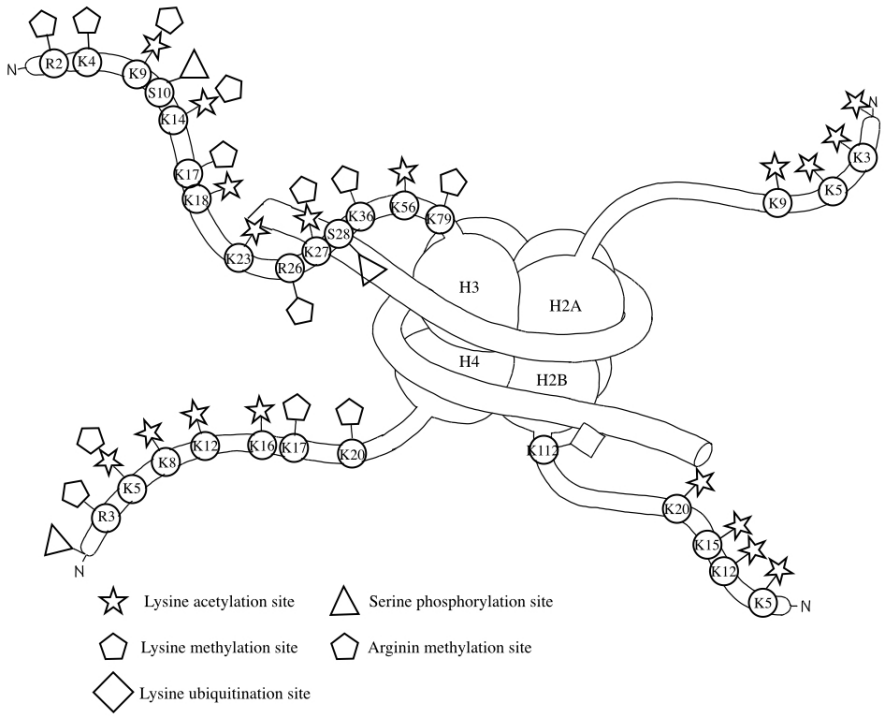

Figure 1: **A mammalian histone octamer of histone H2A, H2B, H3 and H4 and their N-terminal residues.** Mentioned are the amino acids that are known to be modulated and the modifications for each amino acid (methylation, acetylation, ubiquitination or phosphorylation). Modified after Wood and Shilatifard 2004.

region can be actively transcribed again, or their transcription can be blocked and genes thus be silenced.

Typically, the tri-methylation of Lys 4 in H3 (H3K4me3), together with histone acetylations are associated with active transcription (Gaspar-Maia et al., 2011). The methylations of H3K4, H3K36 and H3K79 are considered to mark active transcription, whereas H3K9, H3K27me, H3K27me2 and H3K27me3 and H4K20 methylations are thought to be associated with transcriptional repression and a silenced chromatin states, although in some cases mediated through the recruitment of distinct silencing factors (Schuettengruber et al., 2011; Black et al., 2012; Chen and Dent, 2014) (Fig. 1).

Other mechanisms refining the epigenetic landscape include the incorporation of histone variants like H3.3, H2AZ or macroH2A (discussed elsewhere), and DNA modifications. DNA modifications are chemi-

cal alterations on DNA rich in Cytosine and Guanine, so called CpG[1] sites which can be methylated directly. The so called 5-methylcytosine and its derivates, 5-hydroxymethylcytosine, 5-formylcytosine and 5-carboxylcytosine are the most studied DNA modifications (Kohli and Zhang 2013). DNA CpG methylations are conducted by DNA methyltransferases (DNMTs) and repress the gene expression (Gaspar-Maia et al., 2011). The persistence of DNA methylation signals over several DNA replication steps could be reported in the last years. Cytosinemethylation marks are divided during S-phase in a semiconservative manner (Kolyaba and Classen 2014). Besides these cytosine methylations, newer studies found a N6-methyldeoxyadenosine (6mA) known from prokaryotes, in the early phases of vertebrate embryonic development (Liu et al., 2016).

The DNA-histone interaction can be disrupted by chromatin remodeling enzymes sliding nucleosomes along the DNA, or translocating the nucleosome core particle to another DNA strand. It is thought that DNA parts sterically hindered by the nucleosome structure surrounding it, could be re-accessible after sliding the nucleosome to another position, and thus making room for transcription factors (Smith and Peterson, 2005). This process is guided by the different chromatin marks which are read by protein domains of the chromatin remodeling enzymes. The exchange of histones and reposition or eviction of nucleosomes is mediated through ATP consumption. The general working mechanism for ATPases and similar functioning helicases are repeated circles of enzymatic opening and closing over the DNA, which allows the enzyme to move along single-stranded DNA or RNA (Singelton et al., 2007; Chen and Dent, 2014).

1.1.1 ATP-dependent Chromatin-Remodeling Complexes and the CHD Family

Based on similarities of ATPase subunits genes, the chromatin remodeling complexes have been grouped into four main families: SWI/SNF (mating type switching/sucrose non-fermenting), ISWI (imitation switch), INO80 (inositol), and CHD (chromodomain helicase DNA-binding) proteins (Winston et al., 1992; Marfella and Imbalzano, 2007; Schuettengrube et al., 2011; Gaspar-Maia et al., 2011; Chen and Dent, 2014).

The yeast SWI/SNF (switch/sucrose nonfermentable) family contains a bromodomain, which recognizes the acetylated lysine residues on the N-terminal tails of histones. This group consists of yeast SNF2 and STH1, *Drosophila melangaster* Brahma (BRM), mammalian BRM (SMARCA2) and

[1] p refers here to the phosphodiester bond that links a cytosine and a guanine

brahma-related gene 1 (BRG1 or SMARCA4). BRG1 is also the catalytic subunit of the PBAF remodeler (Marfella and Imbalzano, 2007; Bultman et al., 2000; Moshkin et al., 2007).

The ISWI family is characterized through their SANT domain, which is named after the first proteins identified with this domain; Swi3, ADA2, N-CoR and TFIIB and functions as a histone-binding module. This family comprises yeast Isw1, Isw2 and mammalian homologues SNF2H and SNF2L (Tsukiyama and Wu, 1995; Marfella and Imbalzano, 2007; Schuettengruber et al., 2011).

The INO80 family can form three different complexes: INO80, SNF2-related CBP activator protein (SCARP), and TAT-interacting protein(TIP60)-p400. Members of this family have a DNA helicase activity, they are involved in DNA repair and replication, and an evolutionary conserved function of INO80 family members is chromatin editing. The mammalian INO80 chromatin remodeler has further been linked to DNA repair and especially interstrand cross-linking checkpoint activation (Marfella and Imbalzano, 2007; Fazzio et al., 2008; Gaspar-Maia et al., 2011; Andreev et al., 2019).

The CHD family includes a number of proteins which are highly conserved from yeast to humans (Marfella and Imbalzano, 2007). It comprises ATP-dependent chromatin remodeling enzymes, and is characterized by its tandem chromodomains, helicase domain, and DNA-binding domain (Manning and Yusufazai 2017). Chromodomains were originally characterized in *Drosophilas* heterochromatin protein 1 (HP1) which binds nucleosomes through its chromodomain and contribute to promotion of closed chromatin states (heterochromatin) at homeotic genes (Pearce et al. 1992; Wreggett et al. 1994).

The CHD family consists of nine protein members, further distributed into three subfamilies according to their structural homology. Two chromodomains binding methylated histone-residues, and two Sucrose NonFermentable2 (SNF2)-like helicase-ATPase domains are characteristic for all CHD proteins (Hall and Georgel 2007; Layman et al., 2010). The SNF2-like ATPase domain contains conserved amino acids which were found in proteins involved in a variety of cellular processes including chromatin assembly, transcription regulation, DNA repair, DNA replication, development and differentiation (Tsukiyama, 2002; Smith and Peterson, 2005; de la Serna et al., 2006; Marfella and Imbalzano, 2007) (Fig. 2).

CHD1 and CHD2 are grouped together because both proteins posses a DNA-binding domain. CHD1 binds globally to active euchromatin and

co-localizes with RNA polymerase II in embryonic stem cells (Gaspa-Maia et al., 2009). Further, CHD1 is part of the acetyltransferase SAGA and SILK complex in yeast (Pray-Grant et al., 2005), it interacts with trimethylated histone 3 Lysine 4 (H3K4me3) in embryonic stem cells, and plays together with CHD2 an important role in maintenance and development (Lalani et al., 2005). Interestingly, the HDAC activity of CHD1 has been shown to function as both transcriptional activator (Stokes and Perry, 1995) and repressor (Tai et al., 2003) in mouse. A homozygous knock-out of *chd1* is perinatal lethal in mice (Marfella e t al., 2006). Embryos with CHD1 depletion through RNA interference accumulate high levels of heterochromatin and cannot differentiate (Gaspar-Maia et al., 2011). A newer study linked CHD1 to learning and memory through Controlling the immediate early gene response in the hippocampus (Schoberleitener et al., 2019). CHD2 is found in iPS cells and mesenchymal stem cells and interacts besides the histone variation H3.3 also with HDAC1 and 2 and the NCoR complex (Micucci et al., 2015).

Instead of a DNA-binding domain CHD3, CHD4 and CHD5 contain two tandem plant homeodomains (PHDs), which are zink finger motifs able to interact with methylated histone residues (Bienz 2006). CHD3 interacts with HDAC1/2, ATR and TRIM27. CHD4 was found in hematopoietic and neural stem cells, and interacts with the nucleosome-remodelling (NuRD) complex and binds specifically to H3K4 and H3K9me3 (Xue et al. 1998). CHD3 and 4 are part of the Mi2-NuRD (Mi-nucleosome remodeling deacetylase) complex and as such, involved in transcriptional regulation, replication, DNA repair and cell fate. As Mi-2alpha (CHD3) and Mi-2beta (CHD4) they mediate the ATP-dependent nucleosome remodeling quality of this complex (Tong et al., 1998; Zhang et al., 1999; Xue et al., 1998). A double homozygous knock-out of *chd5* is viable in mice. CHD5 interacts with NuRD and binds to H3K4 and H3K27me3 (Micucci et al., 2015). A depletion of CHD5 in the developing neocortex blocks neuronal differentiation, and leads to an accumulation of undifferentiated progenitor cells (Egan et al., 2013).

The group III of CHD proteins comprises CHD6, 7, 8 and 9 due to their C-terminal tandem Brahma and Kismet (BRK) domains, but these are functionally not fully understood (Daubresse et al. 1999; Micucci et al., 2015; Manning and Yusufyai, 2017). These CHD proteins are homologues of the *Drosophilas* protein Kismet which catalyzes the trimethylation of H3K4, and directs ASH1 and TRX to chromatin (Klymenko and Mueller, 2004).

CHD6 to CHD9 use a SANT domain to bind nonspecific to DNA, and especially linker DNA between nucleosomes (Schusterand and Stoeger

2002; Aasland et al., 1996; Boyer et al., 2004). CHD6 interacts with RNA Polymerase II, and is a DNA damage response factor stabilized during oxidative stress via reduced degradation (Moore et al., 2019). CHD6 seems to disrupt nucleosomes in a distinct non-sliding manner. CHD6 and 7 have a reported affinity for shorter linker DNA, while CHD8 binds longer pieces and thus slides nucleosomes into positions with more flanking linker DNA (Manning and Yusufzai, 2017). In oligodendrocytes stage progression a newer study reported a compensatory mechanism of CHD8 for CHD7 with common binding profiles (Marie et al., 2018). CHD9 is involved in the osteogenic differentiation in human (Shur et al., 2005; Shur et al., 2006).

A *chd6* and *chd9* knock-out seems to have no effect (Manning and Yusufzai, 2017). In contrast to that, knocking out *chd8* causes autism spectrum disorder (Manning and Yusufzai, 2017).

CHD7 over expression has been reported for aggressive subtypes of breast cancer, stomach and colon cancer and glioblastoma (Kim et al., 2011; Chu et al., 2017; Machado et al., 2019). Remarkably, a homozygous knock-out of *chd7* is lethal (Hurd et al., 2007) while a heterozygous mutation causes CHARGE syndrome (Hall, 1979; Hittner et al., 1979; Pagon et al., 1981) (Fig. 2).

1.2 CHD7 and CHARGE Syndrome

The mammalian *chromodomain helicase DNA binding protein 7*(CHD7) protein structure consists of two chromodomains, an SNF2 domain, the helicase - and two BRK domains (Liu et al., 2013). Although CHD7 is highly conserved in mice (identity 94.9 and 97% similarity) one study reports one chromodomain in mouse CHD7 (Marfella and Imbalzano, 2007), while other studies identify two chromodomains (Bosman et al., 2005).

Located on chromosome 8q12.1, the Chd7 gene is 188 kb in size and codes with 37 coding and non-coding exons for 2997 amino acids (Visser et al., 2004).

In the developing embryo CHD7 is essential for the formation of embryonic derived ectodermal neural crest cells (Schulz et al., 2014) which migrate from the neural tube to the periphery to form for example heart and brain. CHD7 binds multiple subunits of the PBAF complex in neural crest cells. In mouse embryonic stem cells and neural crest cells, CHD7 was enriched at enhancer regions, together with H3K4me1 (Gaspar-Maia et al., 2011), and in both, Humans and *Xenopus*, CHD7 activates the transcription

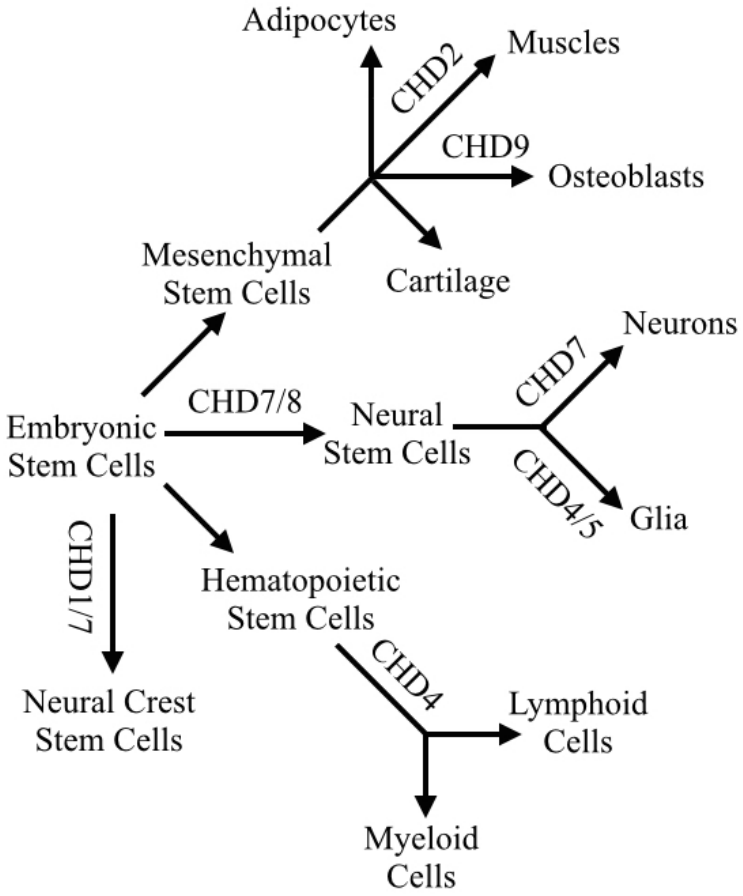

Figure 2: **CHD family members in different stem cell types.** Indicated are CHD proteins with an either activating or inhibiting role in the development of the mentioned stem cell population. Modified from Micucci et al., 2015

factors Slug, Twist and Sox9 which are critical for the migration of neural crest cells from the border regions (Bajpai et al., 2010). CHD7 expression is required in the surface ectoderm, endoderm, and migrating neural crest cells which all contribute to the development of facial structures and the eye (Sperry et al., 2015). Under healthy conditions CHD7 is expressed in heart, optic vesicle, facio-acustic preganglion, brain, olfactory pit and mandibular component of the first branchial arch of mouse embryos (Lalani et al., 2005).

Furthermore, CHD7 interacts with p300, SOX2, an binds to Sox2, Oct4, Nanog, Neurod, Rxrg, and Rarb (Micucci et al., 2015).

A homozygous mutation in the *chd7* gene is lethal at E10.5 probably due to respiratory and cardiovascular defects (Hurd et al., 2007), while a heterozygous *chd7* mutation causes CHARGE syndrome (also known as Hall-Hittner syndrome). It has an estimated incidence of approximately 0.1-1.2 in 10,000 newborns (Blake and Prasad, 2006) and was named as an acronym of the most prevalent birth defects (Coloboma of the eye, Heart defects, Atresia of the choanae[2], severe Retardation of growth and development, Genital and Ear abnormalities) (Hall, 1979; Hittner et al., 1979; Pagon et al., 1981).

The clinical features of CHARGE syndrome were graded into major and minor diagnostic criteria. Coloboma of the eye, cranial nerve dysfunction, choanal atresia and ear abnormalities rated as major CHARGE symptoms. Minor criteria are cardiovascular malformations, genital hypoplasia, cleft lip/ palate, tracheoesophageal fistula[3], distinctive face characteristics, growth deficiency and developmental delay. Occasional features are renal abnormalities, spinal abnormalities (scoliosis), fifth finger clinodactyly[4] and neck and shoulder anomalies (Blake et al., 1998; Blake and Prasad, 2006). Other features associated with CHARGE syndrome include late pubertal development, sleep apnea, intermittent abdominal pain, retinal detachment, cataracts, migraines, seizures, urinary tract infections, hypoglycemia and psychiatric and behavioral disorders (Hartshorne et al., 2016).

Additionally, limb abnormalities, renal abnormalities and thymic hypoplasia were described[5]. Also defects in the olfactory bulb development

[2] A blockage of the passages between the nasal cavity and the naso-pharynx (Blake and Prasad, 2006).

[3] tracheoesophageal fistula: is an abnormal connection between trachea and oesophagus

[4] clinodactyly: a curving of the fifth, small finger towards the fourth finger

[5] (Opthalamic Genetic Disease: A Quick Reference Guide to the Eye and External Ocular Adnexa, by N.L. Couser, Elsevier 2019).

and the absence of the sense to smell (Anosmia) appear to be present in virtually all CHARGE patients (Vissers et al., 2004; Jongmanns et al., 2008). A reduced or absent olfaction is often caused by hypoplasia or aplasia of the olfactory bulbs. Even *chd7* heterozygous knock-out mice show a lack of odor discrimination and hypoplasia of the olfactory bulbs. In olfactory tissue CHD7 colocalizes with Ascl1 and Neurod1 and thus is highly expressed in olfactory epithelium (Micucci, et al., 2015).

However, clinical features in CHARGE syndrome vary from case to case in their symptomatic severity and are incomplete penetrant in humans (Layman et al.,2010; Nishina et al., 2012). In one example of two monozygotic twin sisters and a siblings pair of two brothers, identical *chd7* mutations resulted in a striking intrafamilial variability (Jongmans et al., 2006).

The above described clinical features of CHARGE syndrome were later related to *chd7* mutations. Depending on the symptoms used as selection criteria, 70 to 90% of the CHRAGE patients carry a *chd7* mutation[6]. Up to now, 554 pathogenic *chd7* mutations of 894 patients have been reported[7]. Some resulting in nonsense mutations (44%), frame shift mutations causing deletions or insertions (34%), mutations in the splicing site (11%) or missense mutations (8%) (Janssen et al., 2012). A study analyzing the different *chd7* mutations in humans, predicted a premature protein truncation in 73% of analyzed patients. They include nonsense and frameshift mutations, and conclude this would most likely lead to haploinsufficiency of the CHD7 protein (Lalani et al., 2005). Newer studies also analyze intronic *chd7* mutations and indeed one study found that an insertion of 63 nucleotides into intron 28 created a premature termination codon, and a truncated protein (Villate et al., 2018).

Most of the described *chd7* mutations are thought to be *de novo* mutations, as most individuals diagnosed with CHARGE syndrome seem to have unaffected parents (Liu et al., 2014, Pranckeniene et al., 2019). There are however a few reported cases of inherited familiar *chd7* mutations, with parent-to-child transmission of non-mosaic *chd7* mutations and CHARGE syndrome (Jongmans et al., 2008; Hartshorne et al., 2016). In cases of affected parents a *chd7* mutation is autosomal dominant (Jongmans et al., 2008). Thus, the estimated chances of transmitting a *chd7* mutation to the next generation is 50% but because of the large variability of the clinical features the symptomatic severity for the offspring cannot be predicted (Jong-

[6] A heterozygous mutation of *chd7* can also be found in a minority of Kallmann syndrome patients (Bergman et al., 2011; Kim et al., 2008).

[7] Janssen et al., 2012 created a *chd7* database (https://molgenis51.gcc.rug.nl/menu/main/home)

mans et al., 2006; Jongmans et al., 2008; Bergmann et al., 2011).

Interestingly, somatic mutations and germline mosaicism[8] have been described in the context of CHARGE syndrome[9](Jongmans et al., 2008; Pauli et al., 2009). Germ line mosaicism was found in a father of two affected children, carrying the same *chd7* mutation causing CHARGE syndrome. This mutation could not be found in somatic lymphocytes but in the spermatozoa of the father (Pauli et al., 2009). A somatic mutation in the lymphocytes of an unaffected father could be related to the *chd7* mutation of two affected siblings (Jongmans et al., 2008). In this reported case the gametes were not analyzed suggesting likewise a germline mosaicism of the father which was passed along.

1.2.1 Eye Malformations in CHARGE Syndrome

Almost 80% of CHARGE patients show eye malformations and/or suffer from blindness[10]. Among the most prevalent ocular features of CHARGE syndrome are bi- or unilateral ocular colobomata, which describes a hole in the iris, retina or choroid structure which arrises due to a failure in the optic fissure closure (Bardakjian et al., 2004). The optic fissure is a ventral groove that forms during optic cup morphogenesis. After the blood vessel formation, the optic fissure closes around them. The mechanisms underlying optic fissure closure are poorly understood (Weiss et al., 2012) (Fig. 3).

Initially, the cells of the early optic vesicle express transcription factors like Otx2, Pax6, Rx, Six3, Six6, and Lhx2 (Fuhrmann, 2010; Beccari et al., 2013). These cells further differentiate into the retina pigment epithelium (RPE), the neural retina, and the optic stalk (Fuhrmann, 2010). The regulatory mechanisms underlying neural retina morphogenesis and patterning are not fully understood (Martinez-Morales et al., 2017).

Interestingly, an expression of CHD7 could be found in the developing eye at E11.5 already (Sperry et al., 2015). At E12.5 the lens vesicle and the neuroectodermal layer of the developing eye express CHD7 (Bosman et al., 2005). The neuroectoderm forms the neural retina, retinal pigment epithelium and the iris. Besides that, the eye is surrounded by a layer of neural crest cells forming the sclera, the choroid and a part of the cornea (Fig. 4). These neural crest cells help direct the generation of the optic cup, which involves a complex folding process resulting in formation of the choroid fissure (Sperry et al., 2015). CHD7 has reportedly been expressed

[8]Germline mosaicism where only some of the parental gametes carry the mutation while the somatic cells (often used for genetic testing) have a non mutated genotype

[9]also in Lalani and Belmont 2009, Enz. of Molecular Mechanisms of Disease

[10]Database for ocular diseases (University of Arizona): CHARGE syndrome

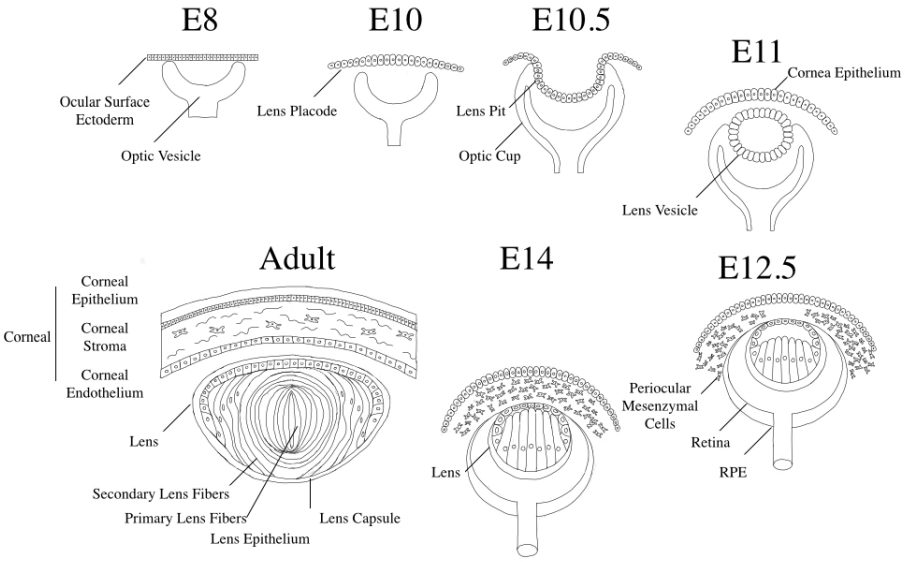

Figure 3: **The development of mammalian eyes.** The mammalian eye develops as optic vesicle out of the prosencephalon (diencephalon). At embryonic day 8 (E8) the optic vesicle is formed. Later on the optic vesicle invaginates to form the lens pit and optic cup. The ocular surface ectoderm forms the lens placode which invaginates to the lens pit soon after (E10.5). At embryonic day 11 (E11) the lens pit is completely invaginated to build the lens vesicle, placed on top of the optic cup. Above this structure the cornea epithelium is closed. Neural crest-derived periocular mesenchymal cells periocular mesenchymal cells migrate between the premature lens and the cornea epithelium. The lens and optic nerve is further specified and the retina and retina pigment epithelium (RPE) are build (E12.5 and E14). In the adult eye the cornea has three layers: the cornea epithelium, the stroma and corneal endothelium directly on top op the lens. The lens is surrounded by the lens capsule. Secondary and primary lens fibers form the core of the lens. Close to the cornea is the lens epithelium positioned. Picture modified from lifemaps.com

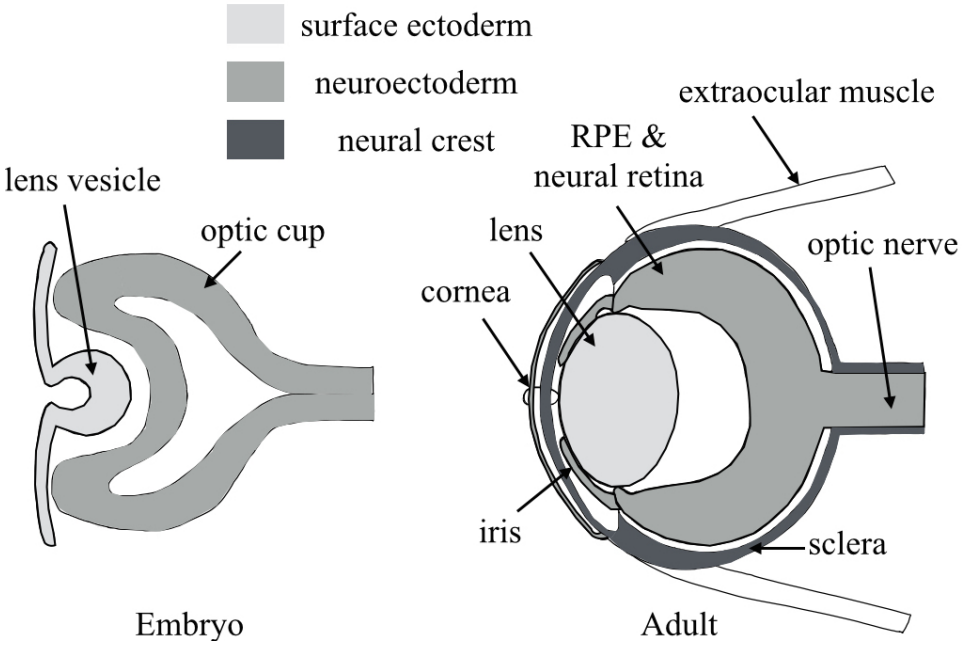

Figure 4: **Ectodermal and neural crest tissue of the eyes.** The embryonic lens vesicle is build out of surface ectoderm, while the optic cup is build out of neuroectoderm. In the adult eye the lens is formed out of surface ectoderm and the retinal pigment epithelium (RPE) and neural retina consists of neuroectoderm. Neural crest cells build the sclera, cornea and choroid (shown in white). Picture modified from Stenkamp, 2015

in neural crest cells (Randall et al., 2009; Bajpai et al., 2010, Schulz et al., 2014). A loss of Chd7 within the retina contributes to ocular malformations in mammals (Sperry et al., 2015).

Another study concluded that the eye development requires CHD7 in the surface ectoderm forming the lens, and in the neural ectoderm building the optic cup and stalk morphogenesis. Further CHD7 would be absolutely required for the specification of the neuraoectoderm (Gage et al., 2015).

Intriguingly, the same *chd7* mutation can affect the right and left eye with different symptomatic severity. A study analyzing 53 CHARGE patients diagnosed with *chd7* mutations, were tested for their vision on the right and left eye separately. Totally blind were 8% on the left, and 11% on the right eye[11](Hartshorne et al., 2016).

[11]Legally blind were the majority with 38% on the left eye and 21% on the right eye. A moderate impaired vision reported 11% for their left eye and 19% for their right eye. Only

A very frequently observed eye malformation in CHARGE patients is, as mentioned before, the coloboma of the eye, originating from a non closed optic fissure (Blake et al., 1998; Lalani et al., 2005; Hartshorne et al., 2016; Nishina et al., 2012). Coloboma can affect virtually all structures of the eye. A coloboma of the iris results for example in a visible key-hole shaped pupil (Bardakjian et al., 2004). The overall prevalence of iris-, retina-, choroid-, disc colobomata in CHARGE syndrome was rated between 77 and 90% in different studies (Blake et al., 1998; Lalani et al., 2005; Hartshorne et al., 2016). A further study focussing on eye malformations found a prevalence of 94% (18 out of 19) of patients with coloboma and *chd7* mutation. In total, 35 eyes displayed a coloboma of the posterior segment and the anatomical severity of the eye malformations were graded according to the presence of colobomata, macula[12] defect, and microphthalmos[13]. They observed that even eyes with large colobomata could form maculas. Again, a low to moderate agreement between the phenotype of both eyes was reported. The authors found a significant correlation between the location of the CHD7 truncation, and the severity of the eye symptomatic (Nishina et al., 2012).

Besides ocular coloboma CHARGE patients also often suffer from retina detachment and cataracts (Hartshorne et al., 2016). More seldom are optic nerve hypoplasia and hyperplastic viteous[14] causing a turbidity of the inner eye fluid due to a persistent fetal vasculature[15]. Additionally, anophthalmia[16], hypertelorism[17] and ptosis[18] are described[19].

a mildly restricted vision had 17% on the left and 23% on the right eye and a normal vision was reported for 19% on the right and left eye (Hartshorne et al., 2016)

[12]Macula: also called fovea; a spot on the retina consisting of mostly cone cells and needed for sharp vision.

[13]Microphthalmia refers to a globe with a total axial length that is at least two standard deviations below the mean for age (Bardakjian et al., 2004).

[14]Also known as persistent fetal vasculature (PFV) which is a developmental defect first described by A.B. Reese in 1955 (American Journal of Ophthalmology, 40(3) https://doi.org/10.1016/0002-9394(55)91866-3) as a congenital malformation of the anterior portion of the primary vitreous.

[15]Database for ocular diseases (University of Arizona): CHARGE syndrome

[16]one or two missing eyes

[17]wide-spaced eyes

[18]a dropped eye lid

[19]In Opthalamic Genetic Disease: A Quick Reference Guide to the Eye and External Ocular Adnexa, by N.L. Couser, Elsevier 2019

1.2.2 Mental Impairments in CHARGE Syndrome

CHARGE patients show a broad spectrum of mental challenges and even impairments, including e.g. developmental delay, autism spectrum, depression, anxiety and hyperactivity. An early study reported low adaptive behavior skills, motor impairments and moderate to strong autism spectrum disorder symptoms in 13 patients with CHARGE syndrome (Smith and Peterson 2005). A very detailed study of the psychological symptoms and behavioral traits in CHARGE syndrome reported a frequent developmental delay in 85% of patients. Most patients reported sleeping problems (59%) followed by aggressive behavior (51%), tactile defensiveness (51%), obsessive compulsive (49%), or self-injuring behavior (47%), anxiety (45%), attention deficit (26%), autism spectrum (26%)[20]. In this study CHARGE patients gave a self-report on what decreases their life quality regarding to their mental health. Besides insomnia, the feeling of anxiety and a poor overall mental health restricted them the most (Hartshorne et al., 2016).

A study further underlining obsessive compulsive and repetitive behaviors, and to less extend aggressive and auto-aggressive behavior in CHARGE patients, reported an average of 11.5 repetitive behaviors per patient per day. This compulsive behavior reportedly interfered with their daily routine (Bernstein and Denno 2005).

A major difficulty of many human studies is to differentiate how the different symptoms of CHARGE syndrome influence each other, and how they intertwine. For example, patients suffering from deaf-blindness might show decreased receptive language skills as a result of their different perception. It is undoubtedly difficult to Control against sensory impairments when psychologically assessing human patients. An early study empathized the challenges of diagnosing autism in individuals with sensory impairments (Smith et al., 2005).

To decipherer the connections between hearing loss, cognitive abilities and the quality of language perceptiveness, a study was conducted. Here Vesseur and colleagues could connect the degree of hearing loss with receptive and expressive language skills, and found a correlation between the receptive language skills and the cognitive abilities. The cognitive abilities were not connected to expressive language skills or the degree of hearing loss. Interestingly, out of the 41 analyzed patients 58.5% scored low on IQ tests (lower then 70)[21](Vesseur et al., 2016). However, the type

[20] tics (17%), conduct disorder (13%), depression (8%) and other (8%) (Hartshorne et al., 2016)

[21] Out of 41 patients with CHARGE syndrome 0 had an IQ over average (IQ bigger 115), 9 (22) had a normal IQ score between 86-115, 8 (19.5) had a subnormal IQ level between 70

of IQ test used was not mentioned, thus it remains unclear wether sensory impairments could influence the results. Furthermore, the possible visual impairments (e.g. coloboma of the eye reported in 77 to 94% of patients (Blake et al., 1998; Lalani et al., 2005; Nishina et al., 2012; Hartshorne et al., 2016)) of the analyzed CHARGE patients were unfortunately left out of the picture.

Another significant correlation was found between sleeping problems, anxiety, self-abuse, conduct problems and autistic-like behaviors in CHARGE patients. The authors connect the sleeping problems with the restricted vision and the possible influence on the melatonin release and circadian rhythm (Vesseur et al., 2016), but not to the reported sleep apnea which occurred in 25% of the cases (Hartshorne et al., 2016). However, Vesseurs study focusses on CHARGE syndrome, so patients were not grouped due to *chd7* mutations but rather due to their symptoms. This is especially disastrous because other mutations like a triplication of Sox11 and an inappropriate p53 activation during the development can mimic clinical CHARGE features (Sperry et al., 2014; Nostrand et al., 2014).

1.2.3 Cerebellum under CHD7 Deficiency

The cerebellum is the center of motor function and locomotion Control in the brain, and inhibitory signals of the cerebella Purkinje cells are the main output of the cerebellum to other brain parts. A fully developed cerebellum is sagittally separated into anterior (lobules I-V), central (lobules VIa to VII), posterior (lobules VIII) and nodular (lobules IX and X), while the medial part of the cerebellum is called vermis. In 35% of CHARGE syndrome patients a cerebella vermis hypoplasia has been reported (Yu et al., 2013) and a newer case study reports a *de novo* duplication in the *chd7* gene causing mildly hypoplastic inferior vermis, and dilatation of the lateral and fourth ventricles in a CHARGE patient (Pranckeniene et al., 2019).

Cerebella hypoplasia has been recapitulate in mice studies, showing that a loss of CHD7 can cause this phenotype (Feng et al., 2017; Whittaker et al., 2016; Donovan et al., 2017). One study related midbrain and vermis hypoplasia with a reduced FGF8 expression and postulates CHD7 as FGF8 regulator (Donovan et al., 2017).

Within the cerebellum CHD7 interacts with Top2B a topoisomerase which is decreasing the tension during the transcription of long genes.

and 85 and 24 (58.5) scored low (less then 70) on IQ tests (Vesseur et al., 2016).

Intriguingly Reelin was reported to be a target of CHD7. In the cerebellum Reelin is released by granular neurons and secreted to Purkinje cells to guide them into the right position. Under CHD7 deficiency the Reelin gene shows a closed chromatin state (Feng et al., 2017) and the Purkinje cell layer is disrupted (Feng et al., 2017; Whittaker et al., 2017).

In CHD7 deficient mice a reduced FGF8 expression in the isthmus organiser (IsO), the embryonic signaling centre of the cerebellum has been reported. During cerebella development *fgf8* and *chd7* loss-of-function alleles interact. Since CHD7 associates with *otx2* and *gbx2* regulatory elements and alters the homeobox gene expression, it has been suggested that CHD7 is needed for maintenance of cerebella identity during embryogenesis (Yu et al., 2013).

1.2.4 Stem Cells under CHD7 Deficiency

In embryonic stem cells the presence of CHD7 correlates with signals of active gene expression and open chromatin. CHD7 is present at enhancer elements of stem cell and pluripotency genes like *sox2*, *oct4* and *nanog*. A major co-localization of BRG1 and CHD7, distal but not proximal to gene promotors was reported in embryonic stem cells. Common co-localization sites of both proteins included master transcription factors of embryonic stem cells, and genes associated with active chromatin architecture (Yang et al., 2017).

In embryonically derived neural crest cells CHD7 binds multiple subunits of the PBAF complex. In genes of the ectodermal linage CHD7 binds preferentially active (H3K4me1, H3K27ac) and poised (H3K4me1, H3K27me3) enhancer elements (Zentner et al., 2011; Gaspa-Maia et al., 2011). Ectodermal lineages and tissues are affected in CHARGE syndrome including the brain, retina and neural crest-derived structures like heart and craniofacial structures.

Some developed tissues still contain multipotent stem cells. In the adult brain, multipotent neural stem cells are located in the subventricular zone of the lateral ventricle and migrate as neuroblasts through the rostral migration stream into the olfactory bulbs to form new interneurons. Another stem cell niche of the adult mouse brain is the hippocampal dentate gyrus which is functionally involved in learning and memory. Neural stem cells of the dentate gyrus migrate from the subgranular zone into the granular layer to form granular neurons (Fig. 5). In rodents 85% of dentate granular neurons form and connected to hilar mossy fibers postnatally (Ribak et al., 1985). In contrast to that, human granular neurons of the

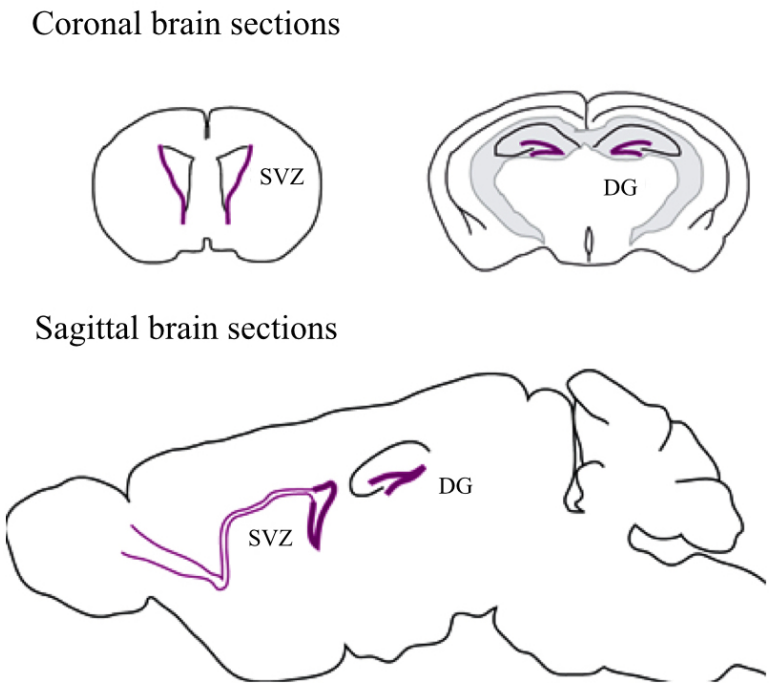

Figure 5: **Neural stem cell niches in the adult mouse brain.** Modified after Zhao et al., 2008

dentate gyrus are formed prenatally (E90), and connect to hilar mossy fibers around E160 to 170 (Humphrey 1967).

CHD7 is highly enriched in neurogenic regions of the adult mouse brain, the subventricular zone, the rostral migratory stream and the subgranular zone. Long time studies with an inducible, conditional knock-out of *chd7* in adult neural stem cells of the subventricular zone showed that CHD7 deficiency lead to a reduction in mature dopaminergic and GABAergic olfactory bulb interneurons. The effect of this knock-out is the downregulation of the CHD7 targets *sox4* and *sox11* in combination with an accelerated proliferation of the stem cell pool. In the SGZ of the hippocampus less BrdU-positive newborn neurons have been found (Feng et al., 2013).

In neural stem cells CHD7 physically interacts with the SOX2 at genes involved in diseases like Alagille syndrome (*jag1*, a Notch signaling ligand), Feingold syndrome (*mycn*, a bHLH transcription factor) and Pallister-Hall syndrome (*gli3*, a mediator of sonic hedgehog signaling). Furthermore, these diseases show a symptomatic overlap with CHARGE syndrome. Both CHD7 and SOX2 have overlapping expression patterns

and functions and contribute to the development of the ectodermal linages including brain, retina and neural crest-derived cells (Micucci et al., 2015).

A study of oligodendrocyte precursor cells could show that CHD7 and CHD8 functions overlap. CHD7 was found to Control oligodendrocyte differentiation through chromatin opening and transcriptional activation of key regulators. During cell state progression CHD7 seemed dispensable because CHD8 compensated in chromatin binding profiles, and genetic interactions (Marie et al., 2018).

CHD7 has been linked to an osteoblast cell fate decision in mesenchymal stem cells. Here CHD7 represses PPAR-γ through a Wnt-mediated mechanism and recruitment of a CHD7, NLK and SETB1 complex. Under CHD7 deficiency this study could show that cells were taking a different fate reasonably through PPAR-γ activity (Takada et al., 2007).

1.3 Epigenetic Proteins with Antagonistic Functions

After the discovery of *polycomb* as Controlling factor of the segmentation in *Drosophila* (Lewis, 1978) the first hints to another group of chromatin modifying proteins were collected in 1985 (Ingham 1985; Kennison and Tamkun 1988). The transcriptional repressive polycomb (PcG) and the (re)activating trithorax group (TrxG) of proteins, were identified as master regulators of *homeotic transcription factors* or *Hox* genes (Lewis, 1978; Zink and Paro 1989). These *homeotic transcription factors* determine the anterior-posterior body axis during the embryonic development in vertebrates and invertebrates.

Since then an antagonistic relationship between the trithorax and polycomb group of proteins has been suggested (Klymenko and Mueller 2004; Dorighi and Tamkun 2013; Schuettengruber et al., 2017 review, Micucci et al., 2015).

The trithorax group of proteins in *Drosophila* and the mammalian myeloid/lymphoid or mixed-lineage leukemia (MLL)-protein-containing complexes activate the same target genes, which are silenced by polycomb group proteins. This is mediated through active histone marks such as methylation of histone 3 lysine 4 (H3K4me3), and the dimethylation of histone 3 lysine 36 (H3K36me2) (Dorighi and Tamkun 2013).

A double knock-out of *ash2* and *trx* in *Drosophila* causes a loss of *Hox* gene expression. This phenotype could be restored through the additionally knocked-out of the polycomb counterpart PcG. ASH1 and TRX are

concluded to be anti-repressors and trithorax and polycomb are described as antagonistic regulators (Klymenko and Mueller, 2004).

A very interesting study emphasizes and antagonistic relationship of trithorax and polycomb group proteins in mice. The mammalian MLL, a homolog of *Drosophilas* TRX shows an axial-skeletal phenotype when knocked-out and an altered *Hox* gene expression in mice. When this knock-out was coupled to its polycomb counterpart *bmi-1* and deleted together, the phenotype normalized (Hanson et al., 1999).

In neural stem cells the trithorax member CHD4 interacts with the polycomb group protein PRC2. CHD4 is expressed during neurogenesis of the cortex, and expressed in murine SVZ neural progenitor cells. Intriguingly CHD4 interacts here with *Polycomb repressive complex 2* (PRC2) and especially its catalytic part *enhancer of zeste* (EZH2). PRC2 usually represses gene expression on a broader scale through the trimethylation of histone 3 lysine 27 (H3K27me3) mediated by EZH2. However, in complex with CHD4 it binds to the promotor of the *glia fibrillary acidic protein* (GFAP) to suppress its expression and thus glia differentiation. In neural stem cells CHD5 interacts with PRC2 and binds H3K27me3 as well (Egan et al., 2013; Micucci et al., 2015).

Several PcG and TrxG proteins function as eraser proteins that prime histones for the implementation of new histone marks. Many of these eraser proteins are also found to be in complex with histone code writers, facilitating immediate transition from active to inactive chromatin states or conversely from inactive to active chromatin states (Kolybaba and Classen 2014).

A new study summarized the relationship of enzymatic histone marks and their transcriptional activating or repressive effect (Fig. 6). As a member of the CHD family CHD7 is related to a transcriptional active chromatin state. A transcriptional repressive histone mark is set by the writing enzyme EZH2, which is the catalytic part of the mammalian PRC2 complex.

1.3.1 Mammalian PcG Complexes and PRC2

There are five main PcG complexes in mammals that recognize and set repressive histone marks: *Polycomb repressive complex 1* (PRC1; Franke et al., 1992), *Polycomb repressive complex 2* (PRC2, Ng et al., 2000), *dRing associated factor complex* (dRAF; Lagarou et al., 2008), *Polycomb repressive deubiquitinase complex* (PR-DUB; Scheuermann et al., 2010), and *Pho-repressive complex*

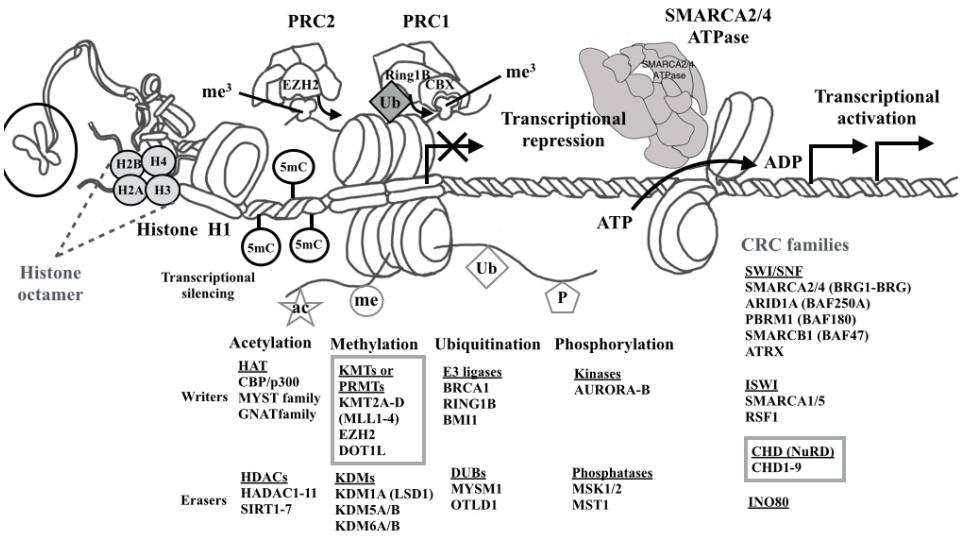

Figure 6: **Chromatin regulatory mechanism mediating transcriptional activation and repression** Modified after Valencia and Kadoch, 2019

(Pho-RC; Klymenko et al., 2006). Additionally PRC3 and 4 are separated by different EED isoforms (Kuzmichev et al., 2002 and 2004).

The human PRC2 complex consists of the proteins *embryonic ectoderm development* (EED), *suppressor of zeste* (SUZ) 12, and the *enhancer of zeste* EZH1 or 2. PRC2 methylates Lysine 9 of histone 3 and mediates mono-, di- and trimethylation of H3K27 (Magueron et al., 2008). The methyltransferase activity of PRC2 is conducted by the SET domain of EZH2 and the resulting suppressive histone marks are needed for neural fate commitment and terminal differentiation of neural stem cells during embryonic development (Magueron et al., 2008).

1.4 EZH2 Deficiency causes Weaver Syndrome

The *Enhancer of Zeste* (E(Z)) was first identified in *Drosophila* as the catalytic part of the PRC2. The mammalian (E(Z)) homologe EZH1 and 2 show conserved domains like the homolog domain 1 and 2 (both needed for protein-protein interactions), and the catalytic SET domain (Cao 2008). In humans, the *ezh2* gene is located on 7q35 with 20 exon's. The protein consists of 746 amino acids.

The pre-SET domain of EZH2 (and other members of the E(z) family) contains a triangular zinc cluster that stabilizes the methyltransferase

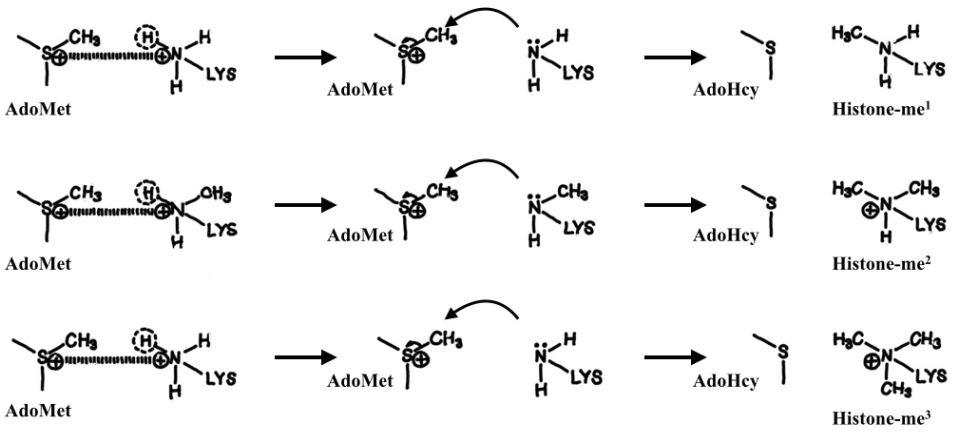

Figure 7: **Mechanism of methyl group transfer to lysine residue used by EZH2.** Modified from Wood and Shilatifard, 2004

activity (Min et al., 2002; Wood and Shilatifard 2004). As methyltransferase is EZH2 capable of transferring and erasing methyl groups, and uses S-adenosylmethionine (SAM or AdoMet) as a methyl group donor. All members of the mammalian DNMT family use SAM or AdoMet as donor (which is synthesized from methionine). The catalytic mechanism of the SET domain itself is mediated together with S-adenosylmethionine and the substrate lysine of a histone tail. A conserved tyrosine of the SET domain deprotonates the epsilon-amino group of the substrate lysine, and prepares it therefore for a nucleophilic attack on the AdoMet methyl group (Trievel et al., 2002). The methyl group is transferred to the lysine of the histone tail, leaving a methylated histone residue and AdoHcy, the byproduct of AdoMet which serves as potent inhibitor of methyltransferases (Hitchler and Domann 2009; Jacobs et al., 2002; Min et al., 2002; Wilson et al., 2002; Zhang et al., 2002). EZH2 is capable of mono- di- and tri- methylating lysine 27 of histone 3 (H3K27me1,H3K27me2,H3K27me3) which silences gene expression (Fig. 7).

EZH2 can also be inhibited by GSK126, a small molecule that is competitive to S-adenosyl-methionine (SAM) and non-competitive with its peptide substrates. GSK126 is highly selective against other methyltransferases. Even EZH1 which is 96% identical to EZH2, is inhibited 150-fold less (McCabe et al., 2012).

In contrast to EZH2, EZH1 has only a weak catalytic function. The PRC2-EZH1 complex seems to be involved in chromatin compaction and it does not need the methyltransferase co-substrate SAM or AdoMet for this activity (Margueron et al., 2008).

A homozygous mutation is the *ezh2* gene is lethal, while a heterozygous mutation of *ezh2* was linked to a medical condition called Weaver Syndrome. Numerous *de novo* and familial missense mutations were found. Their spacial distribution spreads all over the gene structure but some cluster around the catalytic SET domain (Tatton-Brown et al., 2014). These mutations are likely to form a non-functional protein which could even build up artificial complexes. Besides a dominant negative effect of the mutation, these mutations could also lead to a loss of function and haploinsufficiency (Ronan et al., 2013,).

Patients with Weaver syndrome show an overgrowth phenotype in 90% of the cases and intellectual disabilities in more than 80% of cases. Also, dysmorphic facial features, obesity and macrocephaly are common symptoms (Tatton-Brown et al., 2013). In Weaver syndrome the methyltransferase activity of the whole PRC2 complex can be impaired (Gibson et al., 2012). A *ezh2* knock-out reportedly leads to impairment of spatial learning and memory, contextual fear memory and pattern separation in mice (Zhang et al., 2014).

1.4.1 EZH2 and PRC2 in Stem Cells and Differentiation

A knock-out of the complete PRC2 complex has no effect on early linage commitment or embryonic stem cell self-renewal. Embryos that lack PRC2 homozygously fail to pass midgestation and die during and after implantation (Chamberlain et al., 2008; Shen et al., 2008; Pasini et al., 2004; Morin-Kensicki et al., 2001). EZH2, EED and SUZ12 are essential for the embryonic development, deficient mice are embryonic lethal and EZH2-null or EED-null embryonic stem cells could not be established (Gil et al., 2005; Pasini et al., 2007).

In the context of embryonic development and differentiation of stem cells, a time dependent role of EZH2 has been described, because it has been observed that EZH2 expression level drop during cell differentiation. The role of PcG and especially EZH2 in neuronal progenitor cells seems to be the refinement of cell fate commitment (Kuzmichev et al., 2005).

A time-dependent activity of EZH2 has also been reported for neocortical neuronal progenitor cells. A knock-out of *ezh2* lead to a prolonged neurogenic phase and delayed the astrogenic phase. After embryonic day 12.5 a knock-out increased neurogenesis in the cerebral cortex through a more rapid cell cycling of neural precursors which lead to an increase in the number of neurons. The depletion of EZH2 in neuronal precursors did not change their cell fate anymore after a critical time point. This

was related to a lacking repression of the Wnt beta-catenin target Neurogenin1. In general, PcGs seem to regulate the differentiation capacity of neuronal progenitor cells without affecting the differentiation process per se (Hirabayashi et al., 2009).

Furthermore, EZH2 is expressed in actively dividing neural stem cells and progenitors, but not quiescent neural stem cells in the subgranular zone. Here EZH2 regulates the proliferation by suppressing PTEN expression and promoting the activation of the Akt m-Tor pathway (Zhang et al., 2014) A regional loss of EZH2 in the stem cell niches affects the differentiation of neural stem progenitor cells and the maintenance of the stem cell population. In the subgranular zone of the dentate gyrus, an increase in NeuN positive and a moderate increase in Nestin positive cells was observed but no change in GFAP positive cells. It was concluded that EZH2/H3K27me3 would play an important role in the maintenance of stem cell subpopulations within the subventricular zone and the subgranular zone of the dentate gyrus (Rhodes et al., 2018).

1.4.2 EZH2 in Cancer

Since the nature of histone mark H3K27me3 is to repress gene expression an EZH2 deficiency has been linked to over proliferation and cancer. Especially lymphoma, prostate and breast cancer were linked to reduced EZH2 activity (Varambally et al., 2002).

Interestingly, loss of function *and* gain of function mutations in *ezh2* seem to promote cancer growth an aggressiveness in a context dependent manner. In a subset of hormone-refractory, metastatic prostate cancer high EZH2 level were linked to clinical failure. It was traced back to EZH2 mitigating the G2/M transition in cell cycle (Cao et al., 2008). EZH2 was shown to silence tumor suppressor genes (Chen 2010) and was therefore thought to promote cancer growth when functionally impaired. In contrast to that, McCabe and colleagues describe an over expression of EZH2 and an H3K27me3 up-regulation in lymphomas and state that a different substrate preference of the mutated protein could be the reason (McCabe et al., 2012).

In clear cell carcinoma an EZH2 Inhibitor caused regression and reduced the number of tumor suppressor gene *arid1a* mutated tumors (Bitler et al., 2015).

1.4.3 EZH2 Phosphorylation

The EZH2 protein can be phosphorylated at different amino acids with different effects. First, Riising et al. stated that a phosphorylation of EZH2 leads to a functional inhibition of both the recruitment to chromatin, and the gene repressive activity (Riising et al., 2008; Chen et al., 2010; Kaneko et al., 2010; Wei et al., 2011; Wu and Zhang 2011).

Then Chen et al. observed in more detail that CDK1 and 2 phosphorylate EZH2 at Thr350 is functional relevant for the recruitment to histone and the H3K27me3 level (Chen et al., 2010). This phosphorylation of EZH2 through CDK1 and 2 represents an important link to the cell cycle.

Another link of EZH2 to cell growth and nutrient-response allegorizes the phosphorylation through Akt, a kinase of the phosphoinositide 3-kinase (PI3K) signaling pathway. Also in this case a phosphorylation of EZH2 lead to a reduced methyltransferase activity and decreased H3K27me3 level (Cha et al., 2005).

Different studies agreed that EZH2 phosphorylation increases its degradation, followed by reduced H3K27me3 marks and interference with its ability to bind to non-coding RNAs, such as HOTAIR and Xist (Chen et al., 2010; Kaneko et al., 2010; Wei et al., 2011; Wu and Zhang et al., 2011). In mouse embryonic stem cells the origin of EZH2 bound RNAs was further investigated. It became clear that EZH2 preferentially binds to the 5'-region of RNAs originated from genes with low PRC2 occupancy and low H3K27me3 level. The genomic origin of the bound RNAs was compared to the distribution of bound PRC2 on the chromatin. PRC2 seemed to bind preferentially to active promotors and interacted with their nascent transcripts. RNA binding to EZH2 decreased H3K27me3 level at active promotors which could hint to a molecular link between gene state and epigenetic regulation (Kaneko et al., 2013).

1.5 Related Studies in Mice

A combined knock-out of mammalian trithorax and polycomb-group homologues was first described by Hanson et al. 1999. As mentioned before, in this study *mll* a homologue of *Drosophilas trx* was knocked-out in combination with *bmi-1* a homologue of *Drosophilas* polycomb member Posterior sex combs (Psc). In this study, the *Hox* gene defects caused by a *mll* knock-out were normalized in a combination with an *bmi-1* knock-out in mice (Hanson et al., 1999).

1.5.1 CHARGE and CHARGE-like mouse lines

Different approached have been used to generate CHARGE and CHARGE-like mice over the years.

While analyzing chromosome 4 mutants in head-bobbling mice with circling behavior, six nonsense and three splicing site mutations of the *chd7* gene were found. The expression of CHD7 in eye, olfactory epithelium, inner ear and vascular system during the early development was confirmed (Bosmann et al., 2005).

A gene trap null allele was generated through insertion of a lacZ reporter into the *chd7* allele creating a functional null allele coupled with a ß-galactosidase reporter. CHD7 null mouse embryos died around E10.5 and heterozygous mice displayed CHARGE features (Hurd et al., 2007).

The so called *looper* mouse was identified by the ENU mutagenesis screen for deaf mice. The *looper* strain has a nonsense mutation (c.5690C>A, p.S1897X) within the *chd7* gene causing different symptoms. These mice display ossicle malformation, otosclerosis and hearing impairment, retarded growth, heart defect, hyperactivity and depending on the used model eye coloboma. In behavior studies these CHARGE mice circled in the arena and likewise in the water maze test. They run faster and travel further than their Control litter mates. Since the knock-out mice were falling less in the rotator experiment, it was concluded that their motion Control itself was not impaired (Ogier et al., 2013).

A study analyzing a conditional neural crest cell knock-out of *chd7* used Foxg1-Cre;Chd7$^{+/flox}$ and Wnt1-Cre;Chd7$^{+/flox}$ mice and analyzed the skeletal phsnotype, the developing eye, ear, nose, pharyngeal pouch, forbrain and gut (Sperry et al., 2015).

A later study analyzed the so-called *trooper* mouse, a mouse line harboring a pathogenic point mutation in the *chd7* gene. This report focused on middle ear defects and hearing impairment of mice, and showed that a homozygous mutation remains lethal (Ogier et al., 2018).

Up to now, no Weaver disease mouse model (carrying a heterozygous *ezh2* mutation) has been described, but different *ezh2* knock-out mouse lines were created like the Pax7Cre;EZH2$^{fl/fl}$ mouse line (Feng et al., 2016), or Ezh2$flox/flox$;ROSA26 mice (Rhodes et al., 2018).

A double knock-out of *chd7* and *ezh2* has not been described until now.

1.5.2 Previous Data - *chd7* and *ezh2* Single Knock-out

Our pervious data showed that a *chd7* knock-out in the cerebellum leads to cerebella hypoplasia, impaired granular neuron differentiation, induction of apoptosis and an abnormal Purkinje cell localization. We found that CHD7 promotes the open chromatin state of genes like *reelin* which is crucial for Purkinje cell development (Feng et al., 2017). Another study also reported that a deletion of *chd7* from cerebellar granule cell progenitors results in reduced proliferation, cerebellar hypoplasia, developmental delay, motor deficits and caused a downregulation of Reelin in mice (Whittaker et al., 2016).

Interestingly, we further saw that CHD7 occupies active chromatin regions (H3K27ac) (Feng et al., 2017). The opposite task namely H3K27 silencing via mono-, di- and tri-methylation is conducted by EZH2, the catalytic part of the PRC2 complex. As described above a heterozygous mutation in the *ezh2* gene is related to a medical overgrowth condition called Weaver syndrome. Also, the symptoms of CHARGE ($CHD7^{+/d}$) and Weaver syndrome ($EZH2^{+/d}$) are partially oppositional.

Further hinting towards an antagonizing relationship of CHD7 and EZH2, our data showed that a neural stem cell knock-out of *chd7* increases cell proliferation and decreases the stem cell pool (BrdU) in the dentate gyrus. Strikingly, this phenotype could be rescued by voluntary running (Feng et al. 2013) while physical exercise had no effect on the number of stem and label retaining cells in an *ezh2* knock-out conducted with the same parameters (Liu, Y.).

A *chd7* knock-out also affects the neuron morphology. Neurons with *chd7* knock-out show less and shorter branches (Feng et al., 2013) and in contrast to that preliminary data showed that neurons with an *ezh2* knock-out had more branches in comparison to littermate Controls (Liu, Y.).

With these strong hints to an antagonizing relationship between CHD7 and EZH2, we hypothesize that EZH2 might be a good candidate to counteract CHD7 mutation phenotypes.

1.6 Aims and Objectives of this Study

CHARGE syndrome is a combination of birth defects which can result in a severe brain symptomatic that is currently not treatable. Patients suffer from a broad spectrum of brain-related constraints and unlike other

affected organs there is no surgery approach to ease the situation. A better understanding of the disease related changes under CHD7 deficiency, could enable the development of a stem cell treatment in the future. Thus, a disease model of the CHARGE syndrome *chd7* was analyzed. These mice displayed a depleted stem cell pool in the dentate gyrus, a missing cerebella anterior lobe and a disorganized cerebella purkinje cell layer with less primary branches. Besides all that these mice had very severe eye malformations.

Previous data suggested a possible antagonistic relationship between CHD7 and EZH2. Following this hypothesis a genetic rescue of the CHARGE mouse was analyzed and did proof that a reduction of both CHD7 and EZH2 rescues the stem cell pool, the cerebellum and the eye symptomatic almost entirely.

Furthermore, a inducible homozygous knock-out of *chd7* and *ezh2* restricted to neural stem cells, confirmed the rescue of the stem cell pool and revealed that key regulators downregulated under CHD7 deficiency were normally expressed in the double knock out.

2 Results

2.1 The CHARGE Mouse

This mouse line was generated through crossing a CMVCre mouse line carrying a Cre recombinase coupled to a universally expressed viral CMV promotor (CMVCre, C57BL/6N-C2 mouse), with mouse line that possessed a homozygously floxed CHD7 gene (CHD7$^{fl/fl}$, C57BL/6N-C2 mouse). After the first mating the mutant mice of the F1 generation expressed the Cre recombinase, and CHD7 heterozygous in all mouse tissues from embryonic days onwards (CMVCre;CHD7$^{+/fl}$). No crossing within the mouse line was conducted.

A knock-out was confirmed after genotyping the tail DNA of the F1 litter, and further supported by analyzing the CHD7 expression in qPCR and stainings of different tissues.

The absence of the human smelling sense is a known feature of CHARGE patients, thus this tissue was examined. The olfactory bulbs of CHARGE mice were smaller (Fig. 8 A and B) and the tissue expressed significantly less CHD7. It has been shown before that a reduction of CHD7 resulted in less newborn neurons in the olfactory bulbs (Feng et al., 2013). In the CHARGE mouse line, a reduction in the doublecortin expression could be observed, resulting in less newborn neurons in the olfactory bulbs (Fig. 8D to K and L). These results confirm an efficient *chd7* knock-out and the generated CHARGE disease model.

CHARGE patients are reportedly small, and some develop a micro-cephalous. Therefore the body and brain weight of CHARGE mice were measured and analyzed per mouse. Male and female mice were analyzed separately. CHARGE mice of both sexes had a lower body weight in comparison to the Control litter mates (Fig. 9A and B).

The total brain weight was quantified as percentage of the body weight for each mouse. No significant changes were observed when all mice were grouped together per sex (Fig. 9C and D). However, a selection of the most severely affected mice did show a significant reduction in the brain weight of these mice. Here the same number of male and female animals of both genotypes was analyzed together.

Previous studies reported a hyperactive behavior of a mouse line displaying CHARGE features (Ogier et al., 2013). Thus, the here analyzed CHARGE mouse (CMVCre;CHD7$^{+/fl}$) was examined in this regard. To further analyze the movement and the running speed of the CHARGE

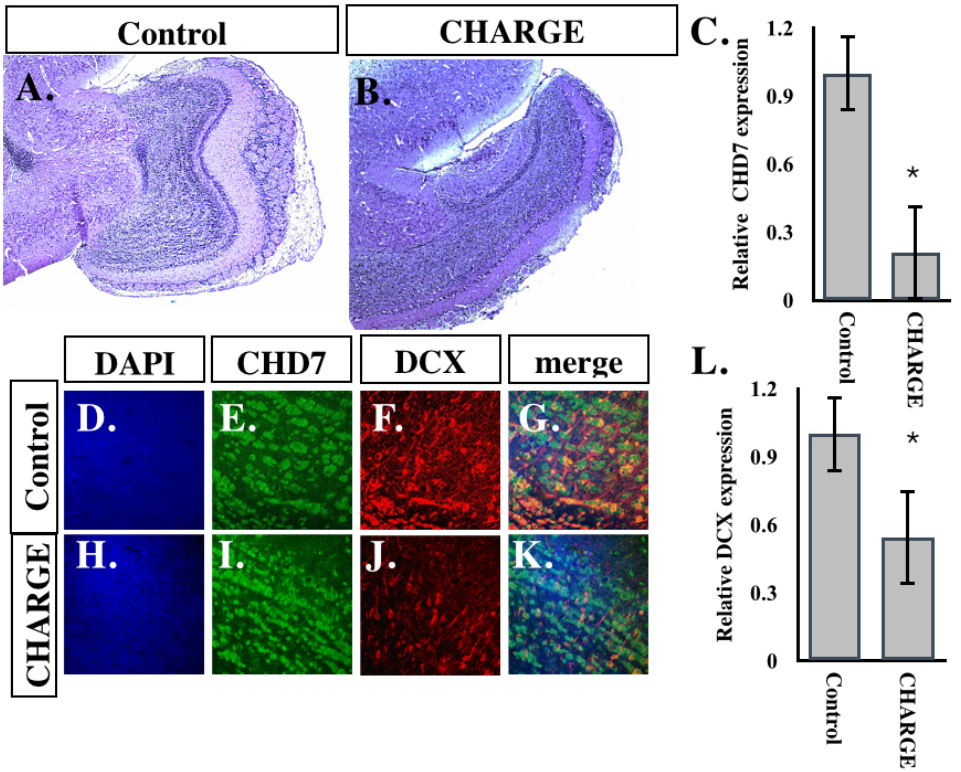

Figure 8: **CHARGE mice have deformed olfactory bulbs with less newborn neurons.** A and B: H & E stainings of the ten week old Control (CMV Cre-) and CHARGE (CMVCre;CHD7$^{+/fl}$) mouse olfactory bulbs. C: qPCR for CHD7 expression in Control and CHARGE mouse olfactory bulb tissue; n=3 animals per genotype, p=0.0433. D to G and H to K: Immunostainings of DAPI, CHD7 and DCX in the olfactory bulbs of Control and CHARGE mouse. L: qPCR of DCX expression in Control and CHARGE mouse olfactory bulb tissue; n=7 Control and n=3 CHARGE mice, p=0.0189. Statistics were done with a students t-test.

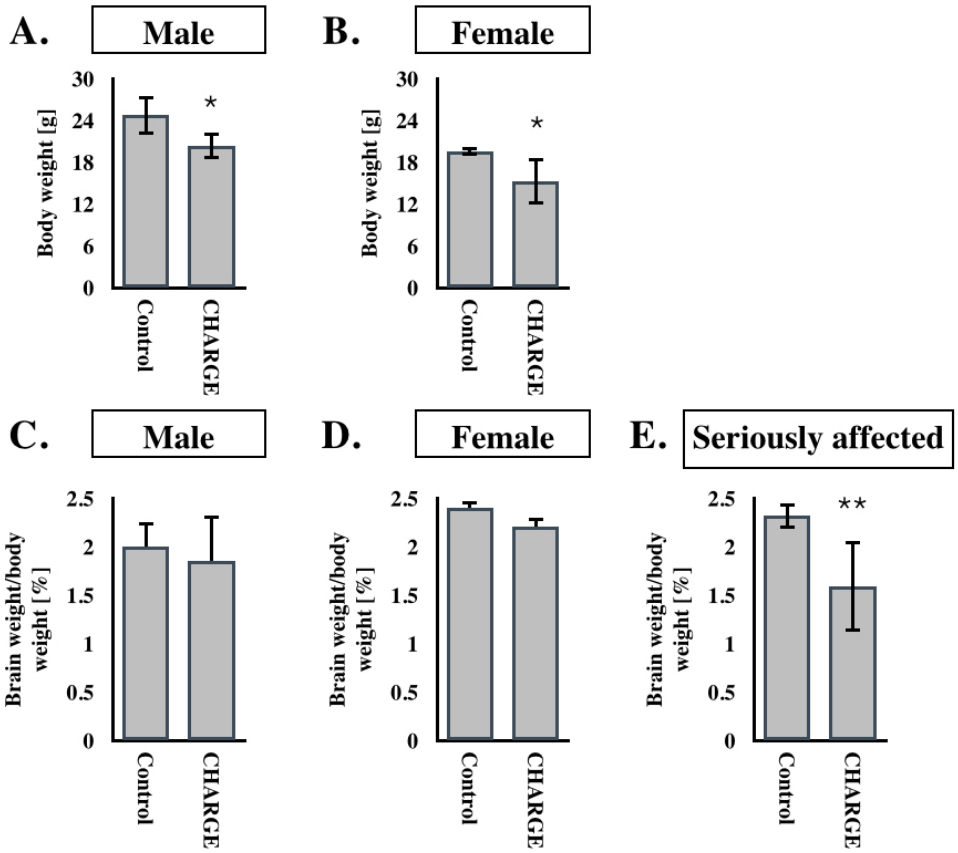

Figure 9: **CHARGE mice are smaller and severely affected mice have a smaller brain.** The ten week old Control (CMV Cre-), CHARGE (CMVCre;CHD7$^{+/fl}$) mouse were weight directly post mortem using a fine scale. A: The weight of male animals of the Control and CHARGE mouse line were compared; n=20 Control and n=9 CHARGE mice, p=0.0366. B: The weight of female animals of the Control and CHARGE mouse line were compared; n=4 Control and n=5 CHARGE mice, p=0.0330. C: The brain weight of male Control and CHARGE mice were measured and calculated in relation to their respective body weight; n=20 Control and n=9 CHARGE mice, n.s. D: The brain weight of female Control and CHARGE mice were measured and calculated in relation to their respective body weight; n=4 Control and n=5 CHARGE mice, n.s. E: Comparing the Control mice to the three most severely affected CHARGE mutants; n=7 Control and n=3 CHARGE mice, p=0.0039. Statistics were done with a students t-test.

mice, an open field test was conducted. Mice were filmed for 15 minutes, and later analyzed by using a computer program (ImageJ macro, Fig. 10A and B). The resulting excel sheets were used to calculate running speed and traveled distance (Fig. 10C and D). Control mice were moving mainly at the corners of the open field, while CHARGE mice did not spare the center field (Fig. 10A and B). The *chd7* mutant mice were traveling significantly faster and further in comparison to their Control litter mates (Fig. 10C and D).

2.1.1 Eye Defect in CHARGE mouse

CHARGE patients suffer from severe and diverse eye malformations including complete blindness.

While the Control mice showed no eye abnormalities, the CHARGE mice had mild to severe eye malformations with high penetrance. The phenotype ranged from structural functionally eyes to a only rudimentary developed eyes with closed eye lids. Virtually all mutant CHARGE mice displayed some kind of eye malformation in one or two eyes (Fig. 11).

The eye symptoms showed a heterogeneity between the left and the right eye.The CHARGE mouse eyes were scored regarding to their visible closed eye lids (100% = eye completely closed, 50% = eye half closed, 0% = not affected). On average the right eye was affected in 70% of the mice, while the left eye displayed a closed eye lid in 30% of the mice. (Fig. 11). Such a symptomatic heterogeneity in the severity of the eye phenotype has been reported for human CHARGE patients likewise (Hartshorne et al., 2016).

Further, the eye structure was analyzed. The eye of the Control animal showed retina, lens, pupil and cornea and had a normal size of around 3 mm in diameter (Fig. 12A). The eye structure of the CHARGE mouse eye is barely recognizable. Remarkably, a thick layer of black pigment epithelium is surrounding the eye (under normal conditions the pigment epithelium is forming a one-cell thick bottom layer underneath the retina). The mutant eye has no visible pupil and the lens is not fully formed. A retina is not recognizable. The eye is structural under-developed and predictably non-functional (Fig. 12B).

Furthermore, the stained CHARGE eye was much smaller in its total size in comparison to the Control mouse eye depicted on the left site (Fig. 12A and B). Only eyes with a visible pupil were analyzed, thus strongly under-developed and structurally deformed eyes (like the one displayed) were not included in this analysis. The eye diameter was measured with

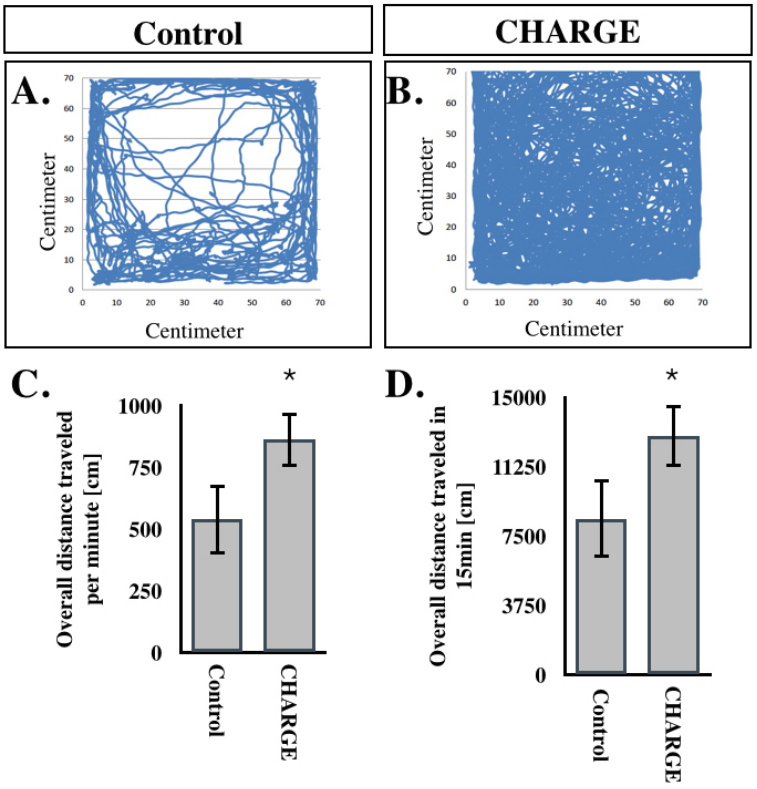

Figure 10: **CHARGE mice run faster (Control and CHARGE mouse).** Eight week old Control (CMV Cre-) and CHARGE (CMVCre;CHD7$^{+/fl}$) mice spend 15 minutes in a 72 to 72 cm white box, moving freely while filmed. A and B: An ImageJ macros was used to automatically track the mice walking path in the box (developed by Yue Zhou). C: The recorded distance traveled per minute; n=5 Control and n=6 CHARGE mice, p=0.0487 between Control and CHARGE mouse. D: The overall distance traveled within 15 minutes each for Control and mutant mouse; n=5 Control and n=3 CHARGE mouse, p=0.0487. Statistics were done with a students t-test.

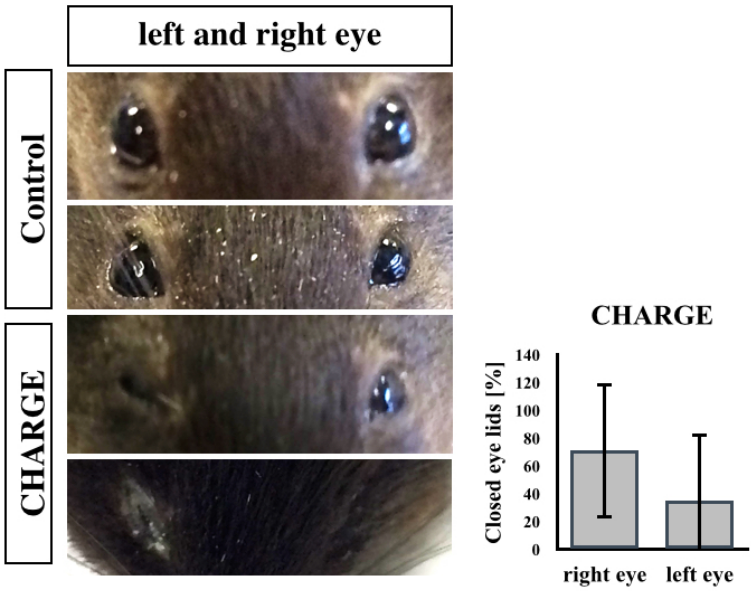

Figure 11: **CHARGE mice have closed eye lids, more often on the right site.** The ten week old Control (CMV Cre-) and CHARGE (CMVCre;CHD7$^{+/fl}$) mice were photographed, and both eyes are shown as zoomed picture of two example mice per genotype. The optically assessable damage of the left and right eye was analyzed with 100% damage representing a closed lid, 50% representing a half closed lid and 0% representing an open eye lid; n=7 CHARGE animals, and 7 left and right eyes respectively (14 eyes).

a scale tool of ImageJ. CHARGE mice had significantly smaller eyes in comparison to their Control litter mates (Fig. 12C). Also the CHARGE eye retina was significantly thinner than the retinas measured for their Control litter mates (Fig. 12D).

To further investigate differences between the CHARGE and Control mouse retina, the retina layers were stained and measured. Again, only eyes with a visible pupil were considered, excluding the most severely affected eyes. Therefore, the separation of the outer nuclear layer (ONL), inner nuclear layer (INL) and granular cell layer (GCL) is visible in both mutant and Control mice by the dark stained nuclei (Fig. 13A and B).

CHARGE mice displayed an outer nuclear layer thickness which was comparable to the measured Control mouse retina thickness (Fig. 13C).

The inner nuclear layer of the retina was significantly thinner in the CHD7 deficient mice (Fig. 13D).

There was no significant difference between the measured ganglion cell layer thickness in Control and CHARGE mice eyes (Fig. 13E).

Since the severe CHARGE eye phenotype hinted towards underdeveloped eyes, markers were stained which are usually expressed early in the eye development. Under-developed cells expressing embryonic markers where not expected under Control conditions, and no MASH1 positive cells where found. However, CHARGE retina showed cells with a signal for MASH1 in the ganglion cell layer (Fig. 14B and F).

The Control retina displayed a clear PAX6 signal in the ganglion cell layer and the inner nuclear layer, which corresponds to other studies (Stanescu-Segal et al., 2015). Little is known about the function of PAX6 in the adult retina, but amacrine and ganglion cells keep the expression under normal conditions (Stanescu-Segal et al., 2015).

Pictures of CHARGE mouse retina were taken with the same confocal laser microscope adjustments but show a much weaker PAX6 signal. Only very few cells can be considered as PAX6 positive (Fig. 14C and G).

2.1.2 Cerebella Defect in CHARGE Mouse

To confirm the *chd7* knock out crebellum tissue of CHARGE (CMVCre;CHD7$^{+/fl}$) and control litter mates were stained for CHD7 and DAPI. The CHD7 signal in the CHARGE mouse cerebellum seems

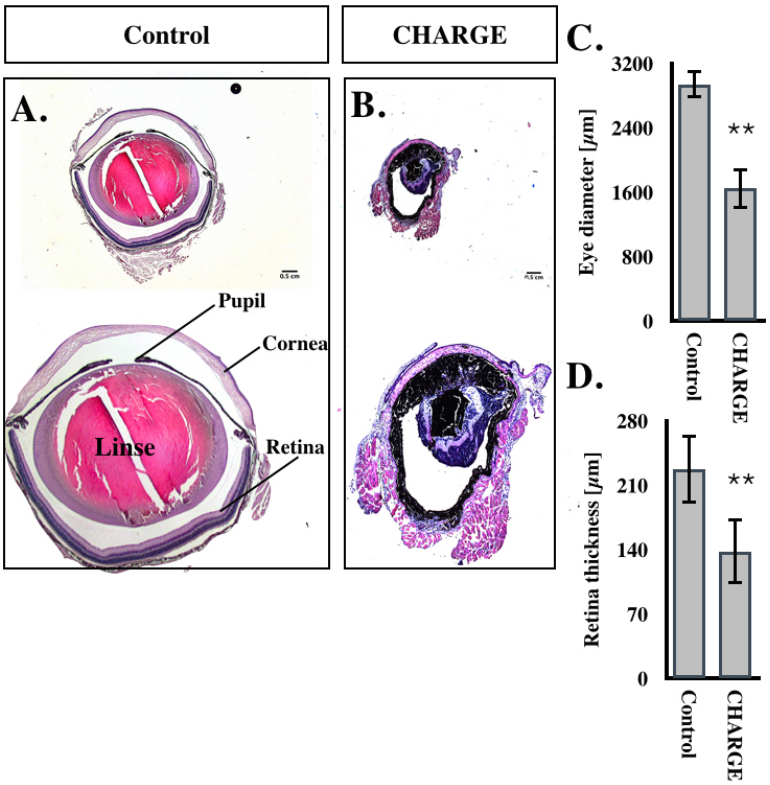

Figure 12: **CHARGE mouse eyes are smaller and the retina is thinner.** A and B: The ten week old Control (CMV Cre-) and CHARGE (CMVCre;CHD7$^{+/fl}$) mouse eyes were stained with Hematoxylin and eosin stain. Pictures were taken with a 1.25 x objective. C: The eye diameter was measured with a scale tool of ImageJ; n=3 Control and n=6 CHARGE eyes, p=0.0038. D: The retina thickness was measured with a scale tool of ImageJ; n=6 Control and n=12 charge eyes, p=0.0038. N-values represent eyes, more then 3 slices per eye were considered. Statistics were done with a students t-test.

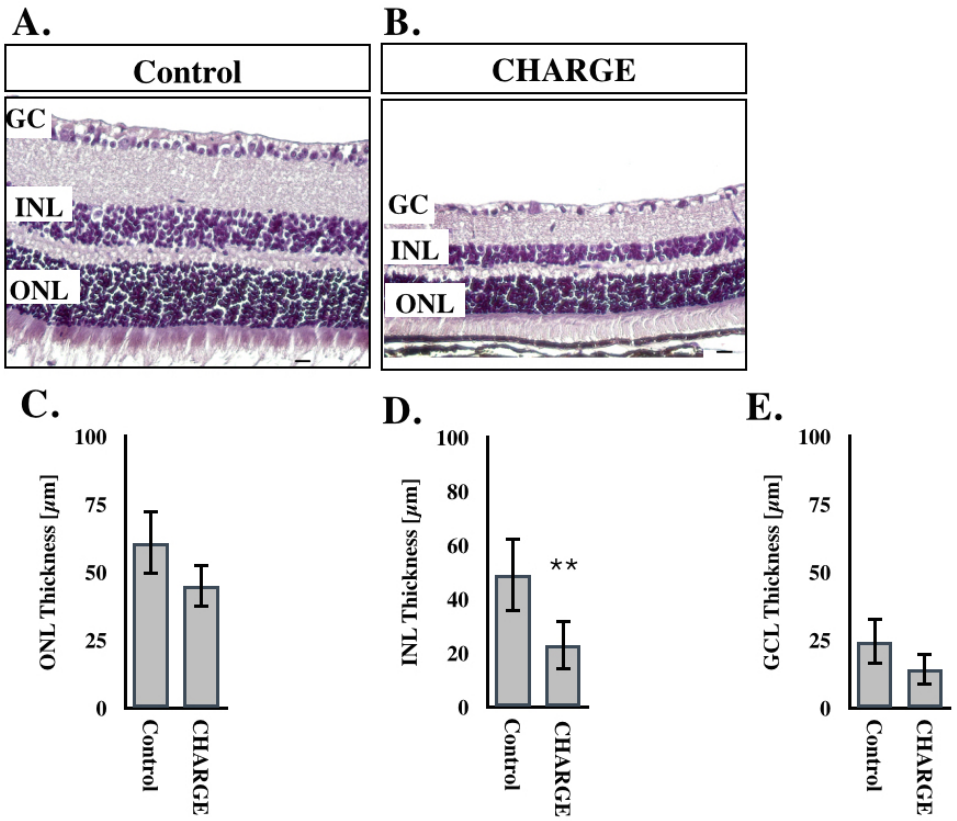

Figure 13: **CHARGE mouse retina has a thinner inner nuclear layer.** The ten week old Control (CMV Cre-) and CHARGE (CMVCre;CHD7$^{+/fl}$) mouse eyes were stained with Hematoxylin and eosin stain. A and B: H & E Retina Staining of Control (left) and CHARGE (right) retina. Pictures were taken with a 10 x objective. The retina thickness was measured with a scale tool of ImageJ. C: Graph showing the measured outer nuclear layer (ONL) thickness in μm for Control and CHARGE mouse; n=6 Control and n=12 CHARGE mouse eyes, n.s. D: Graph showing the measured inner nuclear layer (INL) thickness in μm for Control and CHARGE mouse; n=6 Control and n=12 CHARGE mouse eyes, p=0.0096. E: Graph showing the measured granular cell layer (GCL) thickness in μm for Control and CHARGE mouse; n=6 Control and n=12 CHARGE mouse eyes, n.s. More than 3 slices per eye were considered. Statistics were done with a students t-test.

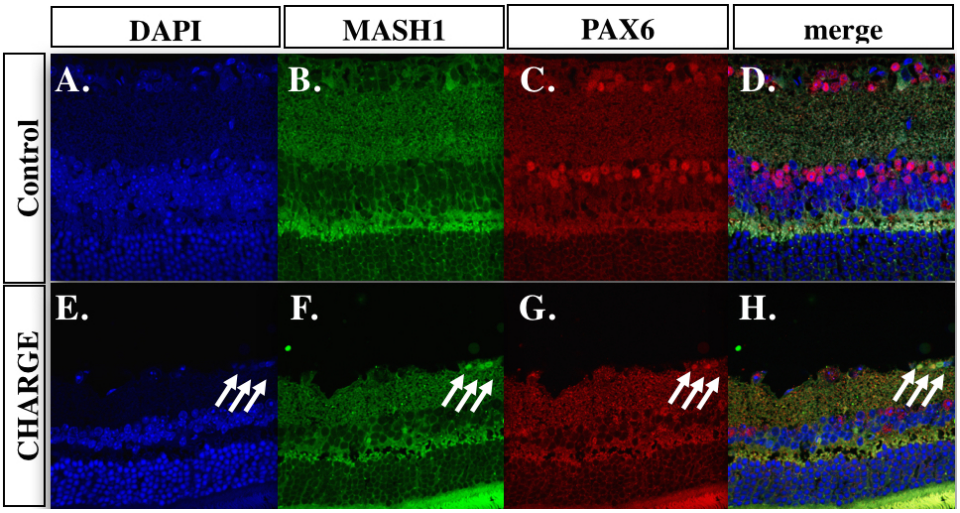

Figure 14: **CHARGE mouse retina has less PAX6 positive cells and expresses ectopic Mash1.** A to H: The ten week old Control (CMV Cre-) and CHARGE (CMVCre;CHD7$^{+/fl}$) mice eyes were stained for MASH1 (white arrows) and PAX6. Pictures were taken with a confocal microscope LSM780 (Zeiss).

reduced, indicating less CHD7 positive granular neurons (Fig. 15A to F).

The cerebellum tissue was homogenized and the RNA was isolated to analyze the CHD7 expression. A qPCR showed a significant reduction in the CHD7 RNA expression level under CHARGE conditions (Fig. 15).

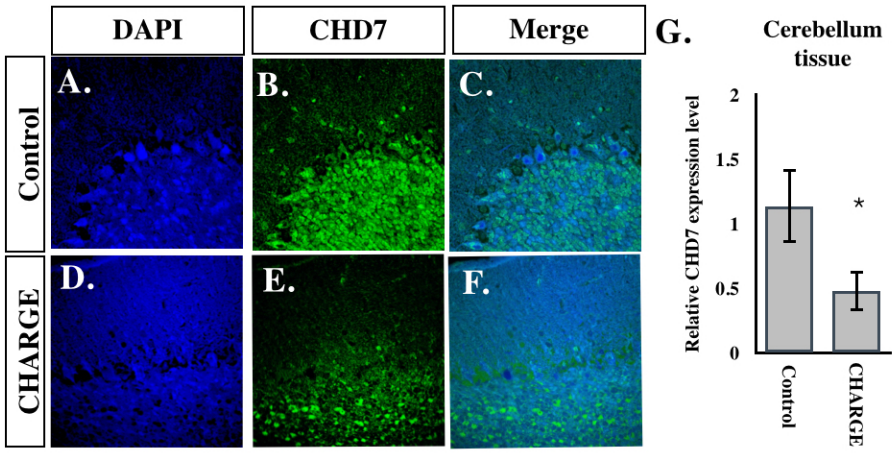

Figure 15: **Immunofluorescence picture and qPCR graph for CHD7 in the cerebellum (Control and CHARGE mouse)** A to F: Stained brain slices of the ten week old CHARGE mouse cerebellum were treated with antibodies against CHD7 and DAPI and pictures were taken with a laser microscope (LSM780, Zeiss). G: qPCR of CHARGE mouse cerebellum analyzing the relative expression level of CHD7 in Control (CMVCre-) and mutant (CMVCre;CHD7$^{+/fl}$) mice. n= four animals per genotype. Statistics were done with a students t-test.

In some human CHARGE syndrome patients cerebella vermis hypoplasia has been reported (T. Yu et al. 2013).

Data from an Atoh1-Cre::Chd7$^{fl/fl}$ mouse line, showed a structural difference in the cerebella anterior lobe (Feng et al., 2017). Thus, this structure was analyzed in the CHARGE mouse.

An superior overview picture of the cerebellum tissue hinted already towards a structural difference of the CHARGE mouse cerebellum (Fig. 16B and E) and a staining revealed that the III anterior lobe is missing in the CHARGE mouse cerebellum (Fig. 16C and F).

The cerebellum was further analyzed with regard to the purkinje cell layer. Strikingly the purkinje cell layer showed some a-typical cell accumulations. While the Control animals had only 1.5% of Purkinje cells with more than three neighboring cells, the CHARGE mutant mice had 27% of purkinje cells displayed three or more neighbors (Fig. 17C).

The Purkinje cell body size was measured but no significant difference between the cell body size of Control and CHAGRE mouse could be

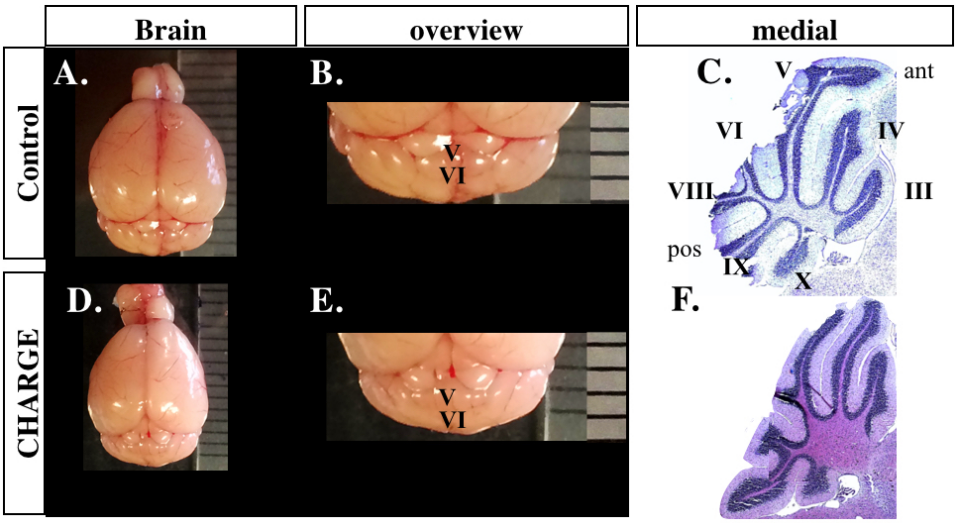

Figure 16: **CHARGE mouse has a defect in the anterior lobe of the cerebellum.** A and D: Photograph of the brain of ten week old Control (CMV Cre-) and CHARGE (CMVCre;CHD7$^{+/fl}$) mice. Brains were placed next to a scale, directly after dissection. B and E: Zoomed picture of the cerebellum with marked V and VI lobe. The scale (mm) is indicated on the right. C and F: Nissl staining of the medial cerebellum. Roman numbers indicate the lobi. Ant = anterior, pos = posterior.

observed (Fig. 17D).

Another characteristic of the CHARGE purkinje cells seemed interesting. In the CHARGE animal, less calbindin positive cells appeared to have primary branches. A quantification revealed that this difference was significant (Fig. 17E).

2.1.3 Less Neural Stem cells in CHARGE Mouse DG

A loss of neural stem cells in the dentate gyrus has been linked to CHD7 deficiency before (Feng et al., 2013), thus the amount of BrdU and nestin positive cells was analyzed, for cells grown under CHARGE and Control conditions. The CHD7 mutant mice showed a significant lower number in BrdU and Nestin double positive cells than their Control litter mates (Fig. 4.2.1).

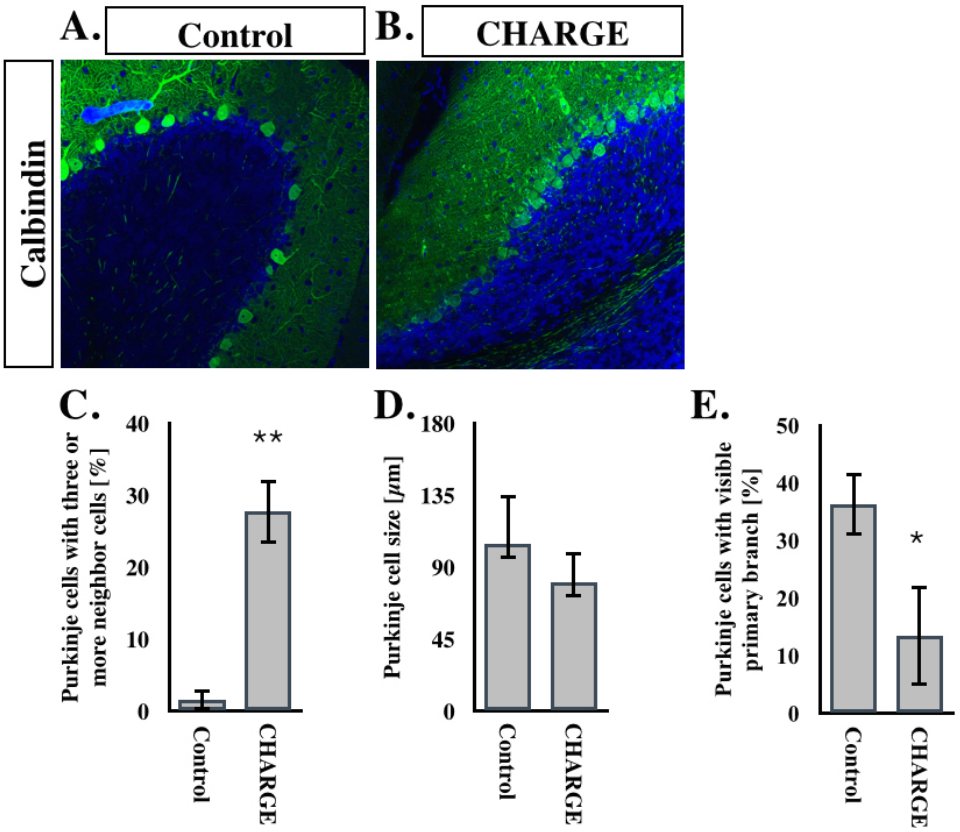

Figure 17: **CHARGE mouse purkinje cells are disorganized and show less primary branches.** A and B: Stained brain slices of the ten week old Control (CMV Cre-) and CHARGE (CMVCre;CHD7$^{+/fl}$) mice cerebellum were stained for Calbindin and DAPI, pictures were taken with a confocal microscope LSM780 (Zeiss). C: Neighboring cells of each purkinje cell were measured; n=347 Control and n=408 CHARGE mouse cells, p=0.0107. D: Quantification of Purkinje cell-body size in Control and CHARGE mouse. Cell-body sizes were measured using a scale tool of the ImageJ; n=33 Control and 37 CHARGE mouse cells, n.s. E: Purkinje cells with visible primary branches were manually quantified. Control Purkinje cells n=392, CHARGE purkinje cells n=779, p=0.0344. N-values represent cell numbers counted from different brain slices. Control Purkinje cells n=33, CHARGE purkinje cells n=37 of three animals per genotype. Several stainings of three mice per genotype were quantified. Statistics were done with a students t-test.

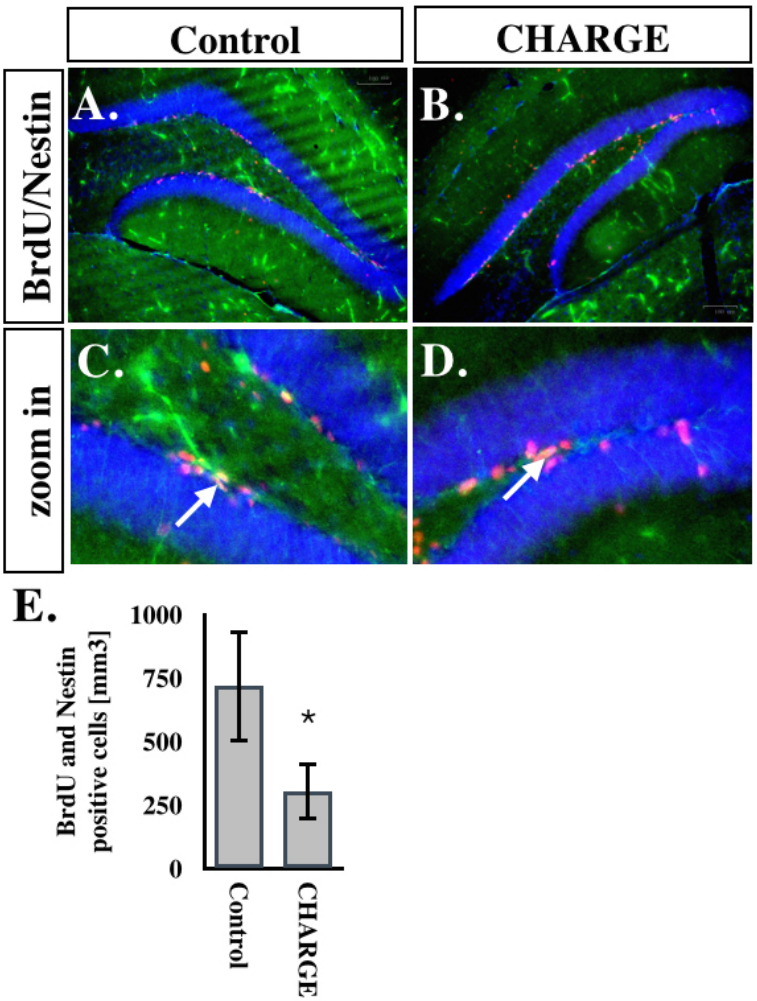

Figure 18: **CHARGE mouse showed less stem and label retaining cells in the dentate gyrus** The ten week old Control (CMV Cre-) and CHARGE (CMVCre;CHD7$^{+/fl}$) mice were treated with BrdU for 5 days and dentate gyrus were stained. A and B: Stained with BrdU, Nestin and DAPI and pictures were taken with a laser microscope LSM780 (Zeiss). C and D: Zoomed in pictures showing cells with BrdU and Nestin staining, marked with white arrows. E: Graph depicting the counted cell amount of BrdU and Nestin double positive cells [mm3]; n=7 Control and n=3 CHARGE animals, p=0.0326. Statistics were done with a students t-test.

2.2 The reCHARGE Mouse

To be able to compare the reCHARGE mouse line to the CHARGE mouse, the same viral, universally expressed CMV promotor was used to knock-out *chd7* and *ezh2* heterozygous in all cells of the body. The CMVCre mouse line (C57BL/6N-C2 mouse) was crossed with CHD7$^{fl/fl}$;EZH2$^{fl/fl}$ mice (C57BL/6N-C2 mouse), to give birth to an F1 litter with the genetic combination of CMVCre;CHD7$^{+/fl}$;EZH2$^{+/fl}$ (herein interchangeably called reCHARGE mouse, or heterozygous double knock-out). This breeding scheme was used for all animals.

Illustrating the double knock-out of *chd7* and *ezh2* beyond the genotyping results, both proteins were stained in the cerebellum of Control, CHARGE and reCHARGE mice. In combination with the purkinje cell staining Calbindin, EZH2 staines purkinje cell nuclei, while CHD7 gives a weak signal for granular cells, and no signal for purkinje cells (Fig. 19 A to G).

To confirm a successful knock-out, EZH2 and CHD7 were analyzed by a qPCR in the cerebellum tissue of reCHARGE mice (CMVCre;CHD7$^{+/fl}$;EZH2$^{+/fl}$) and compared to Control (CMV Cre-) and CHARGE mice (CMVCre;CHD7$^{+/fl}$). While CHARGE cerebellum tissue displayed a reduced CHD7 expression level in comparison to their Control litter mates, the reCHARGE mouse cerebellum tissue confirmed the double knock-out of *chd7* and *ezh2* (Fig. 19D and H).

As CHARGE mice weight less than their Control litter mates, the body weight of the genetic rescue was determined. Males of both genotypes had on average a weight of 23 grams, while the average female weight was 19 grams. There was no detectable difference between reCHARGE (CMVCre;CHD7$^{+/fl}$;EZH2$^{+/fl}$) and Control (CMVCre-) litter mated (Fig. 20A and B). In both male and female Control and reCHARGE mice no difference between the measured brain weight could be observed (Fig. 20C and D).

2.2.1 Eyes in CHARGE vs reCharge Mouse

The very severe and obvious eye malfomations of the CHARGE mouse (CMVCre;CHD7$^{+/fl}$) could not be observed in the reCHRAGE mouse (CMVCre;CHD7$^{+/fl}$;EZH2$^{+/fl}$). While CHARGE mice often display closed eye lids, the reCHARGE mice never showed such a phenotype. The eyes of littermate Control animals were optically indistinguishable from the eyes of the heterozygous double knock-out

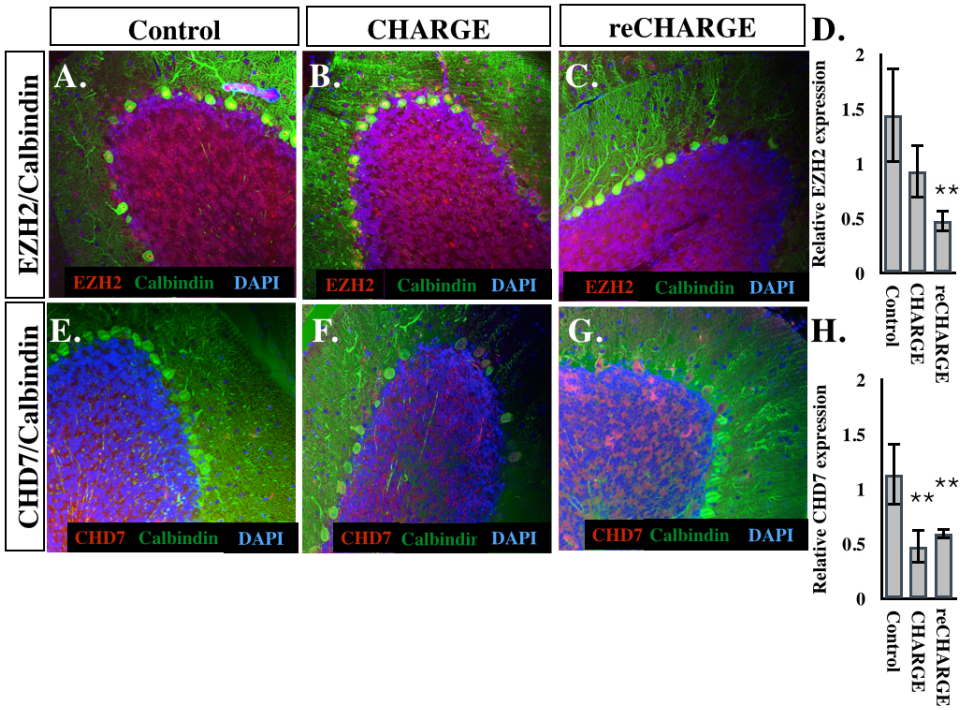

Figure 19: **reCHARGE mouse has a reduced expression of CHD7 and EZH2 in the cerebellum.** A to C: The ten week old Control (CMV Cre-), CHARGE (CMVCre;CHD7$^{+/fl}$) and reCHARGE (CMVCre;CHD7$^{+/fl}$;EZH2$^{+/fl}$) mouse cerebellum were stained with EZH2, Calbindin and DAPI. E to G: The cerebellum of all three genotypes were stained for CHD7, Calbindin and DAPI. D: The qPCR was run using Taqman probes of Actin, EZH2. Shown are the relative expression level calculated by using the SQ values of samples with working standard, normalized to actin; n=3 Control, n=4 CHARGE and n=4 reCHARGE mice, Control to CHARGE n.s., p=0.0053 Control to reCHARGE. H: The qPCR was run using Taqman probes of Actin and CHD7. Shown are the relative expression level calculated by using the SQ values of samples with working standard, normalized to actin; n=3 Control, n=4 CHARGE and n=4 reCHARGE mice, p=0.0097 Control to CHARGE, p=0.0055 Control to reCHARGE. Statistics were done with a students t-test.

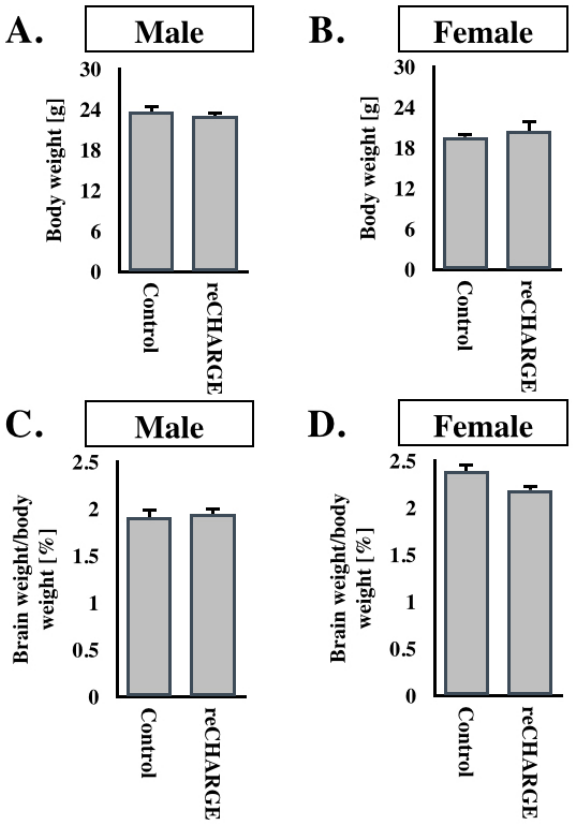

Figure 20: **reCHARGE mouse body and brain weight correspond to the Control values.** The ten week old Control (CMV Cre-), and reCHARGE (CMVCre;CHD7$^{+/fl}$;EZH2$^{+/fl}$) mouse were weight directly post mortem by using a fine scale. A: The weight of male Control and reCHARGE mouse animals were compared; n=20 Control and n=9 reCHARGE mice, n.s. B: The weight of female Control and reCHARGE mouse animals were compared; n=4 Control and n=5 reCHARGE mice, n.s. C: The brain weight of male Control and reCHARGE mice were measured and calculated in relation to their respective body weight; n=15 Control and n=4 reCHARGE mice, n.s. D: The brain weight of female Control and reCHARGE mice were measured and calculated in relation to their respective body weight; n=4 Control and n=5 reCHARGE mice, n.s. Statistics were done with a students t-test.

CMVCre;CHD7$^{+/fl}$;EZH2$^{+/fl}$ (Fig. 21).

Hematoxylin and eosin stainings of Control, CHARGE and reCHARGE eyes revealed that the heterozygous double knock-out had structural well developed eyes; the reCHARGE eyes showed a retina, lens, pupil and cornea. Even though, these eyes were bigger than the CHARGE mouse eyes, they were still significantly smaller than the Control litter mate eyes (Fig. 22A to D).

As seen before the CHARGE retina was thinner. In contrast to that the reCHARGE retina was as thick as the Control mouse retina (Fig. 22E).

The retina layers analyzed in the CHARGE mouse line (CMVCre;CHD7$^{+/fl}$) were also analyzed in the genetic rescue (CMVCre;CHD7$^{+/fl}$;EZH2$^{+/fl}$). All retina layers were stained and measured (Fig. 23A to C). Remarkably some reCHARGE mice displayed an extensive retina growth with a wavy structure (indicated in Fig. 23C).

Under CHARGE and reCHARGE conditions the outer nuclear layer was not significantly altered in comparison to the Control values. However, the reCHARGE outer nuclear layer was significantly thicker than the CHARGE outer nuclear layer but still corresponding to Control values (Fig. 23C).

In comparison to the Control, the CHARGE retina had a reduced inner nuclear layer thickness. In the reCHARGE mice the measured inner nuclear layer thickness corresponded to the Control values (Fig. 23D).

The granular cell layer was not significantly changed in CHARGE or reCHARGE mice. In this regard no significant difference between the mouse lines could be observed (Fig. E).

Correlating to the presented CHARGE mouse results, the reCHARGE retina was also stained for MASH1 and PAX6. Similar to the Control mouse retina, the reCHARGE (CMVCre;CHD7$^{+/fl}$;EZH2$^{+/fl}$) had no MASH1 positive cell (Fig. 24B and J).

The PAX6 signal observed for the reCHARGE retina is in comparison to the signal detected under Control conditions much weaker. There are no PAX6 positive cells in the granular cell layer, and only very few cells can be considered positive in the inner nuclear layer of reCHARGE mouse retina (Fig. 24C, G and K).

In summary, the reCHARGE eyes diameter was smaller than the Control eyes and the retina had a wavy structure which was more pronounced

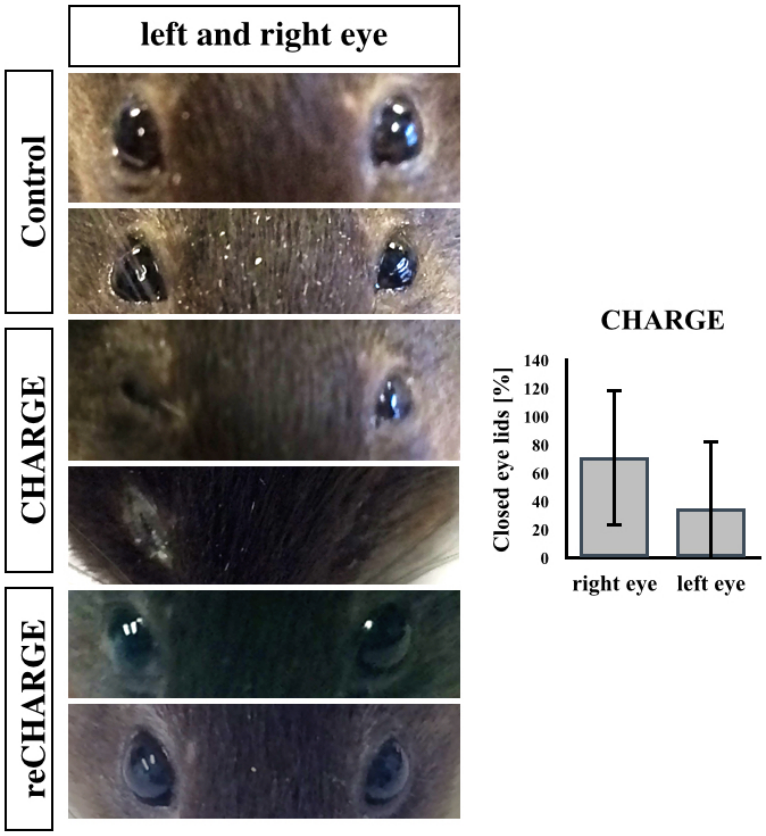

Figure 21: **reCHARGE mouse eyes are unremarkable.** The ten week old Control (CMV Cre-), CHARGE (CMVCre;CHD7$^{+/fl}$) and reCHARGE mice (CMVCre;CHD7$^{+/fl}$;EZH2$^{+/fl}$) were photographed, and both eyes are shown as zoomed picture of two example mice per genotype. The optically assessable damage of the left and right CHARGE mouse eye was analyzed with 100% damage representing a closed lid, 50% representing a half closed lid and 0% representing an open eye lid; n=7 CHARGE animals, and 7 left and right eyes respectively (14 eyes). Control and reCHARGE mice displayed no closed eye lids.

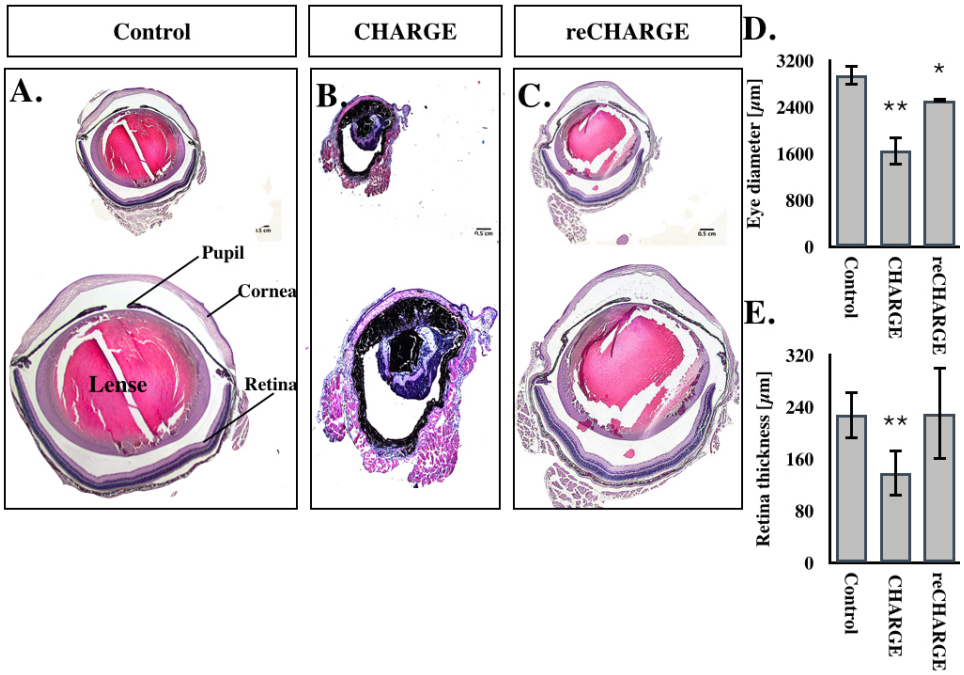

Figure 22: **reCHARGE eyes are smaller but structural unremarkable.** A to C: The ten week old Control (CMV Cre-), CHARGE (CMVCre;CHD7$^{+/fl}$) and reCHARGE (CMVCre;CHD7$^{+/fl}$;EZH2$^{+/fl}$) mice were stained with Hematoxylin and eosin stain. D: Eye diameter was measured with a scale tool of ImageJ; n=3 Control, n=12 CHARGE and n=6 reCHARGE mouse eyes, p=0.0038 Control vs CHARGE mouse eye, p=0.011 Control vs reCHARGE eye. E: Retina thickness was measured with a scale tool of ImageJ; n=3 Control, n=12 CHARGE and n=6 reCHARGE mouse eyes, p=0.0038 Control vs CHARGE mouse eye retina, Control vs reCHARGE eye retina n.s. Statistics were done with a students t-test.

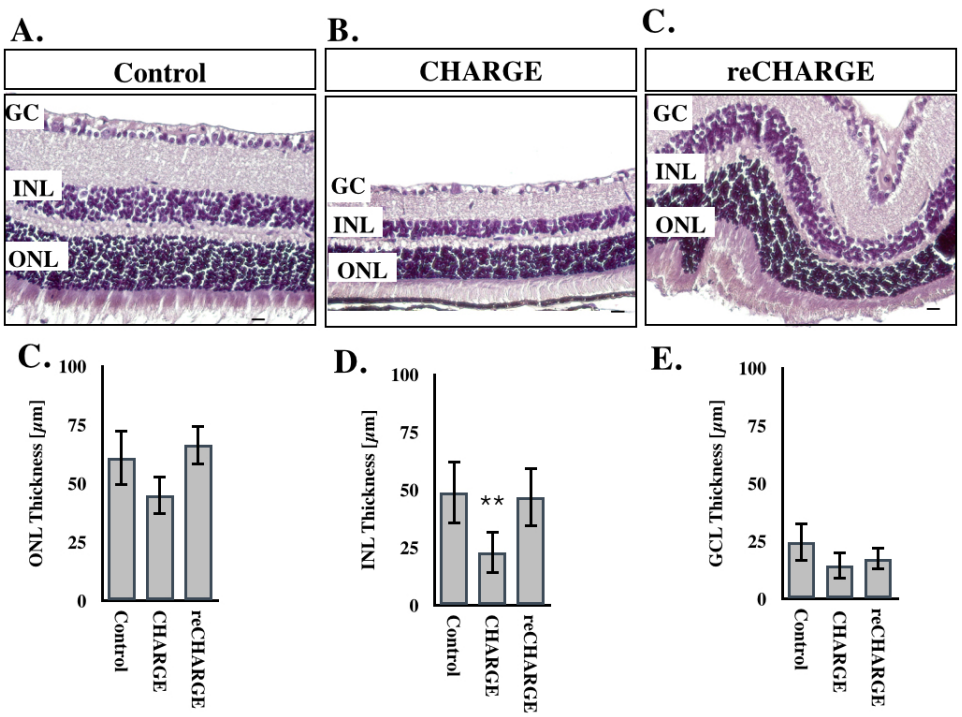

Figure 23: **reCHARGE retina corresponds to Control mouse retina** A to C: The ten week old Control (CMV Cre-), CHARGE (CMVCre;CHD7$^{+/fl}$), reCHARGE (CMVCre;CHD7$^{+/fl}$;EZH2$^{+/fl}$) mice were stained with Hematoxylin and eosin stain and pictures were taken with a 10x objective. C: Graph showing the measured outer nuclear layer (ONL) thickness in μm for Control, CHARGE and reCHARE mouse; n=6 Control, n=12 CHARGE and n=6 reCHARGE mouse eyes, n.s. D: Graph showing the measured inner nuclear layer (INL) thickness in μm for Control, CHARGE and reCHARE mouse; n=6 Control, n=12 CHARGE and n=6 reCHARGE mouse eyes, p=0.0096 Control vs. CHARGE, Control vs reCHARGE n.s. E: Graph showing the measured granular cell layer (GCL) thickness in μm for Control, CHARGE and reCHARE mouse; n=6 Control, n=12 CHARGE and n=6 reCHARGE mouse eyes, Control vs. CHARGE n.s, Control vs. reCHARGE n.s. More then 3 slices per eye were considered. Statistics were done with a students t-test.

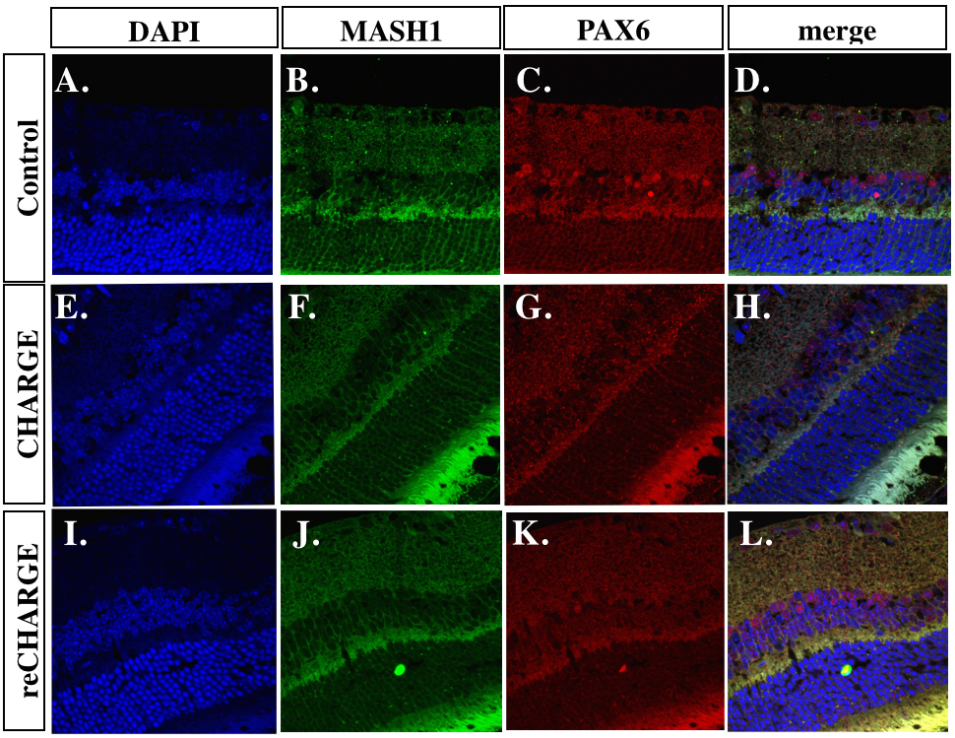

Figure 24: **reCHARGE retina has less PAX6 positive cells but not ectopic MASH1 expression.** The ten week old Control (CMV Cre-), CHARGE (CMVCre;CHD7$^{+/fl}$) and reCHARGE (CMVCre;CHD7$^{+/fl}$;EZH2$^{+/fl}$) mouse retinas were stained for MASH1 (white arrows) and PAX6. Pictures were taken with a confocal microscope LSM780 (Zeiss).

in some individuals than in others. The inner nuclear layer corresponded to the thickness of the Control mice retina and did not show a significant reduction as the analyzed CHARGE retina did.

2.2.2 Cerebellum in CHARGE vs reCharge Mouse

Correlating to the obtained results for the CHARGE mouse cerebellum, the overall structure of the reCHARGE cerebellum was analyzed. The cerebellum tissue was from an apical point of view around 4 mm in size, and the V and VI lobi was visible (Fig. 25A, B, D, E, G, and H).

A heterozygous double knock-out of *chd7* and *ezh2* (CMVCre;CHD7$^{+/fl}$;EZH2$^{+/fl}$) had in contrast to the CHARGE mouse no abnormalities in the cerebella anterior lobe. Corresponding to the Control cerebellum, the lobi III to X of the reCHARGE brain are clearly visible (Fig. 25I).

The purkinje cell layer which was under CHD7 deficiency found to be disorganized, was analyzed in the reCHARGE mouse (CMVCre;CHD7$^{+/fl}$;EZH2$^{+/fl}$). Calbindin stainings of Control, CHARGE and reCHARGE mouse cerebellum were used to analyze the cell distribution of the Purkinje cell layer (Fig. 26A to C).

The cell bodies of neighboring purkinje cells were counted considering two and three neighboring cells as normal, and thus displaying only three or more neighboring cells. The values measured for the reCHARGE condition corresponded to the values measured for the Control litter mates (Fig. 26D).

Further, the purkinje cell body size was quantified by measuring Calbindin stained cells. In comparison to the cell sizes quantified for the Control animals, CHARGE purkinje cells were not significantly smaller. However, the cell size of purkinje cells grown under reCHARGE conditions were significantly bigger than the cell bodies quantified for CHARGE mice (Fig. 26E).

Corresponding to the results obtained in CHARGE mouse cerebellum, visible primary branches of purkinje cells were quantified. The significantly reduced amount of purkinje cells with a primary branch found in CHARGE mouse were not visible in the reCHARGE mouse. The amount of purkinje cells with a visible primary branch of the heterozygous double knock-out corresponded to the Control values (Fig. 26F).

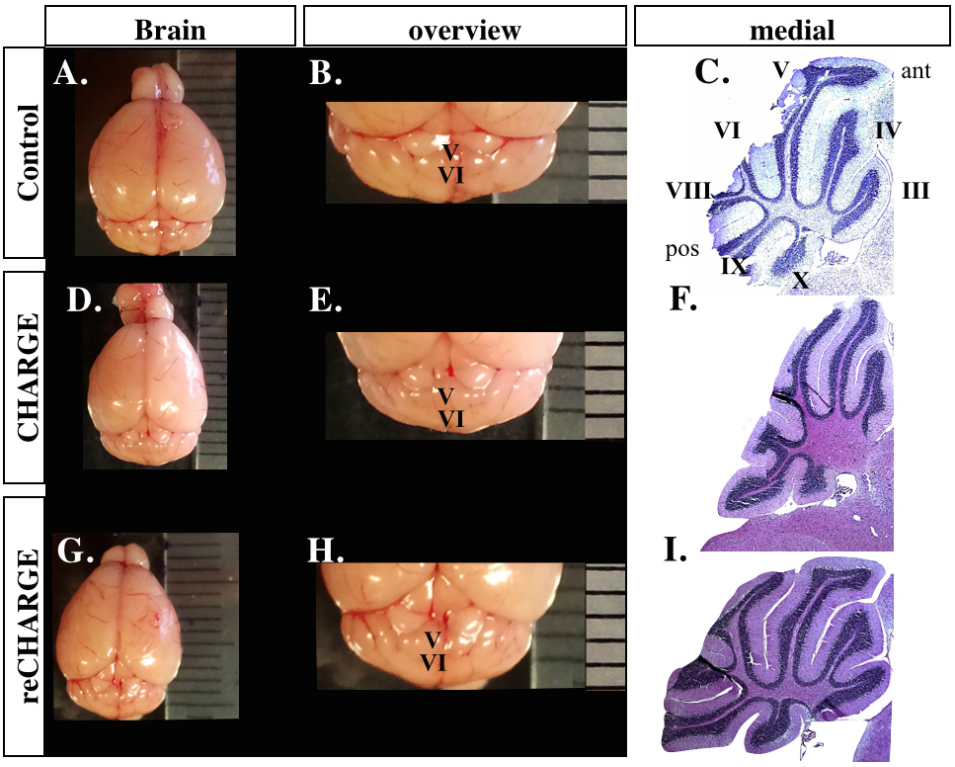

Figure 25: **reCHARGE cerebellum displays no anterior lobe defect** A, D and G: Photograph of the brain of ten week old Control (CMV Cre-), CHARGE (CMVCre;CHD7$^{+/fl}$) and reCHARGE (CMVCre;CHD7$^{+/fl}$;EZH2$^{+/fl}$) mouse. Brains were placed next to a scale directly after dissection. B, E and H: Zoomed picture of the cerebellum marked at V and VI lobe. The scale is indicated on the right [mm]. C, F and I: Nissl staining of the medial cerebellum. Roman numbers indicate the lobi. Ant = anterior, pos = posterior.

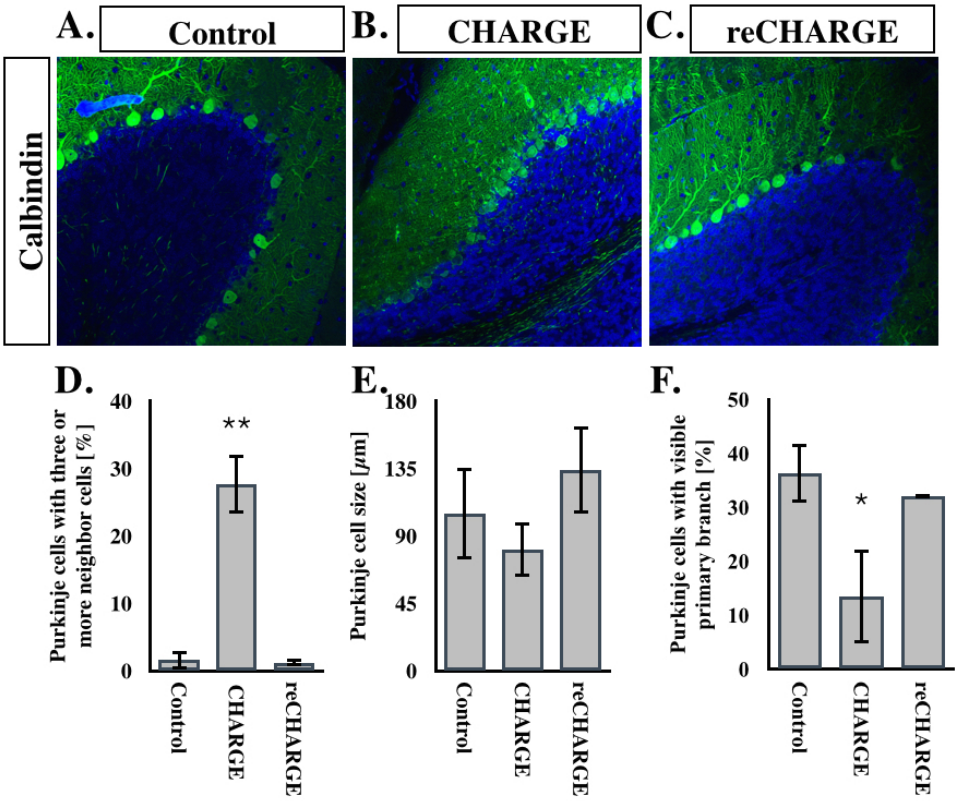

Figure 26: **reCHARGE purkinje cell layer is unremarkable.** The ten week old Control (CMV Cre-), CHARGE (CMVCre;CHD7$^{+/fl}$) A to C: Stained brain slices of the ten week old Control (CMV Cre-) and CHARGE (CMVCre;CHD7$^{+/fl}$) mice cerebellum were stained for Calbindin and DAPI, pictures were taken with a confocal microscope LSM780 (Zeiss). D: Neighboring cells of each purkinje cell were measured; n=347 Control and n=408 CHARGE mouse cells, p=0.0107 Control vs. CHARGE, Control vs reCHARGE n.s. E: Quantification of Purkinje cell-body size in Control and CHARGE mouse. Cell-body sizes were measured using a scale tool of ImageJ; n=33 Control and 37 CHARGE mouse cells, Control vs. CHARGE n.s., Control vs reCHARGE n.s. F: Purkinje cells with visible primary branches were manually quantified; n=141 Control and n=230 CHARGE mouse cells. N-values represent cell numbers counted from different brain slices. Control Purkinje cells n=392, CHARGE purkinje cells n=779, reCHARGE purkinje cells n=324, of three animals per genotype, p=0.0344 Control vs. CHARGE, Control vs. reCHARGE n.s. Several stainings of three mice per genotype were quantified. Statistics were done with a students t-test.

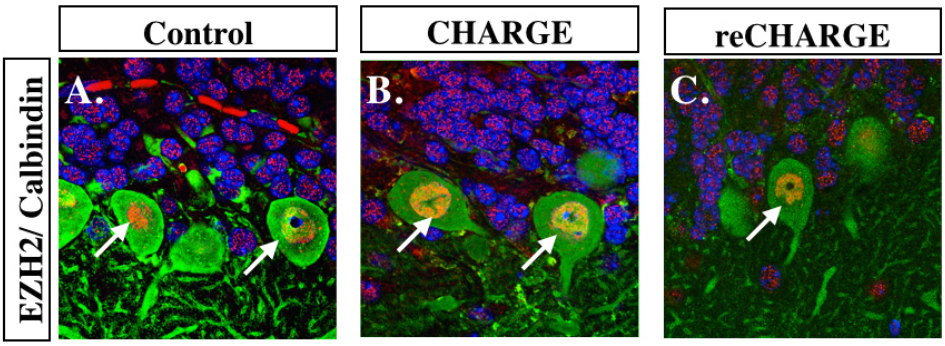

Figure 27: **reCHARGE purkinje cells have a EZH2 signal** A to C: Stained cerebellum brain slices of Control (CMV Cre-), CHARGE (CMVCre;CHD7$^{+/fl}$) and reCHARGE (CMVCre;CHD7$^{+/fl}$;EZH2$^{+/fl}$) mice were stained for Calbindin, EZH2 and DAPI. Z-stacks were taken with an 100x objective of a laser microscope (LSM780, Zeiss).

The EZH2 expression of purkinje cells was likewise analyzed in the reCHARGE mouse. The EZH2 signal is visible in the purkinje cell nucleus (Fig. 27A to C).

2.2.3 Neural Stem Cells in CHARGE vs reCharge Mouse DG

Pervious data showed already a reduction of BrdU and nestin positive cells in the CHARGE mouse dentate gyrus. Thus, these markers were also investigated in the reCHARGE mouse dentate gyrus.

BrdU and Nestin positive cells were analyzed after 5 consecutive days of BrdU treatment. Control (CMV Cre-), CHARGE (CMVCre;CHD7$^{+/fl}$) and reCHARGE mouse (CMVCre;CHD7$^{+/fl}$;EZH2$^{+/fl}$) were stained for BrdU and Nestin (Fig. 28 A to C and zoomed pictures D to F). BrdU and Nestin positive cells were quantified together. A reduction of BrdU and nestin positive cells could be observed in the CHARGE dentate gyrus, while the amount of BrdU and nestin positive cells quantified in the reCHARGE dentate gyrus correlated to values measured for the Control litter mates (Fig. 28G).

2.3 Summary of CHARGE and reCHARGE Mouse

A novel CHARGE mouse line (CMVCre;CHD7$^{+/fl}$) was generated, and analyzed. The olfactory lobes were smaller and expressed less doublecortin, a marker for newborn neurons. CHARGE mice weight significantly less

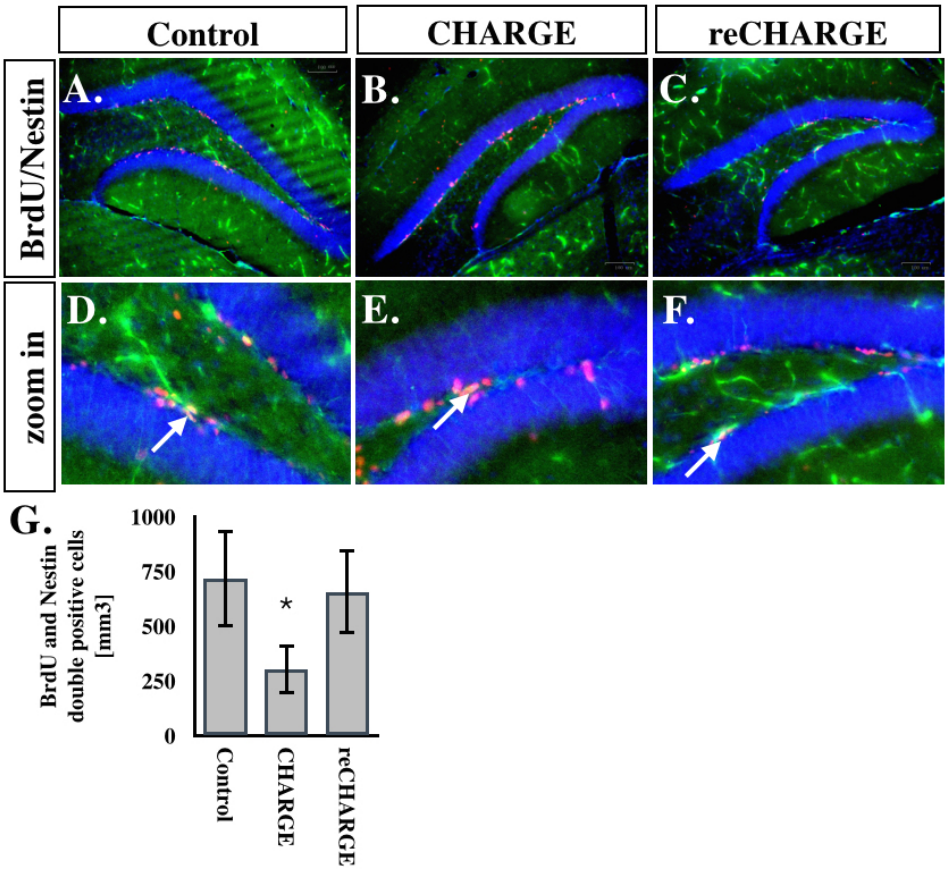

Figure 28: **reCHARGE mice display no stem and label retaining cell defect** The ten week old Control (CMV Cre-), CHARGE (CMVCre;CHD7$^{+/fl}$) and reCHARGE (CMVCre;CHD7$^{+/fl}$;EZH2$^{+/fl}$) mice were treated with BrdU for 5 days and dentate gyrus were stained. A to C: Immunofluorescence picture of BrdU, Nestin and DAPI in Control, CHARGE and reCHARGE dentate gyrus (overlay). Pictures were taken using a confocal laser microscope (LSM780, Zeiss). D to F: Zoom-in pictures showing cells with BrdU and Nestin overlay signal (white arrow). G: Double positive cells were counted manually for each mouse genotype; n=7 Control, n=3 CHARGE and n=3 reCHARGE animals, p=0.0326 Control vs. CHARGE, Control vs. reCHARGE n.s. Four brain slices were count per animal. Statistics were done with a students t-test.

than their Control litter mates, and the most severely affected CHARGE mice had a reduced brain-to-body ratio.

An open field test revealed that CHARGE mice run faster and travel further.

Besides that, the eye phenotype of CHARGE mice showed a heterogeneity between the left and the right eye. Ranging from only rudimentary developed to smaller eyes, the variation within the CHARGE group was quite high. The data showed that less severe affected eyes grown under CHARGE conditions are smaller and have a reduced retina thickness. An analysis of the retina cell layers revealed that the inner nuclear cell layer was thinner in CHARGE mice retinas, than the retinas quantified of their Control litter mates.

The anterior lobe of the cerebellum was underdeveloped under CHARGE conditions and the purkinje cell layer was disrupted. Purkinje cells were measured with regard to their number of neighboring cells, cell body size and the mount of cells with visible primary branches. In the CHARGE cerebellum over 25% of the cells had three or more neighboring cells, while the Control displayed less than 5% of cells with more than three neighboring cells. Also, the amount of purkinje cells with a visible primary branch were significantly reduced in CHARGE mice compared to Control litter mates.

Another small analysis revealed an EZH2 expression in the nucleus of purkinje cells while the protein level of EZH2 and H3K27me3 was not changed in the CHARGE mouse cerebellum.

A genetic rescue of the CHARGE mouse (CMVCre;CHD7$^{+/fl}$) was generated (CMVCre;CHD7$^{+/fl}$;EZH2$^{+/fl}$) and analyzed. This heterozygous double knock-out was confirmed via qPCR, and illustrated by stainings. Mice carrying both heterozygous mutations of *chd7* and *ezh2* showed no alterations in body weight, or brain-to-body ratio. The eyes were unremarkable even though an analysis revealed that the overall eye size was still smaller than measured Control values. Unlike the CHARGE retina the reCHARGE retina thickness corresponded to the Control values. H & E stainings of the reCHARGE retina revealed a wavy structure and unlike the CHARGE mouse retina no retina layer was significantly altered in comparison to retina layers measured for Control litter mates. Furthermore, the ectopic MASH1 expression of the CHARGE mouse retina could not be observed in the reCHARGE mouse retina.

Under reCHARGE conditions no structural damage of the cerebella anterior lobe could be found. Purkinje cells were bigger than CHARGE

purkinje cell bodies, but still within an average range measured for Control mice. Unlike the CHARGE mouse cerebellum, purkinje cells of the reCHARGE cerebellum had three or more neighboring cells as often as they were counted in the Control litter mates, and purkinje cells with primary branches were quantified as often as they were quantified under wildtype conditions.

A RNA sequencing of the cerebellum tissue of Control, CHARGE and reCHARGE mice showed striking similarities between Control and reCHARGE litter mates. Especially, some under CHARGE conditions downregulated genes were rescued efficiently in reCHARGE mice.

Furthermore, neural stem cells of the dentate gyrus grown under reCHARGE conditions showed no significant difference in correlation to cells quantified for Control mice (BrdU and nestin positive cells).

Taken together, the reCHARGE condition represents a partial rescue of the CHARGE mouse phenotype.

2.4 Inducible homozygous Knock-out of *chd7* and *ezh2*

A previous study reported that neural stem cells were altered under CHD7 deficiency. A homozygous, inducible *chd7* knock-out (NesCreERT2;CHD7$^{fl/fl}$) displayed a decreased amount of stem and label retaining cells (BrdU) in the dentate gyrus. These mice displayed furthermore more cell proliferation (Ki67) in the subgranular zone of the dentate gyrus (Feng, W. et al. 2013).

Since the results obtained for the reCHARGE mouse dentate gyrus stem cells showed a rescue, cells carrying a *chd7* and *ezh2* knock-out were further investigated. A nestin promoter was coupled to an inducible Cre recombinase to enable a time dependent homozygous knock-out in the neural stem cells of the adult dentate gyrus. An unconditional homozygous knock-out of either *chd7* or *ezh2* alone is lethal, thus both floxed genes were coupled to an inducible nestin promotor, using the ERT2 system (NesCreERT2). which made the stem cell knock-out inducible by the injection with Tamoxifen. A homozygous double knock-out of *chd7* and *ezh2* was generated (NesCreERT2;CHD7$^{fl/fl}$;EZH2$^{fl/fl}$, interchangeably called double knock-out), analyzed and the results are presented in the following.

2.4.1 The double Knock-out has no Defect in Stem and Label-Retaining Cells of the Dentate Gyrus

As a marker for stem cells, and the promotor guiding the knock-out of *chd7* and *ezh2* in the homozygous double knock-out, the amount of nestin expressing cells were analyzed (Fig. 29).

The ten week old mice were injected on five following days with tamoxifen to induce the knock-out, and after another two, four or six weeks respectively the mice were sacrificed (Fig. 29A). The hippocampal dentate gyrus was analyzed (Fig. 29B). Control (NesCre-) and double knock-out (NesCreERT2;CHD7$^{fl/fl}$;EZH2$^{fl/fl}$) dentate gyrus were stained for nestin (Fig. 32C and D). The nestin positive cells were manually counted in a blind study. Two weeks after the knock-out induction with tamoxifen, the double knock-out had significantly less nestin positive cells. After four and six weeks however, the amount of nestin positive cells was not significantly different to the amount of nestin positive cells counted for the Control litter mates (Fig. 32E).

To further investigate the stem cells in the double knock-out (NesCreERT2;CHD7$^{fl/fl}$;EZH2$^{fl/fl}$), cells were labeled with BrdU and analyzed according to a previous study. In this study a NesCreERT2;CHD7$^{fl/fl}$ mouse line displayed a defect in the BrdU positive cells. Interestingly, this

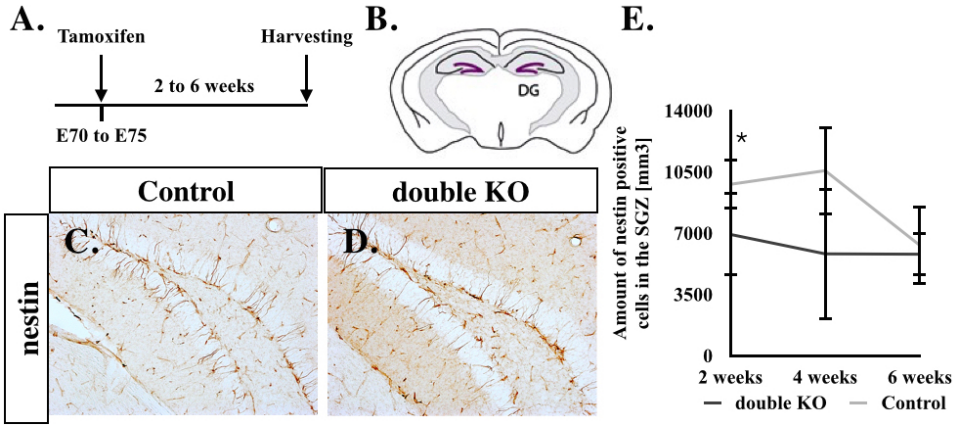

Figure 29: **The amount of nestin positive cells in the double knock-out corresponds to Control values.** A: The ten week old Control (NesCre-) and double knock-out (NesCreERT2;CHD7$^{fl/fl}$;EZH2$^{fl/fl}$) were treated with Tamoxifen for 5 days and after another two to six weeks sacrificed, brains were stained. B: A scheme of the coronally cut mouse brain showing the dentate gyrus. C and D: Example histology pictures stained with Nestin. E: The quantification of nestin positive cells was done manually and 4 to 6 dentate gyrus pictures were count per animal. The time points 2 weeks, 4 weeks and 6 weeks indicate the time after the knock-out induction; n=5 at two weeks, n=5 at four weeks, n=7 at 6 weeks were analyzed for the Control mouse line, and n=4 at two weeks, n=5 at four weeks, n=12 at six weeks were analyzed for the double knock-out. P=0.033 Control vs. double knock-out, two weeks after knock-out induction, other time points n.s. Four brain sections were counted per mouse. Statistical analysis t-test (sigma plot). Statistics were done with a students t-test.

defect could be overcome through voluntary running (Feng et al., 2013).

In brief, the 10 week old mice (NesCreERT2;CHD7$^{fl/fl}$;EZH2$^{fl/fl}$) were injected 5 consecutive days with tamoxifen. After another two weeks, the mice were placed into a running cages and injected with BrdU for twelve days. The following three weeks the running experiment continued after which the mice were sacrificed (Fig. 30A). The hippocampal dentate gyrus was stained and analyzed (Fig. 30B). Z-stacks were taken and the BrdU positive cells in the granular layer were manually counted in a blind study (Fig. 30C to J).

Regarding the amount of BrdU positive cells, a difference could be seen only in running vs. non-running animals. Unlike the *chd7* single knock-out, the double knock-out did not show any significant difference in the amount of neural stem cells between Control and mutant mice (Fig. 30K).

In this context, the position of the BrdU labeled neural stem cells was analyzed. Dividing the granular layer of the dentate gyrus into subgranular layer, middle and upper granular layer the distribution of cells was analyzed, but no significant change could be observed (supplement data Fig. 57).

Taken together, the analyzed stem cells expressing nestin and cells labeled with BrdU showed no difference between the Control and the double knock-out (NesCreERT2;CHD7$^{fl/fl}$;EZH2$^{fl/fl}$).

2.4.2 The double Knock-out has no Proliferation Defect in the Dentate Gyrus

A previous study showed an increased proliferation in the granular zone of the dentate gyrus in a NesCreERT2;CHD7$^{fl/fl}$ mouse line (Feng et al., 2013, supplement Fig. 45). Therefore, the proliferation of the homozygous double knock-out (NesCreERT2;CHD7$^{fl/fl}$;EZH2$^{fl/fl}$) was tested under comparable conditions.

A proliferation marker used in this study was Ki67. This marker overlays with bot CHD7 and EZH2 in the nucleus of neural stem cells (Fig. 31A to J).
For this analysis 10 week old mice were injected with tamoxifen on 5 constitutive days. After another six weeks the mice were analyzed (Fig. 31K). The hippocampal dentate gyrus was stained for Ki67, and the positive cells were count manually in a blind study (Fig. 31L, M and N).

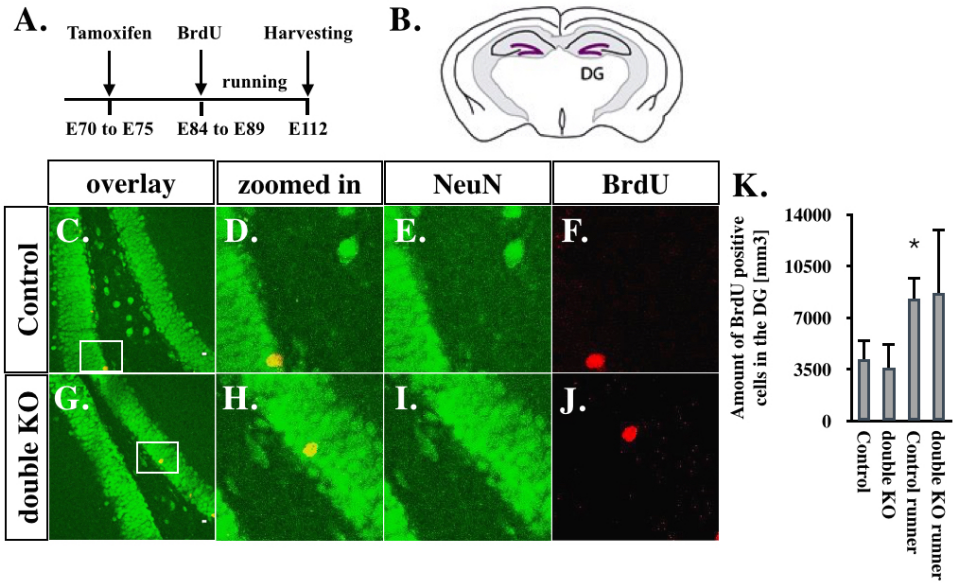

Figure 30: **The amount of BrdU labeled cells in the double knock-out corresponds to Control values.** A: Timing of the running experiment. The ten week old Control (NesCre-) and double knock-out (NesCreERT2;CHD7$^{fl/fl}$;EZH2$^{fl/fl}$) mice were treated for 5 days with tamoxifen and began after two more weeks the running experiment in which they were treated with BrdU for twelve days and sacrificed after 4 weeks in running cages. B: A scheme of the coronally cut mouse brain showing the dentate gyrus. C to J: Section of the dentate gyrus were stained with NeuN and BrdU. D: The quantification of BrdU positive cells was done manually and 4 to 6 dentate gyrus pictures were count per animal; n=5 Control mice, n=6 double knock-out mice, n=5 Control mice in running experiment, and n=7 double knock-out mice were analyzed in the running experiment. P=0.044 between Control group and Control group in running Control group. Statistics were done with a students t-test.

The Ki67 positive cells showed in contrast to the single knock-out of *chd7* no difference between Control and double knock-out (Fig. 31O).

2.4.3 The double Knock-out displays a normal Amount of Newborn Neurons in the Dentate Gyrus

Previous data suggested that an *ezh2* knock-out (NesCreERT2;EZH2$^{fl/fl}$) might affect the number and positioning of immature neurons (data shown in supplement Fig. 44, doublecortin, MCM2, Li, Y.). The homozygous *ezh2* mutant started with more new-born neurons (Doublecortin) than their Control litter mates 2 weeks after the knock-out induction, and showed less new-born neurons after 12 weeks.

This observation suggested an analysis of doublecortin positive cells in the double knock-out (NesCreERT2;CHD7$^{fl/fl}$;EZH2$^{fl/fl}$). For this study, ten week old mice were treated with Tamoxifen to induce the knock-out and analyzed 2 to 6 weeks later (Fig. 32A).

Coronal brain sections of the hippocampal dentate gyrus were histologically stained and analyzed (Fig. 32B, C and D).

In a blind analysis, the doublecortin positive cells were counted manually. Only two weeks after the induction of the double knock-out, the amount of doublecortin positive cells was measured higher in the Control animals. At later time points the difference was not significant. The amount of new-born neurons of the double knock-out mice never exceeded the cell numbers measured under Control conditions. Both cell populations decrease equally over time (Fig. 32E).

Because of the seemingly altered distribution of doublecortin cells in the *ezh2* single knock-out (supplement Fig. 44), the cell distribution of newborn neurons was also analyzed for the double knock-out of *chd7* and *ezh2* (NesCreERT2;CHD7$^{fl/fl}$;EZH2$^{fl/fl}$). Furthermore, the dendritic length and the orientation of doublecortin positive cells in the dentate gyrus was measured, but none of the analyzed parameters were significantly changed in the double knock-out compared to the cells grown under Control conditions (Fig. 58, 59, 60, 61 in the supplement).

Similar to the doublecortin phenotype a single knock-out of *ezh2* (NesCreERT2;EZH2$^{fl/fl}$) seemed to posses first more and then less MCM2 positive cells than the Control mice (supplement Fig. 44, NestinCreERT2 EZH2$^{fl/fl}$, Li, Y.). Two and four weeks after the knock-out induction new-

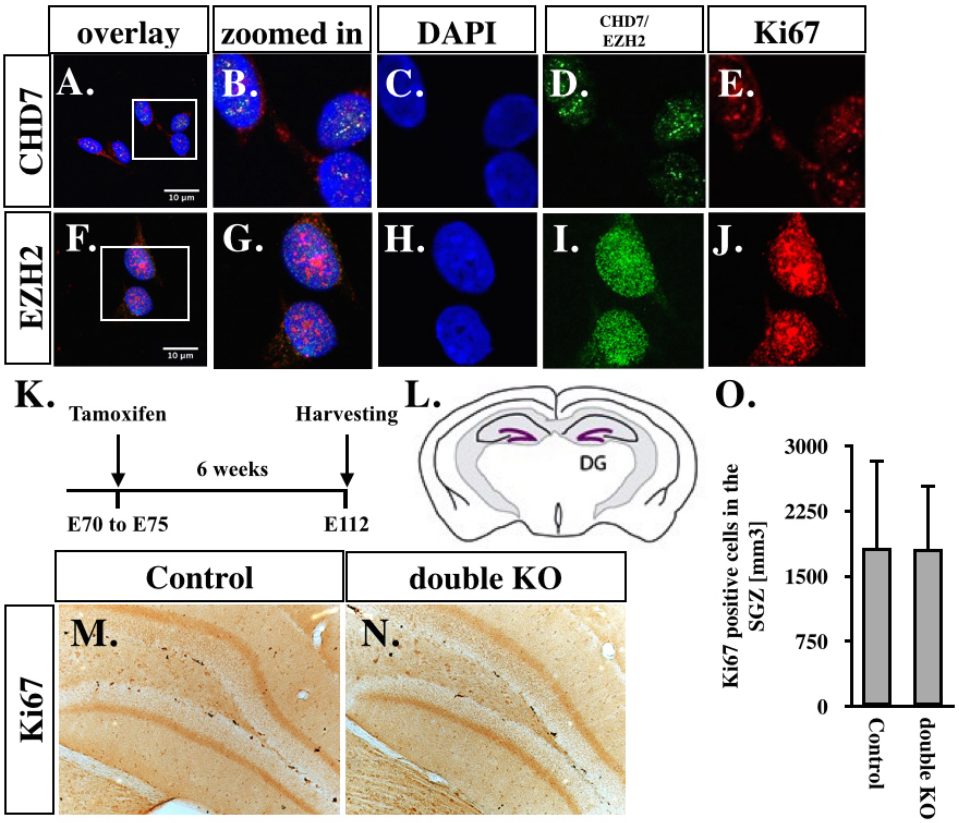

Figure 31: **The double knock-out shows no increase in proliferation** Control (NesCre-) and double knock-out (NesCreERT2;CHD7$^{fl/fl}$;EZH2$^{fl/fl}$). A to J: Neural stem cells stained with Ki67, DAPI and either CHD7 or EZH2. K: Timing of the running experiment. The ten week old mice were treated for 5 days with tamoxifen and were sacrificed six weeks later. L: A scheme of the coronally cut mouse brain showing the dentate gyrus. M and N: Example histology stainings of Ki67 in Control and double knock-out mice. O: Manual quantification of the Ki67 positive cells in the dentate gyrus; n=11 mice per genotype, four brain sections were counted per mouse (n.s.). Statistics were done with a students t-test.

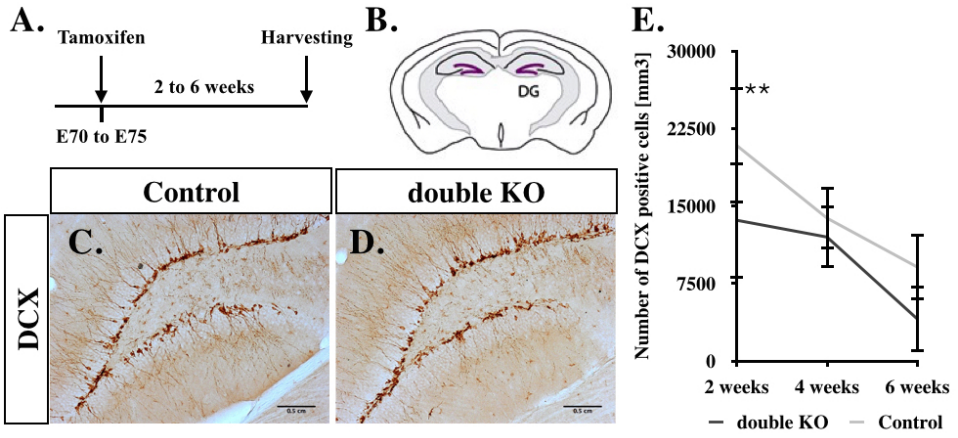

Figure 32: **The amount of newborn neurons correlates with the amount measure in Control mice (NesCre- and NesCreERT2;CHD7$^{fl/fl}$;EZH2$^{fl/fl}$).** A: The ten week old litter mates were treated with Tamoxifen for 5 days and after another two to six weeks sacrificed, and stained. B: A scheme of the coronally cut mouse brain showing the dentate gyrus. C and D: Slices of the dentate gyrus were stained histologically for doublecortin. E: The quantification of doublecortin positive cells was done manually and 4 to 6 dentate gyrus pictures were count per animal. The time points 2 weeks, 4 weeks and 6 weeks indicate the time after the knock-out induction. Animal numbers are mentioned as n-values: n=6 at 2 weeks, n=8 at 4 weeks, n=9 at 6 weeks were analyzed for the Control mouse line, and n=5 at 2 weeks, n=3 at 4 weeks, n=11 at 6 weeks were analyzed for the double knock-out mouse line. P=0.0096 Control vs. Mutant two weeks after knock-out induction. Other time points n.s. Statistics were done with a students t-test.

born neurons expressing MCM2 were first higher in the homozygous *ezh2* knock-out and then lower 8 weeks and 12 weeks after the induction.

Thus, the amount of MCM2 positive cells were quantified in the double knock-out (NesCreERT2;CHD7$^{fl/fl}$;EZH2$^{fl/fl}$). The ten week old mice were treated with tamoxifen and sacrificed after one to six weeks (Fig. 33, A).
Coronal brain slices of the hippocampal dentate gyrus were stained for MCM2 and positive cells were counted manually (Fig. 33B, C and D).

Two weeks after the knock-out induction with tamoxifen the Control mice displayed significantly more MCM2 positive cells. Similarly four weeks after the tamoxifen injections the Control mice showed more MCM2 positive cells. However, this difference was not visible six weeks after the knock-out induction. In the homozygous double knock-out the amount of MCM2 positive cells never exceeded the amount measured in the Control mice (Fig. 33, graph C).

2.5 Summary of the inducible *chd7* and *ezh2* Knock-out

The amount of nestin positive cells in the dentate gyrus of the double knock-out (NesCreERT2;CHD7$^{fl/fl}$;EZH2$^{fl/fl}$) was less two weeks after the knock-out induction, while it normalized four and six weeks after the induction to a non-significant amount, in comparison to the Control litter mates (NesCre-). Likewise the amount of BrdU positive cells in a running experiment analyzed in total six weeks after the knock-out induction, was not significantly different from their Control litter mates.

The amount of Ki67 positive cells, a marker for proliferation was in contrast to a *chd7* single knock-out also not altered, in total six weeks after the knock-out induction.

Cells positive for doublecortin and MCM2, two markers for newborn neurons displayed a significant reduction only two weeks after the knock-out induction while the amount of positive cells normalized six weeks after the tamoxifen injections.

Taken together, the double knock-out showed significantly less nestin, doublecortin and MCM2 positive cells two weeks after the knock-out induction while the amount of nestin, doublecortin, MCM2, Ki67 and BrdU positive cells showed no difference between the Control and the double knock-out six weeks after the knock-out induction.

These results show that important differences which were observed in

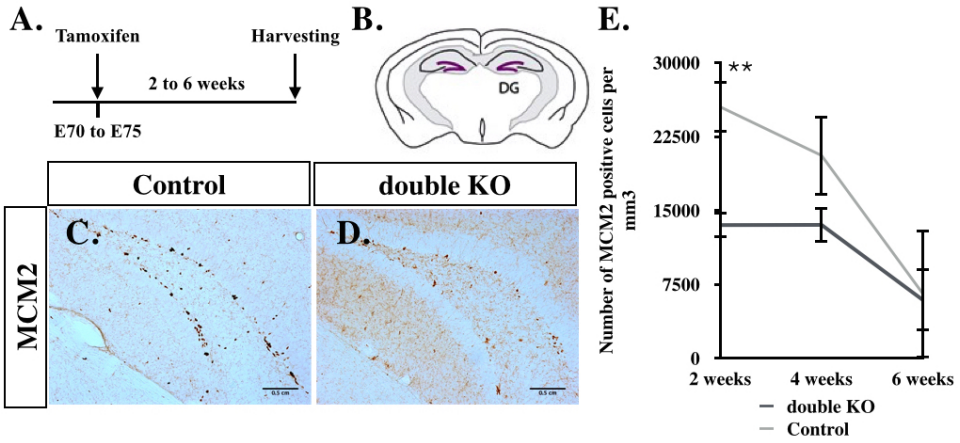

Figure 33: **The amount of early newborn neurons correlates with the amount measure in Control mice** Control (NesCre-) and double knock-out (NesCreERT2;CHD7$^{fl/fl}$;EZH2$^{fl/fl}$) A: The ten week old litter mates were treated with Tamoxifen for 5 days and after another two to six weeks sacrificed. B: A scheme of the coronally cut mouse brain showing the dentate gyrus. C and D: Slices of the dentate gyrus were histologically stained for MCM2. E: The quantification of MCM2 positive cells was done manually and 4 to 6 dentate gyrus pictures were count per animal. The time points 2 weeks, 4 weeks and 6 weeks indicate the time after the knock-out induction: n=5 at 2 weeks, n=5 at 4 weeks, n=6 at 6 weeks were analyzed for the Control mouse line, and n=6 at 2 weeks, n=4 at 4 weeks, n=12 at 6 weeks were analyzed for the double knock-out mouse line. Animal numbers are mentioned as n-values. P=0.0065 Control vs. Mutant two weeks after knock-out induction. Other time points n.s. Statistics were done with a students t-test.

the dentate gyrus stem cell population of a single knock-out of either *chd7* or *ezh2*, were not observed in the homozygous double knock-out of *chd7* and *ezh2* together. In contrast to the *chd7* single knock-out neither BrdU nor Ki67 were different in the double knock-out compared to the littermate Control mice. Also, a difference in the *ezh2* single knock-out namely the MCM2 and doublecortin positive cells shifting from more positive cells in the *ezh2* single knock-out to less cells over time, could not be observed in the double knock-out mice. The amount of new-born neurons was always less in the double knock-out than measured in the Control litter mates and normalized over time.

2.6 Treatment with the EZH2 Inhibitor GSK126

All the herein presented data supported the idea that EZH2 activity reduction could be beneficial for the CHARGE phenotype. This concept could in theory be extended to a novel treatment of CHARGE neural stem cells by inhibiting EZH2 activity. This is especially attractive because EZH2 can be inhibited with a very potent and selective inhibitor called GSK126, which is already tested in clinical trails as cancer treatment.

The question arose whether this inhibitor was potent in cells and *in vivo*, and if it could be used on neural stem cells with a CHD7 knock-down. Beyond that, could this non-permeable drug be a administered to the brain.

2.6.1 *In vitro* - CHD7 Knock-down Cells tolerate a Treatment with the EZH2 Inhibitor

The EZH2 inhibitor GSK126 is already part of several clinical anti-cancer trails and hence a major cytotoxic effect was not expected. It was determined how cells with a CHD7 knock-down reacted to an additional inhibitor treatment, and the resulting downregulation of EZH2 *in vitro*.

Thus, HEK293T cells with and without CHD7 knock-down were tested in combination with the EZH2 inhibitor GSK126. These knock-down cells were generated, sequenced and provided by W. Feng. The CHD7 knock-down could be confirmed via qPCR, and also the EZH2 expression was tested, but found to be unremarkable (Fig. 34A and B).

Next these cells were seeded with a density of 100.000 cells per dish, and incubated with either 0, 1 or 2 μM GSK126. After 72 h of incubation the cells were growing by optical means rather normal (Fig. 34C).

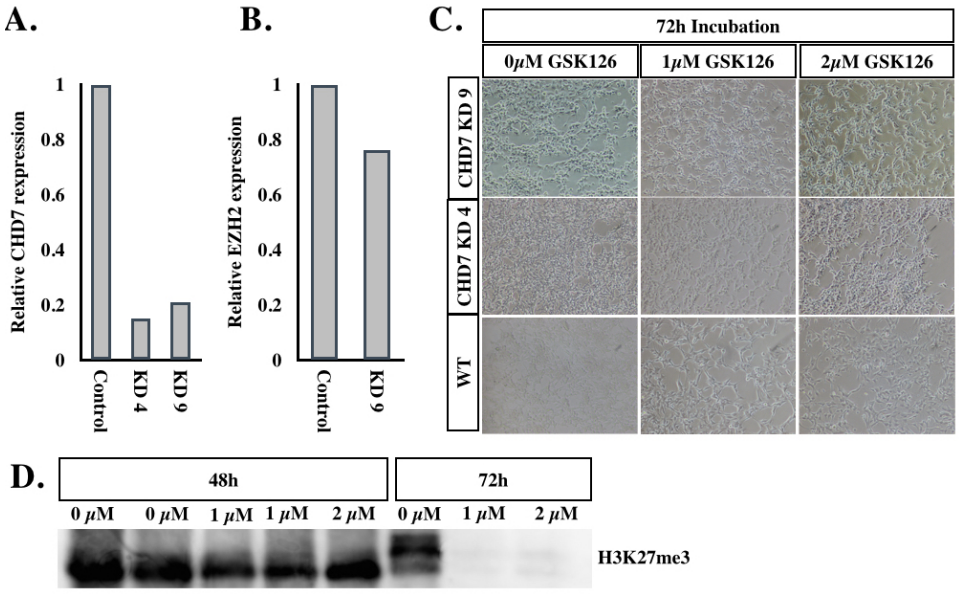

Figure 34: **The EZH2 inhibitor GSK126 is capable of sufficient H3K27me3 downregulation on CHD7 knock-down cells.** A and B: The RNA of HEK293T cells with CHD7 knock-down (provided by W. Feng) was isolated, the cDNA was prepared an a cybergreen qPCR for CHD7, EZH2 was run. C: HEK293T cells with a CHD7 knock-down were incubated with 0, 1 or 2 μM of the EZH2 inhibitor GSK126. Pictures were taken after 72 h incubation. D: Western blot for H3K27me3 (17 kDa) using the harvested HEK293T cells with *chd7* knock-down after 72 h of GSK126 incubation.

After the treatment with the EZH2 inhibitor, the cells were tested for a H3K27me3 reduction, since this would indicate a EZH2 inhibition. For both 1 and 2 μM a reduction of H3K27^3 could be observed (Fig. 34D).

Thus, CHD7 knock-down cells tolerate the EZH2 inhibitor and the inhibitor is sufficient for the downregulation of histone mark H3K27me3.

Here the results of the *in vitro* tests motivated a further *in vivo* analysis of the EZH2 inhibitor GSK126.

2.6.2 *In vivo* - the EZH2 Inhibitor can be Administered to the Brain an reduces H3K27me3 Protein Level

As mentioned before the EZH2 inhibitor GSK126 does not cross the blood-brain-barrier which excludes the possibility of an IV injection to treat neural stem cells or the brain. Hence another approach needed to be tested. To gain a constant infusion of the dentate gyrus stem cells with the

EZH2 inhibitor GSK126, an osmotic pump was surgically installed.

Used were eight week old NesCreERT2 CHD7$^{fl/fl}$ animals, and the knock-out was induced by 5 days of subsequent Tamoxifen injections. After four weeks the pump surgery was performed with Cre positive and Cre negative litter mates. Of both genotypes half of the animals got the EZH2 inhibitor and CldU and the other half got only CldU in physiological NaCl solution. The infusion took place over a period of 5 days and after another two days the mice got a single IdU or BrdU injection and were sacrificed (Fig. 35A).

The osmotic pump was fixed to the hippocampal dentate gyrus to target neural stem cells carrying a *chd7* knock-out with the EZH2 inhibitor (Fig. 35B).

A surgery procedure could be established in a way that seven mice survived the treatment. Unfortunately all of them were Control mice.

Nevertheless, the cut and stained left (not treated e.g. without GSK126) and right dentate gyrus (treated with GSK126 and CldU) of these Control mice could be analyzed after the treatment with the osmotic pump. The inhibitor was infused together with CldU and the pictures show a CldU signal only on the infused brain site (e.g. this site of the brain was connected to the pump). This suggests that the left dentate gyrus had no contact with the pump fluid through the thick brain tissue (Fig. 35C to H).

After the surgery the brain tissue of four mice was dissected, covering a narrow square of 2x2 mm around the pump infusion site and a respective square of the non-infused brain site as Control. Two of them were treated with the EZH2 inhibitor GSK126 (mouse 2 and 4), the other two were treated with NaCl (mouse 1 and 3). The tissue was prepared for western blot and blotted for H3K27me3. Here the tissue of the right dentate gyrus (treated) showed a weaker H3K27me3 level than the left dentate gyrus (not treated) of the same mouse indicating a working treatment with the EZH2 inhibitor GSK126 on the brain tissue of two mice (Fig. 35I).

This experiment shows that it is possible to treat the brain with the EZH2 inhibitor GSK126 *in vivo*, and that the medical infusion could be limited to at least one brain hemisphere.

2.7 Summary of a Treatment with the EZH2 Inhibitor GSK126

The EZH2 inhibitor GSK126 could sufficiently inhibit the EZH2 activity in CHD7 knock-down cells.

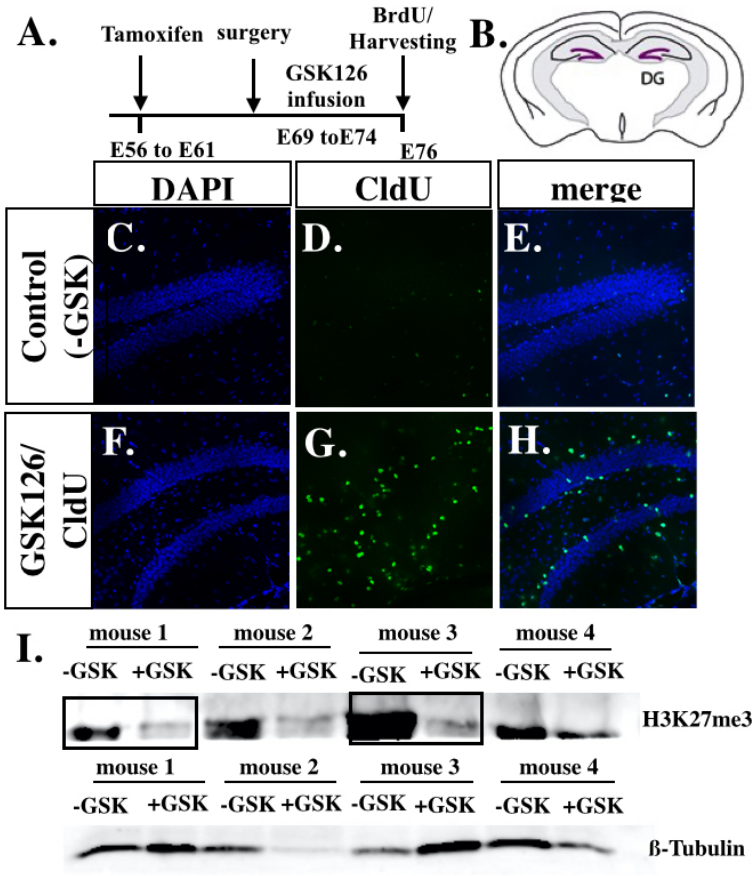

Figure 35: **The EZH2 inhibitor infusion is capable of reducing the H3K27me3 *in vivo*** A: Eight week old NesCreERT2;CHD7$^{fl/fl}$ mice were treated with tamoxifen for five consecutive days to induce the knock-out. After another four weeks the osmotic pump was placed by surgery and infused for five days constantly either GSK126 and CldU, or NaCl and CldU to Control and knock-out mice each. Bevor harvesting the mice, a single BrdU injection was given 2 hours before sacrificing the mice. B: Coronal brain section, the hippocampal dentate gyrus was targeted. C to H: The left and right dentate gyrus of the same animal was stained for CldU and DAPI. I: The tissue of the dentate gyrus was collected after the pump surgery infusion time, in a narrow square of 2x2 mm around the infusion site and non-infused brain site as a Control. The mice were infused with the EZH2 inhibitor GSK126 on the right site of the brain, while the left hemisphere remained untreated (-GSK and +GSK). Tissue of the left and right dentate gyrus of four mice was blotted agains H3K27me3 and beta-tubulin.

Different chemically altered versions of this Inhibitor were tested on HEK293T cells to determine the working concentration and on neural stem cells to analyze the efficient EZH2 inhibition by blotting H3K27me3.

A pump surgery procedure could be established and the treatment was sufficient to show a reduced H3K27me3 level in the brain tissue. The results suggested that the infused fluid does not reach the complete brain but is rather limited to a small area of the brain.

2.8 RNA Sequencing of CHD7$^{+/fl}$ and CHD7$^{+/fl}$EZH2$^{+/fl}$ Cerebellum Tissue

To further analyze the molecular alterations in the gene expression of CHD7 deficient brain tissue and tissue expressing genes under CHD7 and EZH2 loss, a RNA sequencing was performed. For this experiment the RNA expression of CMVCre;CHD7$^{+/fl}$ and CMVCre;CHD7$^{+/fl}$EZH2$^{+/fl}$ mice were compared to each other and to their control litter mates. Thus, the effect of a heterozygous CHD7 or heterozygous CHD7 and EZH2 expression on the RNA level of other genes in the cerebellum tissue was analyzed respectively.

For the RNA sequencing one half of the cerebellum was prepared and the RNA was isolated. The relative CHD7 and EZH2 expression of Control, CHARGE and reCHARGE mice cerebellum was tested by qPCR before the sequencing was performed and showed a downregulation of CHD7 for CHARGE and a downregulation of CHD7 and EZH2 for reCHARGE mice in comparison to the Control litter mates (Fig. 36A and B).

The RNA of the cerebellum tissue (which was previously analyzed by qPCR) was analyzed by RNA sequencing. The resulting data of significantly changed genes show diffenences between the mouse groups (Control, CHARGE and reCHARGE) which are depicted as heat map. The data indicates a clear difference between CHARGE and Control mice. The profiles of two reCHARGE mice seems similar to the control mice profile, while animal reChareg2 showed a heterogenouse gene expression (Fig. 36C).

Significantly downregulated processes of CHARGE vs. Control mice were analyzed and are shown as Processes and Benjamini p-values. In the context of the *chd7* knock out, especially long term memory, mRNA processing and regulation of neuronal plasticity seem remarkable (Fig. 36D).

In granular neuron progenitor cells of the cerebellum which carried a *chd7* knock-out (Fig. 46 from Feng et al., 2017, supplement), regulatory processes of neuronal plasticity were likewise affected. Further, the process of learning and memory was affected in granular neurons while a related process namely long term memory was significantly downregulated in the CHARGE tissue. Also, the ion transport was altered in both knock-outs - ion transport in granular progenitors and potassium ion transmembran transport under CHARGE condition.

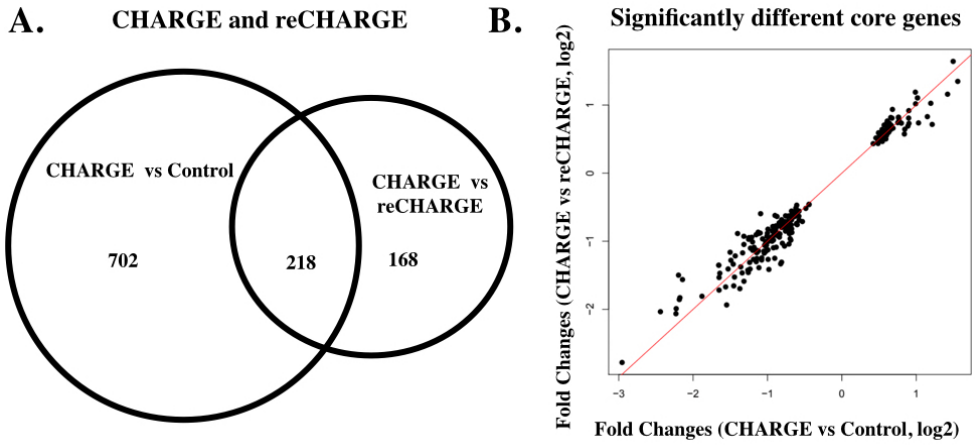

Figure 37: **RNA sequencing graphs of significant changed genes in CHARGE vs. Control and reCHARGE vs. Control** This graph was produced in team work with C. Shao.

The RNA sequencing data was analyzed in regard to the rescued genes observed for the reCHARGE condition in comparison to the CHARGE mouse gene expression (Fig. 37 and Fig. 38A). A comaprison the changed gene expression of core genes showed that under CHARGE conditions 702 genes were altered in relation to control conditions, while 168 genes were differently regulated in CHARGE versus reCHARGE conditions. Remarkably 218 genes were rescued from CHARGE to reCHARGE condition(Fig. 37A)). These altered core genes were either slightly up- or down regulated (Fig. 37B).

A volcano plot depicts significantly and not significantly changed genes. Especially intriguing are the depicted genes which are significantly changed but rescued under reCHARGE conditions in comparison to the measured CHARGE gene expression. The graph clearly shows that under reCHARGE conditions some up- and more downregulated genes of the CHARGE condition, are efficiently rescued (Fig. 38B).

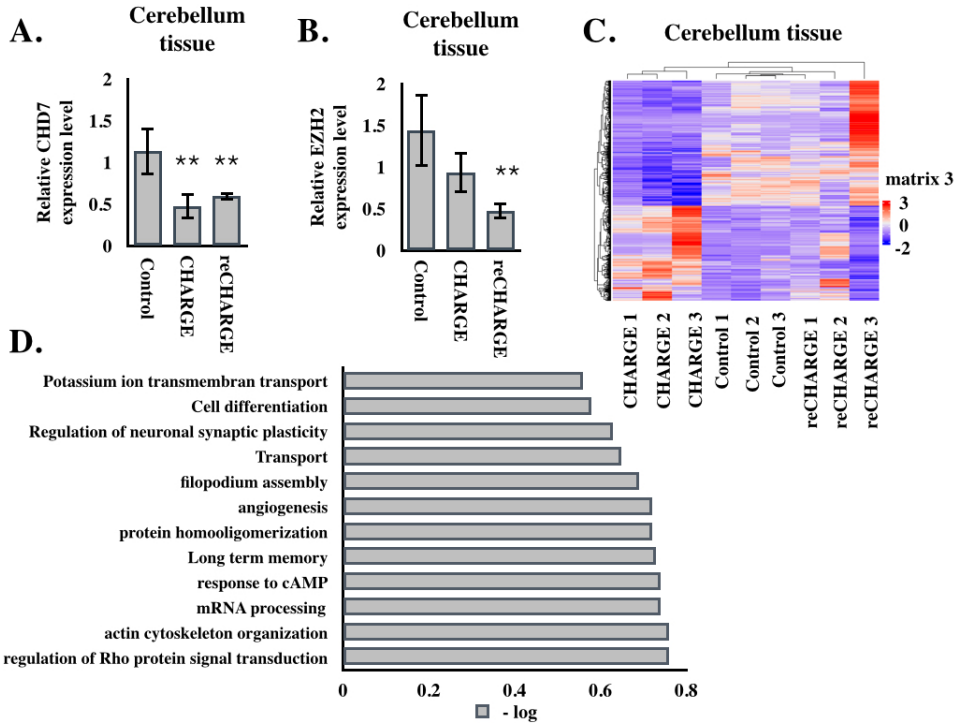

Figure 36: **The RNA profile of CHARGE mouse cerebellum differs to the expression of Control mouse cerebellum, while reCAHRGE mouse expression is more similar to the Control mouse expression.** The cerebellum of Control (CMV Cre-), CHARGE (CMVCre;CHD7$^{+/fl}$) and reCHARGE (CMVCre;CHD7$^{+/fl}$;EZH2$^{+/fl}$) mice were dissected and shock frozen into liquid nitrogen. A: The RNA of the cerebellum tissue was isolated and analyzed with qPCR for the CHD7 expression. Values were normalized to Actin and samples with working standard are shown; n=3 Control, n=4 CHARGE and n=4 reCHARGE mice, p=0.0096 Control vs. CHARGE, p=0.0055 Control vs. reCHARGE. C: Three mice per genotype were send for RNA sequencing. B: The RNA of the cerebellum tissue was isolated and analyzed with qPCR for the EZH2 expression. Values were normalized to Actin and samples with working standard are shown; n=3 Control, n=4 CHARGE and n=4 reCHARGE mice, Control vs. CHARGE n.s., p=0.0053 Control vs. reCHARGE. C: Three mice per genotype were send for RNA sequencing. Resulting heat map of the RNA sequencing showing the significantly changed genes for all three genotypes. This graph was produced by C. Shao. D: Significantly altered cellular processes between CHARGE mouse and Control are depicted. Statistics were done with a students t-test.

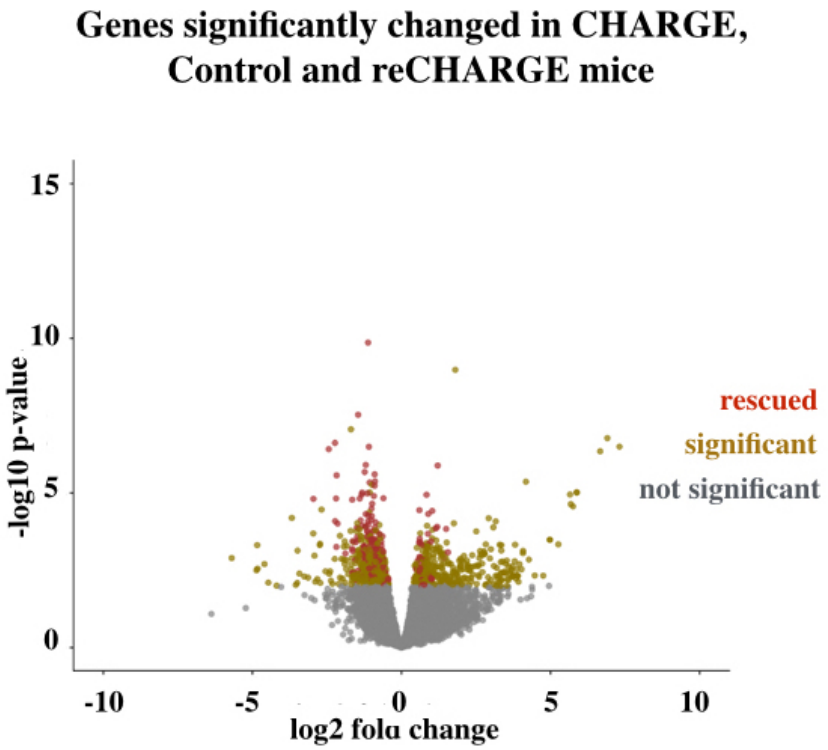

Figure 38: **reCHARGE rescues certain genes up- and downregulated under CHARGE conditions.** The volcano plot depicts the log2 fold change of genes of CHARGE and reCHARGE mouse cerebellum tissue. Efficiently rescued genes are depicted. This graph was produced by C. Shao.

3 Discussion

3.1 The CHARGE Mouse

A novel CHARGE mouse could be generated and analyzed. (CMVCre;CHD7$^{+/fl}$). Due to the CMV promotor which is capable of knocking-out genes already in the germ line and thus maybe deleting the floxed genes in planed future Control mice, only CMVCre and CHD7$^{fl/fl}$ mice were crossed.

The CHARGE mouse olfactory bulbs were smaller and structural different to the olfactory bulbs of their Control litter mates. Less doublecortin was expressed in this CHD7 deficient tissue, which corresponded to a previous analysis were less BrdU and doublecortin positive cells were found under CHD7 deficiency (Feng et al., 2013). A decreased amount of newborn neurons may claim a share in the poor olfactory bulb overall structure.

Since CHARGE syndrome results in a smaller body size, a total of 29 mice were weighed (Fig. 9). The adult male and female mice weighed significantly less than their Control litter mates. The brain-to-body ratio was in general not affected, only three severely affected mice displayed significantly reduced brain weights.

Already with these few experiments a variation in the phenotype of the CMVCre;CHD7$^{+/fl}$ mice was visible.

A high symptomatic variation has also been reported for human CHARGE patients and CHARGE syndrome has been described as a very heterogene disease consisting of several clinical features. One study analyzed CHARGE family cases and found a wide clinical variability (Jongmans et al., 2008). Furthermore, symptoms of CHARGE syndrome overly with other syndromes like Kubiki-syndrome (Schulz et al., 2014). And a inappropriate p53 activation during the development reassembled CHARGE features (van Nostrand et al., 2014). It was argued that the presence of genetic modifiers, the type of mutation in *chd7* as well as interactions with the environment could explain the difference in the phenotypic expression of CHARGE patients (Bosmann et al., 2005).

However, in mice bearing the same *chd7* mutation, having the same genetic background and experiencing the same surrounding, some of these variables can be excluded. The CMV promotor is active during embryonic development, but it is not fully understood at which embryonic day the knock-out happens. Already small differences in the knock-out induction can cause a difference in the later developing structures, may causing the observed variety in the symptoms.

Further, the CHARGE mice were easily distinguishable from the Control litter mates due to their striking behavior. Videos were recorded showing head shaking movements, tremble moving patterns and fast circle running. The so-called 'head bobbling' has been described before (Bosman et al., 2005) and also a hyperactive phenotype of CHARGE mice was reported (Ogier et al., 2014). To evaluate how fast the CHARGE mice were moving, an open field test was conducted. The resulting videos were analyzed by using ImageJ macros and showed a clear difference between Control and CHARGE mutant mice (Fig. 10).

These recorded moving patterns in the open field suggest that the CHD7 deficient mice do not avoid the center of the open field as much as the Control mice do, which might indicate a less fearful behavior (open field figure 10A and B). CHARGE mice run faster and travel farther than their Control litter mates (Fig. 10C and D).

However, the experiments were conducted in a mouse housing room, not excluding the vocalization of other mice which were not tested at the same time. The open field cage was sterilized after each mouse to eliminate the smell of other mice. For a professional open field experiment it is agreed that the experimenter should leave the room or at least hide behind a curtain to exclude a possible reaction of the running mice to the presence of the experimenter. Irrespective of these technical problems (which were the same for all mice tested), the obtained data shows a significant difference between CHARGE mouse and the Control litter mates.

Another bias of the behavior studies was the influence of blindness and a possible impaired inner ear in CHARGE mouse, which the Control mice do not recapitulate. Especially the ear malformations are intensively investigated in CHARGE and CHARGE-like mice (Bosman et al., 2005; Ogier et al., 2014; Ogier et al., 2018). A problem in the inner ear and the equilibrium sense could quite likely influence the stereotypic head-shake movements and maybe even the circle running. The here analyzed CHARGE mice could recapitulate the ear malformations described for CHARGE patients. However, the inner ear was not investigated in these mice.

For future behavior projects, it would be crucial to exclude blindness and deafness as influencing the overall behavior.

Experiments evaluating functional vision and auditory sense (not including any technical devices) are described as jumping from a defined hight (visuality) and fear reaction to loud noises. Both tests are unfortu-

nately quite restricted and seem not very reliable thus non of these tests was conducted.

Nevertheless, the hyperactive circling behavior phenotype of the CHARGE mice was already obvious in the home cage, and a similar observation was made in the so called looper mouse (Ogier et al., 2014).

It has been discussed for a long time which brain regions are involved in hyperactivity. The cerebellum is one of the regions thought to be involved in hyperactivity, as it gives important movement feedback to the rest of the brain. Since Purkinje cells give the inhibitory cerebellar output and are also the only output to the rest of the brain, a different cell structure, cell amount or activity of the Purkinje cells could potentially influence the behavior and were indeed found to be altered in the analyzed CHARGE mouse. However, other brain regions which are thought to be involved in hyperactive behavior were not analyzed in the CHARGE mice.

The cerebella purkinje cell layer was unremarkable in the genetic rescue of the CHARGE mouse, the reCHARGE mouse. It would be interesting to analysis the reCHARGE mouse in regard to their behavior.

For human patients, hyperactivity and autistic behavior trades were also symptoms of the CHARGE syndrome (Graham et al., 2005; Prancke-niene et al., 2019), but other studies emphasize that sleep difficulties (59%), aggressive behavior (51%), tactile defensiveness (51%) and obsessive compulsive behavior (49%) are more common. In the study by Hartshorne et al. attention deficits and the autistic spectrum were reported for 26% of the patients (Hartshorne et al., 2016). Doubtless only some of these behaviors can be monitored in a mouse model. But the sleep circle and a possible aggressive behavior of CHARGE mice would be an interesting point, since this has not been evaluated in CHD7 deficient mice up to now.

3.1.1 Eye Defect in CHARGE Mouse

In 77% to 90% of the human CHARGE patients coloboma of the eye due to a failure of the optic or choroid fissure to close during fetal development, resulting in visual impairments up to complete blindness, are reported (Hartshorne et al. 2016). Surprisingly a mouse model repeating the variety of eye malformations observed in human patients was missing. Only a few isolated malformations have been reported like lid oedema, narrow palpebral fissures and eye nerve hypoplasia (Ogier et al., 2014), cataracts and dry eye conditions (Bosmann et al., 2005).

The eye phenotype of the CHARGE mouse (CMVCre;CHD7$^{+/fl}$) described herein was striking. Three eyes had to be excluded from further analysis because they did not share any structural orientation points. Furthermore, nine out of 14 CHARGE eyes had a closed lid (narrow palpebral fissures) suggesting either one-eyed or two-eyed blindness of the respective animal. Interestingly, the left and the right eye displayed a symptomatic heterogeneity. Almost half of the mice displaying eye malformations possessed two differently affected eyes. The right eye was on average 70% affected while the left eye had in 30% of the mice a closed eye lid. Similar heterogene eye expression patterns have been reported for CHARGE patients wherein the right eye was stronger affected (Hartshorne et al., 2016).

Here it was shown that CHD7 deficiency leads to significantly smaller, and in some cases deformed eyes (Fig. 12). The retina of CHARGE mouse eyes was thinner and especially the inner nuclear layer was significantly decrease under CHD7 deficient conditions (Fig. 13).

Stainings revealed less PAX6 positive cells in the inner nuclear and ganglion cell layer of the CHARGE mice. Little is known about PAX6 task in the adult retina (Stanescu-Segal et al., 2017), but during the development PAX6 is usually responsible for a refined development of retinal progenitor cells, and under PAX6 deficiency only amacrine interneurons are developed (Marquardt et al., 2001). A missing cell fate refinement due to less PAX6 expression could thus lead to a reduced cell variety and maybe even to cell development defects and maybe to increase cell death. This would be interesting to investigate further. A lack of PAX6 could hence hint towards a singular cell development leaving out for example mueller glia, horizontal or ganglion cells. Noteworthy a Pax6 down-regulation has also been linked in different animal models to retinal degeneration (Stanescu et al., 2007; Stanescu-Segal et al., 2017) thus probably participating in the reduced retina thickness observed under CHARGE conditions. However, following experiments like qPCRs or western blots would be needed to further proof a reduced PAX6 expression in the retina and in specific cells.

Also, the ectopic expression of basic helix-loop-helix (MASH1) in the ganglion cell layer of the CHARGE mouse retina was remarkable. MASH1 is needed for retina neuron differentiation (Kageyama et al., 1997) and usually only expressed for a limited time during the retina development. However, positive cells in the ganglion cell layer hint towards non-differentiated cells. These cells are unlikely müller glia cells, which usually reside in the inner nuclear layer of the retina. MASH1 is a marker for bipolar cells of the inner nuclear layer (Jasoni and Reh, 1996) but again a positioning in the ganglion cell layer is unusual.

However, continuative studies are needed to further elucidate why the inner nuclear layer of the CHARGE retina is thinner and/or contains less cells. One approach would be a BrdU treatment of retina cells mainly labeling müller glia cells. Animals with marked retinas were prepared already, but could not be investigated within the time frame of this project.

Additionally, it would be interesting to isolate the complete retina to further analyze and culture the cell composition and single cell types for further analysis. Different approaches would then be possible from knock-out studies to sorting experiments with labeled cells.

3.1.2 Cerebella Defect in CHARGE Mouse

Prior to this analysis W. Feng observed a missing anterior lobe of the cerebellum under CHD7 deficient conditions (supplement Fig. 47). Since the analyzed knock-out was an Atho-1::Cre CHD7$^{fl/fl}$ knock-out limited to the cerebellum, the question arose whether this observation could be confirmed in the CHARGE mouse cerebellum. In agreement with these findings the anterior lobe of the cerebellum in 10 week old CHARGE mice is underdeveloped, the III lobe is missing (Fig. 16). Since this structure develops latest of all structures in the cerebellum, it could display a delayed development in comparison to the cerebellum of the Control mice.

Feng et al. found that CHD7 positive cells are mainly found in the inner granule layer (IGL) of the cerebellum. He also showed that during the development PAX6 positive cells (granule neurons and progenitors) are also positive for CHD7, while SOX2 (Bergmann glia cells) and Calbindin positive cells (Purkinje cells) show only a weak CHD7 expression. Also, there were detectably less Ki67 positive cells in the BrdU positive population suggesting an inappropriate cell cycle exit of granular progenitor cells (Feng et al., 2017). Since CHD7 deficiency results in an underdeveloped state of the cerebellum some of these usually embryonically expressed markers were analyzed in the adult CHARGE mouse to observe differences and similarities between a CHD7 knock-out restricted to the cerebellum and one that is affecting the whole brain.
The mouse cerebellum develops postnatally and within this development granular cells secret Reelin to Purkinje cells while the Purkinje cells secret Sonic hedgehog to the granular cells. This mechanism is needed for both cell types to find their right position in the cerebella structure (Feng et al., 2017). In agreement with these previous findings the CHARGE mouse (CMVCre;CHD7$^{+/fl}$) shows a disrupted Purkinje cell layer.

In this project it could be quantified that each purkinje cell is build up by more than three neighboring cells in almost 30% of analyzed cells under CHARGE conditions (Fig. 17). This disorganization of purkinje cells under CHD7 deficiency has been reported (Feng et al., 2017; Whittaker et a., 2017). Additionally, herein it was shown that most Purkinje cells developed under CHD7 deficiency have significantly less primary branches in comparison to the Control mice (Fig. 17).

The cell processes are needed to pass along signals and can thus be assessed as elementary for the cell function. As purkinje cells are the primary inhibitory output of the cerebellum, this is a striking phenotype. Furthermore, a bulk of purkinje cells which were not able to build primary processes needed for the integration into the cerebellum tissue, would fit into the bigger picture.

It has been reported that CHD7 deficient mice lack reelin due to a closed chromatin state. Reelin is a key factor secreted by granular neurons to guide purkinje cells into the right position in the cerebellum tissue and it seems purkinje cells may also need a further signaling to integrate into this cell layer (Feng et al., 2017). Reelin was also tested in the CHARGE mouse line but outliner rendered the animal number to low to be significant (Fig. 48).

Interestingly, a structural defect in the cerebella anterior lobe (which was also reported in Feng et al., 2017) was not observed in the genetic rescue called reCHARGE mouse (CMV Cre CHD7+/fl EZH2 +/fl). They were indistinguishable from the Control mice anterior lobe.

3.1.3 Neural stem cells in CHARGE Mouse

The hippocampal dentate gyrus is a brain region involved in learning and memory. Adult neural stem cells reside in this area and develop eventually into newborn neurons, which integrate into the subgranular zone. A defect in these cells may be associated with learning difficulties.

CHARGE mice were less fearful in the open field test and stayed in the center of the open field without worry, which may hint towards an impaired (fear-context) learning. Thus, stem and label retaining cells were marked with BrdU in the CHARGE mouse dentate gyrus to analyze this cell population.

A quantified staining for BrdU and nestin together revealed less double positive cells in the dentate gyrus of CHARGE mouse (Fig. 4.2.1). Indicating less stem cells in this region. Possible learning difficulties resulting

from this phenotype would be worth to investigate because of these hints.

3.2 Summary of the CHARGE Mouse Data

The CHARGE mouse (CMVCre;CHD7$^{+/fl}$) could be generated an displayed a variety of symptoms, some of which could be analyzed in this study. CHARGE mice had smaller olfactory bulbs corresponding to the human phenotype (Vissers et al., 2004). The olfactory bulbs showed less doublecortin expression, hinting towards a decreased amount of newborn neurons.

Mutant CHARGE mice were significantly smaller than their litter mates. Severely affected CHARGE mice even displayed a smaller brain-to-body ratio. Further, the CHARGE mice were hyperactive and spend more time in the center of the unknown open field maybe suggesting a maybe less fearful nature or less understanding of their situation.

The eye phenotype had a high penetrance in the CHARGE mouse line and an analysis showed a heterogeneity in the severity of the symptoms with a bias towards the right eye (narrow palpebral fissures). CHARGE eyes were significantly smaller, with a thinner retina and especially the inner nuclear layer of the retina was significantly thinner.

PAX6 positive cells of the inner nuclear and ganglion cell layer were found in the Control retinas. A finding that correlates to a report about PAX6 expression in inner nuclear and ganglion cell layer in p428 in mice (Stanescu-Segall et al., 2015). Under CHARGE conditions PAX6 positive cells seemed reduced in comparison to their Control litter mates, but further experiments are needed to validate this observation.

Stainings revealed that some cells of the CHARGE granular cell layer ectopically express MASH1, a marker usually not found in the adult eye. The cells seemed out of place since MASH1 expressing cells are usually found in the inner nuclear layer, not in the ganglion cell layer. These cells may correlate to the missing PAX6 development refinement. This ectopic expression of MASH1 might reflect the underdeveloped status of the retina, but this also needs further analysis.

The cerebella analysis could confirm a missing anterior lobe, and a disrupted and bulky purkinje cell layer. A quantification of these cells revealed that almost 30% of purkinje cells have more than three neighboring cells under CHARGE conditions. Moreover these cells have significantly less primary branches which all hints towards an underdeveloped brain

structure.

Furthermore, an analysis of stem and label retaining cells of the dentate gyrus revealed less BrdU and nestin positive cells (e.g. stem and label retaining cells) under CHARGE conditions in comparison to their Control litter mates.

3.3 The reCHARGE ouse

As genetic counter part to the CHARGE mouse (CMVCre;CHD7$^{+/fl}$) the reCHARGE mouse (CMVCre;CHD7$^{+/fl}$;EZH2$^{+/fl}$) was generated and analyzed. As mentioned before the CMV promotor could affect the germ line such that no in-line breedings were made.

CHARGE mice are significantly smaller. The reCHARGE mice showed no significant difference in body weight or brain-to-body ratio (Fig. 20).

This is remarkable in the light of undergrowth reported for CHARGE syndrome (CHD7$^{+/fl}$) and overgrowth as obvious feature for Weaver syndrome (EZH2$^{+/fl}$). Here a combination of reduced CHD7 and EZH2 expression resulted in mice of average size.

3.3.1 Eyes in CHARGE vs reCHARGE Mouse

The CHARGE mice displayed closed eye lids, underdeveloped and smaller eyes with a thinner retina and a thinner inner nuclear layer.

The reCHARGE mice had no obvious eye phenotype (Fig. 21), and the eye structure was not significantly altered. The left and right eye were both equally well developed and seemed structurally functional. Measurements of the eye size revealed a smaller eyes (Fig. 22) but the retina thickness was indistinguishable from the Control mice retina.

Remarkable, the reCHARGE retina phenotype showed wavy foldings in some mice (Fig. 23C). This wavy structure could be caused by an over-proliferation, through reduced EZH2 activity and thus reduced H3K27me3. A wavy retina can otherwise be seen in inflammatory tissue, but unlike retina inflammations the cell layer structure of reCharge mouse retina comprising the cell bodies, was separated nicely into inner-, outer nuclear and ganglion cell layer. Further analysis revealed no significant changes in comparison to their Control litter mates.

The question remains how the EZH2 downregulation rescues the eyes development. One suggested candidate was PAX6, a master regulator of the eye development. Similar to the CHARGE phenotype, an eye dependent knock-out of *pax6* leads to small eyes with multiple defects. In other tissues PAX6 was already identified as EZH2 target, which was reasoned could in hint to a possible explanation for the eased eye phenotype of the reCHARGE mouse. Less repressive histone marks on the *pax6* gene would thus promote the expression of PAX6 and could be potentially beneficial for the eye development. Thus, this marker was also stained in the reCHARGE eye but revealed a likewise reduced expression, as seen in the CHARGE mouse. These stainings hint towards a different mechanism the normalized retinas grown under reCHARGE conditions but further expression analysis would be needed.

A MASH1 staining showed no positive cells in the reCHARGE retina knock-out corresponding to the results of their Control litter mates.

3.3.2 Cerebellum in CHARGE vs reCHARGE Mouse

Unlike the CHARGE mouse, the anterior lobe of the reCHARGE mouse cerebellum showed in non of the stained mice a defect.

The purkinje cells had an average size (Fig. 26) and the phenotype of a bulky and crowded purkinje cell layer observed in the CHARGE mouse cerebellum was not visible in the reCHARGE mouse cerebellum (Fig. 26).

Another significant phenotype seen in CHARGE mice cerebellum concerned the visible branches of the purkinje cells. Here in the CHD7 deficient phenotype purkinje cells with a visible primary branch were significantly underrepresented. In contrast to that the reCHARGE mouse purkinje cells showed as many branches as the Control mice did (Fig. 26).

Purkinje cell nuclei showed a profound EZH2 staining signal in both CHARGE and Control mice, although the EZH2 protein level seemed to be unaffected (Fig. 17). Purkinje cells are GABAergic neurons and as such it has been suggested that EZH2 Controls their embryonic cell fate (Feng et al., 2016), but this study also described cerebella hypoplasia which has not been described under EZH2 deficiency in the Weaver syndrome and does not fit to the known overgrowth phenotype. Furthermore, an EZH2 expression in mature purkinje cells was not described. Similar to observations made in the CHARGE mouse the purkinje cells of reCHARGE mice displayed a nuclear EZH2 signal. However, further studies are needed to decipherer differences between CHARGE and reCHARGE purkinje cells.

In the future a RNA sequencing could resolve the different gene expression of purkinje cells while CHIP and ATAC sequencing experiment could tell more about the epigenetic status of theses cells.

3.3.3 Neural Stem Cells in CHARGE vs reCHARGE Mouse

The collected data showed that the CHARGE mouse had a lower number of BrdU and nestin positive cells which was matching already published data of CHD7 deficient in neural stem cells (Feng et al., 2013, supplement Fig. 45).

To create comparable data, the reCHARGE mouse was analyzed at the same time with the same labeling protocol used for the CHARGE mouse. Cells were counted in a blind study. The amount of BrdU and nestin double positive cells of the reCHARGE mouse dentate gyrus was not significantly different from the amount of cells quantified for the Control litter mates, thus displaying a rescue of the CHARGE condition in this aspect.

A knock-out of *ezh2* has been shown to increase the amount of stem cells (Nestin) and newborn neurons (NeuN) in the dentate gyrus (Rhodes et al., 2018). The loss of EZH2 and H3K27me3 seems to induce stem cell development. This may hint towards a mechanism on how a loss of EZH2 can be beneficial for neural stem cells lacking CHD7.

To further investigate stem cells carrying a *chd7* and *ezh2* knock-out, an inducible *homozygous* knock-out was created (NesCreERT2;CHD7$^{fl/fl}$;EZH2$^{fl/fl}$) and analyzed, confirming this result.

3.4 Summary of CHARGE vs reCHARGE Mouse Data

The comparison of CHARGE and reCHARGE mouse under similar conditions was considered as rescue, when the reCHARGE mouse displayed no symptoms in contrast to the CHARGE mouse.

A rescue could not be achieved in the eye size which was still significantly smaller than the Control eye, and regarding the retina PAX6 expression. Also reCHARGE retinas were partially wavy which may hint towards an over-proliferation. Further studies would be needed to confirm this data. An open field analysis has not been attempted with the

reCHARGE mouse.

Additionally, a rescue could be observed in the following experiments. The reCHARGE mouse had in comparison to the CHARGE mouse a normal body size, structural functional eyes, and a retina thickness that corresponded to the measured Control values. Furthermore, the cerebella anterior lobe was unremarkable, and the purkinje cells layer displayed a normal structure and cells with a normal amount of visible primary branches. A analysis of the dentate gyrus stem cells revealed a normal amount of stem and label retaining cells in the reCHARGE mouse, unlike the reduced amount of BrdU and nestin positive cells quantified in the CHARGE mouse dentate gyrus.

As discussed somewhere else herein a RNA sequencing revealed that many genes falsely regulated under CHARGE conditions corresponded to the wildtype under reCHARGE conditions.

Taken together, a heterozygous expression of EZH2 was capable of normalizing some severe symptoms reported for the CHARGE condition.

3.5 Inducible homozygous Knock-out of *chd7* and *ezh2*

Here it could be observed that the dentate gyrus of the CHARGE mice (CMVCre;CHD7$^{+/fl}$) contains less BrdU and nestin positive cells (stem and label retaining cells), and the same observation was made in an inducible knock-out, lacking CHD7 which was restricted to the neural stem cells (Fig. 28 and NesCreERT2;CHD7$^{fl/fl}$, Feng et al., 2013 supplement Fig. 45).

To investigate a possible rescue of the CHD7 phenotype in hippocampal neural stem cells, a homozygous inducible double knock-out of *chd7* and *ezh2* was created. Since a homozygous knock-out of either *chd7* or *ezh2* is lethal, an inducible knock-out system was used and linked to a stem cell promotor (nestin - Nes) creating a NesCreERT2;CHD7$^{fl/fl}$;EZH2$^{fl/fl}$ mouse line. Repeating the same timing W. Feng used to analyze his *chd7* knock-out (NesCreERT2;CHD7$^{fl/fl}$) the double knock-out was analyzed. In contrast to the CHD7 deficient neural stem cells, a homozygous double knock-out of *chd7* and *ezh2* showed no reduction in the amount of stem cells. Likewise animals of the running experiment showed a normal amount of stem cells (NesCreERT2;CHD7$^{fl/fl}$;EZH2$^{fl/fl}$, Fig. 30).

Also, the amount of stem cells was analyzed by using a nestin staining and counting manually all the stained cells 2 weeks, 4 weeks and 6 weeks after the induction of the double knock-out (Fig. 29). Only 2 weeks after

the induction of the double knock-out, the number of nestin positive cells in the granular zone was significantly altered. The other time points showed the same amount of stem cells in double knock-out and Control litter mates. So there was no stem cell defect detectable in the double knock-out.

The development of newborn neurons (MCM2, DCX) seems to be altered in a homozygous *ezh2* knock-out (NesCreERT2;EZH2$^{fl/fl}$, supplement Fig. 44). Preliminary data showed a dynamic reaction of the stem cell pool to the homozygous *ezh2* knock-out. Within the first 2 weeks after the induction of the homozygous *ezh2* knock-out the amount of newborn neurons was slightly higher than in Control mice, but it dropped after about a month past the induction in comparison to the Control mice (Li, Y. , supplement Fig. 44). This observation initiated the analysis of MCM2 and DCX in the homozygous double knock-out of *chd7* and *ezh2*.

Doublecortin positive cells were only 2 weeks after the knock-out induction of the double knock-out significantly lower than the amount counted for the Control litter mates (Fig. 32C).

Within the dentate gyrus, newborn neurons migrate from the subgranular zone towards the end of the granular layer. In a stem cell dependent *ezh2* knock-out (NesCreERT2;EZH2$^{fl/fl}$) more newborn neurons expressing doublecortin were observed in the upper part of the granular layer (Li, Y., supplement Fig. 44). This could have different reasons, for example a misguidance of the cells or a different developmental time frame that lead to a longer doublecortin expression after the cells reached their integration position already. However, nothing similar has been observed in the inducible double knock-out of *chd7* and *ezh2* together. Cell orientation, cell distribution over the granular layer and cell position in the complete dentate gyrus showed no difference in newborn neurons (DCX, BrdU) compared to the Control (supplement Fig. 58, 59, 60, 61 NesCreERT2;CHD7$^{fl/fl}$;EZH2$^{fl/fl}$). Also, the dendritic length of doublecortin positive cells was not significantly changed as it has been observed in a homozygous *chd7* single knock-out (Feng et al., 2013).

Corresponding to nestin and doublecortin observations, the MCM2 quantification also revealed a lower number of positive cells 2 weeks after the knock-out induction (Fig. 33C). It seems that stem cells and newborn neurons are reduced under double knock-out conditions but only 2 weeks after the induction of the knock-out.

This could be explained in different ways. Considerable evidence has shown that tamoxifen administration can be neurotoxic, resulting in

impaired learning in rodents (Eberling et al., 2004). Thus, a time dependent reduction in the amount of stem cells might be an artefact of the tamoxifen treatment. However, this would be a general phenomenon, and in the presented case only the mutant mice displayed this deficit while the tamoxifen treated Control did not show a reduced stem cell amount.

Developing neural stem cells might be sensitive to the knock-out of *chd7* and *ezh2* at a certain time point. The development of neural stem cells to mature neurons, takes about eight weeks in the mouse dentate gyrus. Within the first days a type I and type II stem cell still expresses nestin, before the fate determination is finished in type III stem cells around the end of the first week. Now markers like MCM2 and doublecortin are expressed, until around the second week when these markers for newborn and immature neurons are followed by NeuN and Calretinin (Duan et al., 2008). The balance between neural stem cell self-renewal and cell differentiation is maintained, through epigenetic processes and especially CHD7 and EZH2 have both been linked to the cell fate decision. It was reported that EZH2 plays an important role in the temporal regulation of neural progenitor cells, prolonging the neurogenic phase. The levels of H3K27me3 would gradually increase over time at the *ngn1* promoter, and it would be plausible that, at a certain threshold, their chromatin state would become inactivated by PRC1, resulting in the suppression of *ngn* expression and the transition of NPC fate. In this report it was proposed that the developmental-stage-dependent accumulation of H3K27me3 at specific gene loci functions as a timer to drive cell fate switching (Hirabayashi et al., 2009). Fate confusion could, in theory, lead to an unfinished development and ultimately to cell death.

At a later time point the cell amount of all tested markers normalizes in the double knock-out (NesCreERT2;CHD7$^{fl/fl}$;EZH2$^{fl/fl}$). This may reflect a compensatory mechanism or a balance of both chromatin remodeler after a rough transition phase. It also might make a difference to developing stem cells, wether the cells were growing under a reduced CHD7 and EZH2 level from the beginning, or if said cells lost them at a maybe critical time point during the development.

A homozygous knock-out of *chd7* leads to an increased proliferation (Ki67) in the subgranular zone of the dentate gyrus (NesCreERT2;CHD7$^{fl/fl}$, Feng et al., 2013, supplement Fig. 45). Quantified four weeks after the knock-out induction the amount of proliferation seemed normal when both *chd7* and *ezh2* were knocked-out together (Fig. 31, NesCreERT2;CHD7$^{fl/fl}$;EZH2$^{fl/fl}$). No difference could be observed.

3.6 Summary of the inducible homozygous *chd7* and *ezh2* Knock-out

A homozygous double knock-out of *chd7* and *ezh2* had a normal amount of BrdU labeled cells. An investigation over several weeks showed only two weeks after the knock-out induction a significant reduction in stem cells, and newborn neurons (nestin, DCX, MCM2). At four and six weeks, no difference between the mutant mice and their Control litter mates could be observed.

Further doublecortin positive cells showed no abnormalities in cell distribution, cell orientation and dendritic length (data shown in supplement). Also, the proliferation, measured by Ki67 positive cells was unremarkable in a homozygous double knock-out of *chd7* and *ezh2*.

In summary the double knock-out of textitchd7 and *ezh2* could rescue the *chd7* knock-out phenotype in neural stem cells of the dentate gyrus.

3.7 Treatment with the EZH2 Inhibitor GSK126

Since the CHARGE syndrome is a developmental disease the question remained wether the situation of already affected patients could be eased through a stem cell treatment. This question was linked to further questions. What is the effect of a *chd7* knock-out on different not yet investigated brain regions. Is the structure disrupted in a way that new healthy stem cells would be capable of changing the signal output? Could an EZH2 inhibitor have a negative effect on otherwise non affected brain regions?

To further investigate these questions a few *in vitro* pre-tests and *in vivo* experiments were conducted.

3.7.1 *In vitro* - CHD7 Knock-down Cells tolerate a Treatment with the EZH2 Inhibitor

Cells carrying a stable *chd7* knock down were analyzed in regard to their CHD7, and EZH2 expression via qPCR and showed a significant downregulation of CHD7.

These cells were further cultured and treated with the EZH2 inhibitor GSK126 with either 0, 1 or 2 μM of the GSK126 EZH2 inhibitor. The cells tolerated this treatment, and the inhibition of EZH2 was successful after 72

hours of treatment, shown by western blot for H3K27me3.

Another test was the treatment of HEK293T and neural stem cells with different versions of the GSK126 EZH2 inhibitor chemically altered to maybe later be capable of crossing the blood-brain-barrier. The H3K27me3 protein level was reduced in HEK293T and neural stem cells. However, the reduction on neural stem cells seemed not clearly concentration dependent, which may reflect the chemical alteration which may alter the inhibitory function of this specific inhibitor.

3.7.2 *In vivo* - the EZH2 Inhibitor can be Administered to the Brain and reduces H3K27me3 Protein Level

To further investigate whether the EZH2 inhibitor GSK126 could be a potent CHARGE medication, a brain application was designed. Since the inhibitor does not cross the blood-brain-barrier the brain infusion was achieved through an osmotic pump. With an infusion period of five days constantly infusing 2 μM of the GSK126 inhibitor with 0.5 μl per hour in the right dentate gyrus. The surgery procedure could be established and seven mice survived the treatment. Unfortunately all of them were Control mice and only some received an inhibitor treatment.

Combining the inhibitor treatment with CldU it could be shown that the infusion into the dentate gyrus effectively labels cells with CldU. This occurred in a limited fashion as cells of the left dentate gyrus displayed no CldU signal. Further it could be shown that H3K27me3 level of the dentate gyrus tissue were reduced in two treated mice (Fig. 35I).

3.8 Summary of the Treatment with the EZH2 Inhibitor GSK126

A CHD7 knock down cell line can be treated with the EZH2 inhibitor GSK126 and displays a reduced H3K27me3 level after 72 hours of incubation.

Different chemical altered versions of GSK126 were tested on HEK293T cells and on neural stem cells to reveal functional alterations of the GSK126 inhibitor[22].

Testing the brain compatibility of the non-altered version of the EZH2 inhibitor GSK126 an osmotic pump was surgically fixed to the mice den-

[22] In a next step the chemical variations reducing H3K27me3 will be tested in an *in vitro* model of the blood brain barrier. This will be conducted outside the scope of this project.

tate gyrus. A combination of the inhibitor with CldU revealed that even after five days of constant infusion, only one brain hemisphere contained marked cells. Maybe suggesting that only a regional effect of the inhibitor can be obtained by this approach. However, the infusion was capable of reducing H3K27me3 protein level in the brain tissue. Unfortunately the treatment was not tolerated by the *chd7* knock-out mice while some Control mice survived.

3.9 RNA Sequencing of CHD7$^{+/fl}$ and CHD7$^{+/fl}$EZH2$^{+/fl}$ Cerebellum Tissue

Given the before mentioned results a RNA sequencing was intended to give new insights into the differentially expressed genes under CHD7 or CHD7 and EZH2 loss.
To further investigate the cerebellum tissue of Control (CMVCre-), CHARGE (CMVCre;CHD7$^{+/fl}$) and reCHARGE mouse (CMVCre;CHD7$^{+/fl}$EZH2$^{+/fl}$), the RNA of half of the cerebellum tissue was isolated and tested via qPCR. The expression level of CHD7 and EZH2 and confirmed the reduction of CHD7 in CHARGE and a reduced CHD7 and EZH2 expression level in reCHARGE mouse (Fig. 36A and B).

The analysis of the RNA sequencing data revealed that significantly changed genes showed similarities within the group of CHARGE and Control animals. The reCHARGE mouse tissue however had an expression pattern closer to the Control mice and the gene expression of several genes was rescued under reCHARGE conditions.

An analysis of the RNA sequencing data of all regulated genes in CHARGE vs Control mice revealed that processes for regulation of transcription, DNA-template, and nucleosome assembly are significant altered. Remarkably, also H3K27me3 appeared in the list of significantly changed genes (supplement Fig. 49), and intriguingly processes of chromatin silencing are up-regulated (supplement Fig. 50). A missing re-activation of genes through loss of CHD7 led to increased chromatin silencing under CHARGE conditions. This result underlines the main hypothesis of this work. Further studies are needed to reveal the molecular pathways how CHD7 influences chromatin silencing.

Further up-regulated genes in CHARGE vs Control cerebellum tissue include DNA methylation on cytosine, regulation of gene expression and epigenetic, DNA replication-dependent nucleosome assembly, protein heterotetramerization, chromatin silencing at rDNA and especially regulation of transcription (supplement Fig. 50).

Downregulated are cell differentiation, cell transport and mRNA processing. Interestingly, also Rho protein signal transduction and filopodium assembly were downregulated under CHARGE conditions. A misregulation in the Rho family of small Ras-related GTPases can interfere with cytoskeleton formation and filopodium assembly (Ohta et al., 1999). Neurons deprived of filopodia display defects in growth direction and synaptic formation (Bentley et al., 1986; Bardsley et al., 1999; Maletic-Savatic et al., 1999). The regulation of synaptic plasticity was likewise downregulated in the CHARGE cerebellum tissue (supplement Fig. 51).

Interestingly, a study analyzing CHD7 up-regegulation in glioblastoma found that altered genes were highly associated with pathways such as *biological adhesion*, *cell adhesion* and *locomotion* in gene ontology (GO) analysis (Machado et al., 2019). In the cerebellum tissue of the here analyzed CHARGE mouse cell adhesion and angiogenesis were significantly downregulated (supplement Fig. 51).

All significantly changed genes are summarized in a volcano plot (Fig. 38B) depicting the genes rescued under reCHARGE conditions in comparison to CHARGE mouse cerebellum tissue. The rescued genes cover a part of the significantly changed genes, but not all significantly changed genes. This fits to the expectation of a partial rescue seen in the reCHARGE cerebellum. Especially the downregulated genes found under CHARGE conditions are rescued quite efficiently. This observation could be related to the reduced EZH2 expression of reCHARGE mouse reduces the repressive histone mark H3K27me3 and is capable of gene activation. To further investigate this CHD7 target genes would need to be investigated regarding their H3K27me3 level.

The RNA sequencing of the complete cerebellum tissue can hint towards misregulated over all processes which might hint towards altered processes in the cerebellum of CHARGE patients. From this starting point more detailed investigations, maybe analyzing different cell types, can follow.

3.10 Summary of all Data

Within the framework of this project, a CHARGE mouse (CMVCre;CHD7$^{+/fl}$) and a genetic rescue the reCHARGE mouse could be generated and analyzed. The reCHARGE mouse displayed a partial rescue of most of the analyzed CHARGE symptoms. The reCHARGE mouse had in comparison to the CHARGE mouse a normal body size,

structural functional eyes, and a retina thickness that corresponded to the measured Control values. Furthermore, the cerebella anterior lobe was unremarkable, and the purkinje cells layer displayed a normal structure and cells with a normal amount of visible primary branches. Moreover a RNA sequencing revealed that many genes falsely regulated under CHARGE conditions corresponded to the wildtype under reCHARGE conditions. A analysis of the dentate gyrus stem cells revealed a normal amount of stem and label retaining cells in the reCHARGE mouse, unlike the reduced amount of BrdU and nestin positive cells quantified from the CHARGE mouse dentate gyrus.

Furthermore, the EZH2 inhibitor was tested on CHD7 knock down cells and neural stem cells and was capable of reducing H3K27me3. A brain application was established and revealed that EZH2 inhibitor infused tissue has a reduced H3K27me3 level.

3.11 Future Perspective

The herein collected and presented data shows a rescue of the CHD7 single knock-out phenotype in many aspects. A further investigation could focus on the genetic properties of purkinje cells and granular neurons carrying a *ezh2* and *chd7* knock-out.

Also, BrdU positive cells in the CHARGE and reCHARGE retina would be interesting to analyze to decipherer a possible developmental defect under CHARGE conditions and a possible over-proliferation in the reCHARGE retina.

Another interesting experiment would be a complete behavior profile of CHARGE and reCHARGE mouse, ad best both mouse lines would be Controlled against an eye or inner ear phenotype. An analysis could focus on aggressive behavior or sleeping abnormalities.

Furthermore, the surgical application of the EZH2 inhibitor GSK126 could give new insights into a possible treatment of stem cells under CHARGE conditions. Since the H3K27me3 protein level could be decreased with this treatment, a analysis of the stem cell pool and a possible rescue of the same would be an interesting experiment.

4 Material and Methods

4.1 Mouse Lines

All mouse lines were breed and housed in the DKFZ animal facility (barrier 5) under standardized conditions (temperature, humidity). The genetic background was a C57BL/6N-C2 mouse for all crossed mouse lines.

CHD7$^{+/fl}$ mice were obtained from EUCOMM, and the neomycin selection cassette was removed by crossing with Flp deleter mice. NesCreERT2, NesCre$^{fl/fl}$ and animals were generated as described elsewhere (Corsini et al., 2009).

CMVCre mice were provided by Prof. Augustin and are described as follows. In this transgenic strain, deletion of loxP-flanked genes occurs in all tissues, including germ cells. The cre gene in this strain is under the transcriptional Control of a human cytomegalovirus minimal promoter and is likely to be expressed before implantation during early embryogenesis. It also appears that the cre gene is X-linked since transgene transmission through males is restricted to female offspring[23].

The NesCre^{ERT2} double knock-out of CHD7$^{fl/fl}$ and EZH2$^{fl/fl}$ was crossed between the single knock-out lines.

To induce the knock-out in NesCreERT2 mouse lines Tamoxifen (Sigma, T-5648-5G, 10 mg/ml) was used. Diluted in 4.5 ml sunflower oil (Sigma, S-5007) and 500 μl EtOH, Tamoxifen was injected intraperitoneal (i.p.) twice per day on 5 following days.

For BrdU injections 15 mg/ml were dissolved in sterile NaCl and heat up to $50°C$. Injected were 50 mg/kg once per day. Mice that could not be injected got BrdU in the feeding water with a concentration of 1 mg/ml for 1 week.

Experiments conducted with these mouse lines were proceeded under the allowance of the german regional animal welfare commission. Two animal experiment applications were written in for this project (G-278/15, G-285/16), both were granted by the german regional council.

[23]The Jackson Labratory, https://www.jax.org/strain/006054

Mouse line	Reference name	Genotype
NesCreERT2; CHD7$^{fl/fl}$	CHD7 single knock-out	Cre recombinase expression is limited to the nestin expressing cells, which such as stem and neural progenitor cells. Through the combination with the estradiol receptor the Cre recombinase is inducible through Tamoxifen injections. A homozygous CHD7 knock out is limited to these cells.
NesCreERT2; EZH2$^{fl/fl}$	EZH2 single knock-out	Cre recombinase expression is limited to the nestin expressing cells, which means stem and neural progenitor cells. Through the combination with the estradiol receptor the Cre recombinase is inducible through Tamoxifen injections. A homozygous EZH2 knock out is limited to these cells.
NesCreERT2; EZH2$^{fl/fl}$;CHD7$^{fl/fl}$	Double knock-out	Cre recombinase expression is limited to the nestin expressing cells, which means stem and neural progenitor cells. Through the combination with the estradiol receptor the Cre recombinase is inducible through Tamoxifen injections. A homozygous CHD7 and EZH2 knock out is limited to these cells.
CMVCre; CHD7$^{+/fl}$;EZH2$^{+/fl}$	reCHARGE mouse	The viral CMV promotor is linked to the expression of the Cre recombinase. This promotor is not selectively expressed and can cause a knock-out in any tissue. A heterozygous CHD7 and EZH2 knock out is not limited to any tissue.
CMVCre; CHD7 $^{+/fl}$	CHARGE mouse	The viral CMV promotor is linked to the expression of the Cre recombinase. This promotor is not selectively expressed and can cause a knock-out in any tissue. A heterozygous CHD7 knock out is not limited to any tissue.
EZH2$^{fl/fl}$	Breeding mouse line	The EZH2 sequence is flanked by flox sequences
CHD7$^{fl/fl}$	Breeding mouse line	CHD7 sequence is flanked by fox sequences
CHD7 $^{fl/fl}$; EZH2$^{fl/fl}$	Breeding mouse line	The EZH2 and CHD7 sequence is flanked by flox sequences but no Cre rekombinase is expressed.
C57BL/6N	Breeding mouse	Wildtype mouse
CMVCre	Breeding mouse line	The viral CMV promotor is linked to the expression of the Cre recombinase. This promotor is not selectively expressed and can cause a knock-out in any tissue.

Figure 39: **Used mouse lines with reference name and explanation of the genotype**

Primer:		
CHD7	Primer Chd7 flox CAS_R1:	5'-TCG TGG TAT CGT TAT GCG CC-3'
	Primer Chd7 flox 5P_F:	5'-TGC AGA TGG GAC GTT TTC AG-3'
	Primer Chd7 flox 5P_R:	5'-CTG CAA GAA CAC AGG GCA AG-3'
EZH2	Ezh2_40378_nr_F:	5'-TGG ATA AGC CAC ATA TCA TCG G-3'
	Ezh2_40378_nr_R:	5'-GAT GGC TCA GCA GGT AAA GAC C-3'
CreERT2	Cre_1_Fw	5'-GGC TGG TGT GTC CAT CCC TGA A-3'
	Cre_2_Rv	5'-GGT CAA ATC CAC AAA GCC TGG CA-3'
Cre	212	5'-CTG CCA GGG ACA TGG CCA GG-3'
	213	5'-GCA CAG TCG AGG CTG ATC AGC-3'
CMV Cre	CMV-Cre1	5'-GGC GCG GCA ACA CCA TTT TT-3'
	CMV-Cre2	5'-CCG GGC TGC CAC GAC CAA-3'
	B2-1	5'-CAC CGG AGA ATG GGA AGC CGA-3'
	B2-2	5'-TCC ACA CAG ATG GAG CGT CCA-3'

Figure 40: **Genotyping primer for different mouse lines**

4.1.1 Genotyping

To determine the genotype of the different mice, tail biopsies were taken. The tail pieces were digested in 200 μl NID buffer (50 mM KCl; 10 mM Tris-HCl, pH 8.3; 2 mM $MgCl_2$; 0.1 mg/ml Gelatin; 0.45% NP40; 0.45% Tween 20) with 2 μl Proteinase K (10 mg/ml). After an over night incubation at $56°C$ the mixture was finally incubated at $96°C$ for 10 minutes and briefly centrifuged. For a standard PCR 1-2 μl DNA solution was used.

With a standard protocol only the annealing temperature was changed according to the primer requirements. Together with a DNA marker the samples were visualized with gel red on a 2% electrophorese gel after running for 1 h at 130 V. Pictures were taken and the analyzed genotyping results were included into a mouse data base (Tierbase, Movi).

4.1.2 Running Experiment

Litter mates of the same age (10 weeks) got 5 days of Tamoxifen injection (10 mg/ml, 100 μl twice per day). After another two weeks the stem and label retaining cells were marked by BrdU at 5 days of injection. With the last day of BrdU injection the mice were transferred into running cages and the following four weeks three to four mice per cage shared one running wheel. Then these mice were sacrificed with CO_2, perfused and the dissected brain was fixed in 4% PFA. To recognize BrdU positive cells an antibody was used (Fig. 30).

4.1.3 Pump Surgery

Before the surgery, the osmotic pumps need to be assembled and filled with the EZH2 inhibitor GSK126 under steril conditions. A 2 μM concentration of GSK126 was used. Under a cell culture hood the pumps are unpacked, filled by using a needle and fixed together. This means the cannula was fixed to a metal part connecting it to the pump. The fixed and filled pumps are kept in a 50 ml Falcon in NaCl and are sterilized right before use with 100% EtOH and rinse in fresh NaCl.

For the procedure, eight to ten week old litter mate mice were used (NesCreERT2;CHD7$^{fl/fl}$). The mice got Tamoxifen (10 mg/ml) twice per day, injected i.p. and after two more weeks the pump surgery was performed.

To prepare the surgery a heating mat was warmed and placed in front of a head holder for stereotactic injections. Natriumchlorid, Ketamin/ Xylazin in NaCl (1 ml / 0.5 ml/ 8.5 ml, 10 μg/g) were prepared in a syringe, eye creme, clean surgical tools in 100% Ethanol bath, and a needle with surgical suing material was prepared.

The mice were deeply anesthetized with Ketamin/ Xylazin in NaCl and prepared for the surgery by shaving, fixing the skull into a stereotactic head holder (Kopf) and disinfecting the skin.

A small incision opened the view from the skulls bregma to the hind head. To form a small pocket under the skin, blunt-ended sizers are positioned under the skin on the back of the mouse and softly opened. Later on, the pump will be positioned in this pocket. Subsequently a long glass needle was fixed to the stereotaxic apparatus and placed right above bregma. The system was set to zero and the dentate gyrus was targeted by using the following coordinates x +/- 1.6, y -2.0, z -2.3. Under

the microscope this exact position was used to open the skull with a needle.

While opening the skin pocket with forceps, the pump was positioned on the back of the mouse. The skull hole was cleaned and a tiny bit of a fluid glue was distributed in a circle around the hole. The insertion needle was pushed through the hole in the skull and the plastic tap was glued to the skull. While the glue dried, the plastic cap on top of the tap was cut-off, and the skin insertion was sewn with surgical filament. After releasing the mouse out of the stereotaxic head holder, every mouse got another shot of diluted Ketamin (1:10 in NaCl) and was placed on a heating mat with $37°C$ and monitored while waking up. Pain killers were given ad libitum in the drinking water (Fig. 35).

4.2 Stainings

The brains of perfused mice were fixed with 4% Paraformaldehyde in PBS over night, and then cut into 40 μM slices with a Vibratome (Leica). Brain sections were kept in PBS and washed with fresh PBS before staining.

Eyes and brains used for H & E stainings were fixed with 4% Paraformaldehyde in PBS over night, orientated in a wax block. Eyes were washed two times for 15 minutes in PBS, slowly dehydrolized by reducing the PBS content and increasing the alcohol amount. Meaning that after two times of 30 minutes incubation with 70% alcohol, two times one hour incubation with 85% and 95% alcohol followed subsequently. The eyes stayed over night in pure alcohol and were put in xylene for two hours on the next morning. Paraffin or wax was added with $60°C$ and exchanged against new paraffin after another hour. Finally the eyes were placed in the plastic mold and paraffin was added and dyed. Eyes were cut into 6 μM parrafin sections, and sections with a visible pupil and optic nerve were selected for stainings.

4.2.1 Immunofluorescence

To reduce autofluorescence, the fixed brain slices were kept in PBS with 100 mM Glycine before blocking them in 5% NSS (diluted in PBST (PBS 0.2% Triton X)) for 30 minutes. If BrdU was stained the sections were treated with 2N HCl at $37°C$ before blocking them. After washing the tissue, the secondary fluorescent antibody and 1:10000 DAPI diluted in 5% NSS (diluted in PBST) incubated for 1 hour. With a final washing step the sections were mount on glass objectives with Eukitt for fluorescent stainings. Fluorescent images were taken with confocal laser-scanning

Name	Company	Host	IF	IHC
Calbindin	abcam	Mouse	1:100	
CldU	abcam	Mouse	1:100	
DCX	Santa Cruz	Goat	1:100	1:500
BrdU	Abcam	Rat	1:100	
NeuN	millipore	Mouse	1:150	
Nestin	BD	Mouse	1:100	1:500
Ki67	Abcam	Rabbit	1:200	1:500
Mash1	BD	Mouse	1:200	
MCM2 (BM28)	BD	Mouse/ Goat	1:200	1:500
Pax6	Covance	Rabbit	1:100	
EZH2	Cell signaling	Rabbit	1:100	
CHD7	Abcam	Rabbit	1:200	1:500

Figure 41: **Primary antibodies used for IF and IHC stainings**

microscopes (LSM780, LSM700, Zeiss) (Fig. 30, Fig. 14, Fig.17, Fig. , Fig. 24).

4.2.2 Immunohistochemistry

Fixed brain sections were kept in PBS and washed with fresh PBS before staining, and then incubated in 2 M HCL for 30 minutes at room temperature. After three more PBS washing steps a mixture of 0.6% H_2O_2 dilution in 1:1 PBS/Methanol was used to block endogenous peroxidase. To remove membrane proteins the samples are washed three times for 15 minutes with PBST (PBS 0.2% Triton X). Then the tissue was blocked for 30 minutes with a solution of 5% NSS in PBST to reduce unspecific antibody binding.

An incubation with the first antibody diluted in 5% NSS PBST at four degree takes a night. Left over antibody was washed away in three PBST washing steps. The biotinylated secondary antibodies (Donkey anti-goat

NAME	COLOR	AGAINST	HOST
A11042/594	594	CHICKEN	GOAT
A11058/594	594	GOAT	DONKEY
A11055	488	GOAT	DONKEY
A21206/488	488	RABBIT	DONKEY
A11012/594	594	RABBIT	GOAT
A21062/350	405	MOUSE	RABBIT
A21442/594	594	RABBIT	CHICKEN
A11059/488	488	MOUSE	RABBIT
A11062/594	594	MOUSE	RABBIT
A21209/594	594	RAT	DONKEY
A21202	488	MOUSE	DONKEY
A21203	594	MOUSE	DONKEY
A31553	405	MOUSE	GOAT

Figure 42: **Secondary antibodies used for IF and IHC stainings**

and donkey anti-mouse, Vector Laboratories) were diluted in 5% NSS PBST and left for 30 minutes on the slices, before left over solution was washed away by another turn of three PBST washing steps. While the samples were washing the AB-Complex was diluted 1 to 100 in PBST, and incubates at room temperature. After the last washing step the horseradish peroxidase system (ABC Kit, Vector Laboratories) or short AB-Complex solution was added to the tissue, and incubated for 30 minutes. With the following two washing steps, first PBST and then PBS the samples were ready to be visualized by DAB staining (Sigma-Aldrich). The reaction can be stopped after 5 minutes by tap water, and the stained tissue was transferred to a glass objectives and dried for at least 30 minutes before mounting them with Eukitt and a glass cover slip. Bright field pictures were taken with a basic microscope (Fig. 29, Fig. 32, Fig. 33, Fig. 26, Fig. 27, Fig. 28).

4.2.3 Haematoxilin and Eosin Staining

An Haematoxilin and Eosin staining was used on paraffin sections to show structural differences in the brain tissue. In a first step the paraffin surrounding the brain was removed by washing with Xylene, and then re-hydrolyzed by two decreasing alcohol concentrations (100% and 70%). The Haematoxylin solution remains for 8 minutes on the brain sections and was removed by rinsing water after this time period. After adding Eosin (0,1% in 70% EtOH) for 1.5 minutes the brain sections are de-hydrolyzed again by increasing alcohol concentrations and a final Xylene washing step. With a cover glass and Eukitt mounting medium the stained brain slices can be covered and analyzed after dried (Fig. 8, Fig. 12, Fig. 13, Fig. 16, Fig. 22, Fig. 23, Fig. 25).

4.3 Western Blot

In brief, a abcam western blot protocol was used[24] and the Imobilon Western Chemoluminescent HRP Substrate protocol from Milipore was used for the chemoluminscent detection. Dissected and snap frozen brain tissue was mechanically homogenized in lysis buffer, and sonicated for 10 minutes per sample. After spinning the samples for 20 minutes at 12000 rpm and $4°C$, the supernatant was collected and the protein concentration was measured by wavelength using a Nano drop.

[24]https://www.abcam.co.jp/ps/products/131/ab131366/documents/Western%20blotting%20-%20a%20beginner's%20guide.pdf

The volume for 20 μg protein was calculated and the samples diluted 1 to 6 in laemmli buffer. Right before loading the sample on a precast gel (Mini-Protean TGX 10% and 12%, Biorad) the samples were heated to $99°C$ for 5 minutes. The precast gels were placed into a western blot running cassette and filled with with 1x Tris-glycine running buffer. With 80 V for 30 minutes, and 120 V for another hour the samples were separated by size in the electrophorese gel.

After a sufficient size preparation the gel-bound-protein was coupled to a nitrocellulose membrane and surrounded by thick buffer soaked papers to form a wet blot sandwich. For big proteins like EZH2 and CHD7, the transfer (in 100 ml 10x Tris, 200 ml Methanol and 700 ml H_2O) was obtained at 100 V for 1 h.

To visualize the transfer quality, a Ponceau Red (2% Ponceau S, 30% trichloracetic acid, 30% sulfosallicylic acid) protein indicator fluid was incubated for 5 minutes, analyzed and then washed off with PBST (1000 ml PBS and 1 ml Tween20). Floating in a 5% milk the membrane was blocked for 1 h at $4°C$ to reduce non-specific antibody binding. After a brief washing step in PBST, the membrane was cut into pieces and incubated over night at $4°C$ with the first antibody diluted 1 to 1000 in PBST.

For the incubation with the secondary antibody, the membrane was briefly washed with PBST and then incubated for 1 h at room temperature. The secondary horseradish-coupled antibody is diluted 1 to 4000 in PBST and visualized with chemiluminescent HRP substrate (Millipore). An equal amount of luminol reagent and peroxide solution was mixed and used when reached room temperature. After an incubation of 5 minutes the left over substrate fluid was removed, and the membrane was covered in transparent foil and a picture was taken (Fig. 34).

4.4 RNA Isolation and cDNA Preparation

In brief, a RNAprep combining Trizol (TRI Reagent Protocol, Sigma-Aldrich) and colums (RNeasy Mini Kit, Qiagene) was used.

Snap frozen tissue $-80°C$ was mechanically homogenized in 500 μl TRI reagent and incubated for 5 minutes at room temperature. After adding 100 μl Chloroform the samples were mixed and incubated for 5 minutes at room temperature. The following centrifugation (12000 rpm, $4°C$, 20 minutes) separated the RNA from the Protein and DNA content. The aqueous phase was then processed mixed with fresh mixed 70% alcohol and the RNeasy protocol was followed. Briefly the precipitated RNA was

NAME	HOST	DILUTION WB	COMPANY	CAT NO
BDNF	mouse	1:500 - 10000	sigma	SAB14021 27-100UG
BetaIII tubulin	rabbit	1:500 - 10000	cell signaling	2128s
Chd7	rabbit	1:500 - 10000	cell signaling	ab3124
EZH2	rabbit	1:500 - 10000	cell signaling	#5246
GAPDH	rabbit	1:500 - 10000	cell signaling	2118L
H3K27me3	rabbit	1:500 - 10000	millipore	ABE44

Figure 43: **Primary antibodies used for western blot**

filtered and washed through silica colums and eluated. The concentrations were measured by wavelength using a NanoDrop system (Thermofisher).

To transcribe the RNA to cDNA a QuantiTec Reverse Transcription Kit (Qiagen, 205310) was used according to the protocol.

4.4.1 qPCR

With the resulting cDNA, a qPCR was set up using a TaqMan gene expression assay protocol. In a 20 μl reaction 1 μl primer (20x TaqMan Gene Expression Assay), 10 μl enzyme (TaqMan Gene Expression Master Mix), 4 μl cDNA template and 5 μl RNase free water was mixed. The standard protocol had a $60°C$ annealing temperature for all primers and the program loop was repeated for 40 to 50 times. In this system the primer mix contains two flanking primers and one carrying the Fluorophor (FAM primer). With increasing amount of PCR product the amount of bound FAM primer increases and leads to a measurable fluorescent signal. With a qPCR machine (Biorad), the product amount and starting quantity (SQ) was analyzed (Fig. 8, Fig. 19, Fig. 36, Fig. 34.

Alternatively a cybergreen qPCR system was used which quantifies the amount of resulting DNA through intercalating into the DNA. If this system was used it is indicated, otherwise TagMan probes were used (Fig. 34).

Relative expression level were calculated as follows: the house keeping gene was subtracted from the tested gene of mutant and Control mice

(calculating the delta CTE and delta CTC value). The delta CTC value was subtracted from the delta CTE value to calculate the delta-delta CT value. In the last step $2^{-deltadeltaCT}$ value was calculated and the values of gene expression were compared.

4.4.2 RNA Sequencing

The cerebellum of the dissected brain was cut in half and one half was snap frozen. After isolating the RNA and producing the cDNA according to 4.4 RNA isolation and cDNA preparation, the cDNA was analyzed via qPCR (4.4.1 qPCR). Samples were selected, diluted in water in a 96 well plate on ice, and send on ice for sequencing to the DKFZ core facility. (The resulting raw data was kindly analyzed by C. Shao.)

4.5 Cell Culture

4.5.1 Neural Stem Cell Culture from Adult Mouse Subventricular Zone

Neural stem cell were isolated as described elsewhere (Fischer et al., 2011). In brief, eight weeks old mice were used and the subventricular zone was isolated. The collected tissue was cut into small pieces and collected in a 2 ml tube. After centrifuge for 1 minute at 250 g the supernatant was removed under a cell culture hood, and 1 ml of Accutase was added to the brain tissue. It takes around 20 minutes at $37°C$ to separate the cells and this can be improved by pipetting up an down or filtering through a blue cap tube. With another centrifugation (5 minutes at 250 g) the supernatant was removed and the cells are resuspended in fresh serum free medium (DMEM/F12 (1:1) + L glutamine and 15 mM HEPES (Invitrogen cat. no.11330-032), growth factors (EGF (Sigma cat. no. E4127), FGF (Sigma cat. no. F0291)), B-27 and ITSS).

Neural stem cells of the subventricular zone can be cultured as spheres or as attached monolayer in serum free medium (SFM) at $37°C$ with 95% air and 5% CO_2. For a monolayer culture dishes have to be coated with coating buffer (Laminin (0.5 mg/ml, Roche 11243217001) 250 μl, PDL/PLL (2 mg/ml in H_2O, Sigma P7280-5mg) 750 μl, PBS to 50 ml) for at least 4 hours at $37°C$. After this incubation time the coating buffer was removed and the plates were dried under UV light in a cell culture hood (NSC monolayer Fig. 34).

To passage these cells, either the medium with the floating spheres was collected, centrifuged, the supernatant removed and 1 ml of Accutase was

added, or the medium was carefully removed from the monolayer and 1 ml Accutase was added. It took 10 minutes of incubation at $37°C$ until the cells were separated and after another centrifugation the left-over Accutase was removed within the supernatant. Finally the cells were resuspended in fresh serum free medium and plated on either a coated or a non-coated plate.

When cells were frozen they were passaged as mentioned and re-suspended into a different medium in the last step. This serum free medium did not contain growth factors (SFM is DMEM/F12 (1:1) + L glutamine and 15 mM HEPES (Invitrogen cat. no.11330-032)) but 10% dimethyl-sulfoxide (DMSO) instead. The cell suspension was gently mixed and aliquoted with 1 ml into polypropylene cryovials (Nunc Cryo Tubes cat. no. 357418) and frozen at $-80°C$ using Cryobox.

To defrost the cells the cryo-vials were gently warmed up to $37°C$, mixed with fresh serum free medium and centrifuged (5 minutes at 200 g). The supernatant was removed and the cells were either seeded as monolayer of neurosphere with 95% air and 5% CO_2 as mentioned (Fig. 53, Fig. 34).

4.5.2 EZH2 Inhibitor Treatment

The EZH2 inhibitor GSK126 (in PBS/ 10% DMSO) was used for different purposes.
For treating cultured cells the inhibitor was mixed with the cell medium to a final concentration of 0, 1 and 2 μM and incubated for 48 and 72h (Fig. 34, Fig. 53).

As a drug for treating neural stem cells in the living animal the inhibitor was diluted in NaCl to a final concentration of 2 μM, filled into a osmotic pump under sterile conditions, and the loaded pump was kept in 70% EtOH in a 50 ml Eppendorf tube with closed litt. Right before positioning of the pump the EtOH was washed away with steril NaCl (Fig. 35).

4.6 Plasmid Multiplication and Isolation

Plasmids were multiplied via heat shock into DH5alpha *E.coli*. In brief, the competent bacteria was thaw on ice and the plasmid DNA was added with a buffer. The bacteria was heated for $42°C$ for 2 minutes and cells were placed on ice again. The prepared *E.coli* were distributed on culturing plates carrying a antibiotic. The antibiotic was selected due to the antibiotic

resistance gene on the respective plasmid wished to multiply. After an over night incubation the growing bacteria colonies were picked and placed in liquid LB medium (800 ml H_2O, 10 g Bacto-tryptone, 5 g yeast extract and 10 g NaCl, pH 7.5 sterile). Another incubation of at least three hours was set to multiply the bacteria carrying the plasmid. After this incubation the bacteria was centrifuged an the plasmid was isolated by using a QIAprep Spin Miniprep Kit following the kit instructions.

References

[Aasland et al., 1996] Aasland, R., Stewart, A., and Gibson, T. (1996). The SANT domain: a putative DNA-binding domain in the SWI-SNF and ADA complexes, the transcriptional co-repressor N-CoR and TFIIIB. *Trends Biochem Sci*, 3:87–8.

[Aid et al., 2007] Aid, T., Kazantseva, A., Piirsoo, M., Palm, K., and Timmusk, T. (2007). Mouse and rat BDNF gene structure and expression revisited. *Journal of Neuroscience Research*, 85:525–535.

[Akhtar et al., 2000] Akhtar, A., Zink, D., and Becker, P. B. (2000). Chromodomains are protein-RNA interaction modules. *Letters to Nature*, 407:405–408.

[Alonso et al., 2002] Alonso, M., Vianna, M. R., Depino, A. M., e Souza, T. M., Pereira, P., Szapiro, G., Viola, H., Pitossi, F., Izquierdo, I., and Medina, J. H. (2002). BDNF-triggered events in the rat hippocampus are required for both short- and long-term memory formation. *Hippocampus*, 12:551–560.

[Amador-Arjona et al., 2015] Amador-Arjona, A., Cimadamore, F., Huang, C.-T., Wright, R., Lewis, S., Gage, F. H., and Terskikh, A. V. (2015). Sox2 primes the epigenetic landscape in neural precursors enabeling proper gene activation during hippocampal neurogenesis. *PNAS*, pages 1–10.

[Anchan et al., 1997] Anchan, R., Drake, D., Haines, C., Gerwe, E., and LaMantia, A. (1997). Disruption of local retinoid-mediated gene expression accompanies abnormal development in the mammalian olfactory pathway. *J Comp Neurol.*, 2:171–84.

[Andreev et al., 2019] Andreev, V., Hristova, R., Asparuhova, M., Danovski, G., Stoynov, S., and Gospodinov, A. (2019). Mammalian INO80 chromatin remodeler cooperates with FANCM to mediate DNA interstrand crosslink-induced checkpoint activation and repair. *DNA Repair (Amst.)*, 74:38–50.

[Bajpai et al., 2010] Bajpai, R., Chen, D., Rada-Iglesias, A., Zhang, J., Xiong, Y., Helms, J., Chang, C., Zhao, Y., Swigut, T., and Wysocka, J. (2010). CHD7 cooperates with PBAF to control multipotent neural crest formation. *Nature*, 7283:958–62.

[Bardakjian et al., 2004] Bardakjian, T., Weiss, A., and Schneider, A. (2004). Microphthalmia/anophthalmia/coloboma spectrum. *Gene Review (Internet)*.

[Beardsley, 1999] Beardsley, J. (1999). Getting wired. *Scientific American*, 280(6):24–26.

[Beccari et al., 2013] Beccari, L., Marco-Ferreres, R., and Bovolenta, P. (2013). The logic of gene regulatory networks in early vertebrate forebrain patterning. *Mech. Dev.*, 130:95–111.

[Bentley and Toroian-Raymond, 1986] Bentley, D. and Toroian-Raymond, A. (1986). Disoriented pathfinding by pioneer neurone growth cones deprived of filopodia by cytochalasin treatment. *Nature*, 323 (6090):712–5.

[Bernstein and Denno, 2005] Bernstein, V. and Denno, L. (2005). Repetitive behaviors in CHARGE syndrome: differential diagnosis and treatment options. *Am J Med Genet A.*, 3:232–9.

[Blake et al., 1998] Blake, K., Davenport, S., Hall, B., Hefner, M., Pagon, R., Williams, M., Lin, A., and Graham, J. J. (1998). CHARGE association: an update and review for the primary pediatrician. *Clin Pediatr.*, 3:159–73.

[Blake and Prasad, 2006] Blake, K. and Prasad, C. (2006). CHARGE syndrome. *Orphanet J Rare Dis.*, 1:34.

[Bosman et al., 2005] Bosman, E., Penn, A., Ambrose, J., Kettleborough, R., Stemple, D., and Steel, K. (2005). Multiple mutations in mouse Chd7 provide models for CHARGE syndrome. *Hum Mol*, 22:3463–76.

[Boyer et al., 2004] Boyer, Latek, and Peterson (2004). The SANT domain: a unique histone-tail-binding module? *Nat Rev Mol Cell Biol.*, 2:158–63.

[Brill et al., 2009] Brill, M., Ninkovic, J., Winpenny, E., Hodge, R., ans R Yang, I. O., Lepier, A., GascÛn, S., Erdelyi, F., Szabo, G., Parras, C., Guillemot, F., Frotscher, M., Berninger, B., Hevner, R., Raineteau, O., and Goetz, M. (2009). Adult generation of glutamatergic olfactory bulb interneurons. *Nat Neuroscience*, 12:1524–33.

[Bultman et al., 2000] Bultman, S., Gebuhr, T., Yee, D., la Mantia, C., Nicholson, J., Gilliam, A., Randazzo, F., Metzger, D., Chambon, P., Crabtree, G., and Magnuson, T. (2000). A Brg1 null mutation in the mouse reveals functional differences among mammalian SWI/SNF complexes. *Mol Cell*, 6:1287–95.

[Cao et al., 2008] Cao, Q., Yu, J., Dhanasekaran, S., Kim, J., Mani, R., Tomlins, S., Mehra, R., Laxman, B., Cao, X., Yu, J., Kleer, C., Varambally, S., and Chinnaiyan, A. (2008). Repression of e-cadherin by the polycomb group protein EZH2 in cancer. *Oncogene*, 58:7274–84.

[Cao and Zhang, 2004] Cao, R. and Zhang, Y. (2004). SUZ12 is required for both histone methyltransferase activity and the silencing function of the EEd-EZH2 complex. *Molecular cell*, 15:57–67.

[Cech and Steitz, 2014] Cech, T. R. and Steitz, J. A. (2014). The noncoding RNA revolution - trashing old rules to forge new ones. *Cell Review*, 157:77–94.

[Cha et al., 2005] Cha, T.-L., Zhou, B. P., Xia, W., Wu, Y., Yang, C.-C., Chen, C.-T., Ping, B., Otte, A. P., and Hung, M.-C. (2005). Akt-mediated phosphorylation of EZH2 suppresses methylation of lysine 27 in histone H3. *Science*, 310:1–5.

[Chamberlain et al., 2008] Chamberlain, S., Yee, D., and Magnuson, T. (2008). Polycomb repressive complex 2 is dispensable for maintenance of embryonic stem cell pluripotency. *Stem Cells.*, 6:1496–505.

[Chen et al., 2010] Chen, S., Bohrer, L., Rai, A., Pan, Y., Gan, L., Zhou, X., Bagchi, A., Simon, J., and Huang, H. (2010). Cyclin-dependent kinases regulate epigenetic gene silencing through phosphorylation of EZH2. *Nat Cell Biol*, 11:1108–14.

[Chen and Dent, 2014] Chen, T. and Dent, S. Y. (2014). Chromatin modifiers and remodelers: regulator of cellular differentiation. *Nature Reviews*, pages 93–106.

[Chu et al., 2017] Chu, X., Guo, X., Jiang, Y., Yu, H., Liu, L., Shan, W., and Yang, Z. (2017). Genotranscriptomic meta-analysis of the CHD family chromatin remodelers in human cancers - initial evidence of an oncogenic role for CHD7. *Mol Oncol.*, 11(10):1348–1360.

[Croce and Helin, 2013] Croce, L. D. and Helin, K. (2013). Transcriptional regulation by Polycomb group proteins. *Nature Strucktural and Molecular Biology Review*, 20:1147–1155.

[Davidovich et al., 2013] Davidovich, C., Zheng, L., Goodrich, K., and Cech, T. (2013). Promiscuous RNA binding by polycomb repressive complex 2. *Nat Struct Mol Biol.*, 11:1250–7.

[de Dieuleveult et al., 2016] de Dieuleveult, M., Yen, K., Hmitou, I., Depaux, A., Boussouar, F., Dargham, D. B., Jounier, S., Hubertclaude, H., Riebierre, F., Baulard, C., adn Bongsoo Park, N. P. F., Keime, C., Carriere, L., Berlivet, S., Gut, M., Gut, I., Werner, M., Deleuze, J.-F., Olaso, R., Aude, J.-C., Chantalat, S., Pugh, B., and Gerard, M. (2016). Genome-wide nucleosome specificity and function of chromatin remodelers in ES cells. *Nature Research Letter*, 000:1–4.

[de la Serna et al., 2006] de la Serna, I., Ohkawa, Y., and Imbalzano, A. (2006). Chromatin remodelling in mammalian differentiation: lessons from ATP-dependent remodellers. *Nat Rev Genet.*, 7:461–73.

[Dixon et al., 2015] Dixon, J. R., Jung, I., Selvaraj, S., Shen, Y., Antosiewicz-Bourget, J. E., Lee, A. Y., Ye, Z., Kim, A., Rajagopal, N., Xie, W., Diao, Y., Liang, J., Zhao, H., Lobanenkov, V. V., Ecker, J. R., Thomson, J. A., and Ren, B. (2015). Chromatin architecture reorganization during stem cell differentiation. *Nature*, 518:331–336.

[Donovan et al., 2017] Donovan, A., Yu, T., Ellegood, J., Riegman, K., de Geus, C., van Ravenswaaij-Arts, C., Fernandes, C., Lerch, J., and Basson, M. (2017). Cerebellar vermis and midbrain hypoplasia upon conditional deletion of Chd7 from the embryonic mid-hindbrain region. *Front Neuoanat.*, page doi: 10.3389/fnana.2017.00086.

[Dorighi and Tamkun, 2013] Dorighi, K. M. and Tamkun, J. W. (2013). The trithorax group proteins Kismet and ASH1 promote H3K36 dimethylation to counteract Polycomb group repression in *Drosophila*. *Development*, 140:4182–4192.

[Duan et al., 2008] Duan, X., Kang, E., Liu, C. Y., li Ming, G., and Hongjun-Song (2008). Development of neural stem cell in the adult brain. *Current Opinion in Neurobiology*, 18(1):108–115.

[Eberling JL1, 2004] Eberling JL1, Wu C, T.-T. R. J. W. (2004). Estrogen- and tamoxifen-associated effects on brain structure and function. *Neuroimage.*, 21(1):364–71.

[Egan et al., 2013] Egan, C. M., Nyman, U., Skotte, J., Streubel, G., Turner, S., OConnell, D. J., Rraklli, V., Dolan, M. J., Chadderton, N., Hansen, K., Farrar, G. J., Helin, K., Holmberg, J., and Bracken, A. P. (2013). CHD5 is required for neurogenesis and has a dual role in facilitating gene expression and polycomb gene repression. *Dev Cell*, 26:223–236.

[Farh et al., 2015] Farh, K., Marson, A., Zhu, J., Kleinwietfeld, M., Housley, W. J., Beik, S., Shoresh, N., Whitton, H., Ryan, R. J. H., Shishkin, A. A., Hatan, M., Carrasco-Alfonso, M. J., Mayer, D., Luckey, C. J., Patsopoulos, N. A., Jager, P. L. D., Kuchroo, V. K., b. Epstein, C., Daly, M. J., Hafer, D. A., and Bernstein, B. E. (2015). Genetic and epigenetic fine mapping of casual autoimmune disease variants. *Nature*, 518:337–343.

[Fazzio et al., 2008] Fazzio, T., Huff, J., and Panning, B. (2008). An RNAi screen of chromatin proteins identifies tip60-p400 as a regulator of embryonic stem cell identity. *Cell*, 134(1):162–74.

[Feng et al., 2013] Feng, W., Kahn, M. A., Bellvis, P., Bernhardt, O., Herold-Mende, C., and Liu, H. (2013). The chromatin remodeler CHD7 regulates adult neurogenesis via activation of SoxC transcription factors. *Cell Stem Cell*, 13:62–72.

[Feng et al., 2017] Feng, W., Kawauchi, D., Koerkel-Qu, Q.-H., Deng, H., Serger, E., Sieber, L., Lieberman, J., Jimeno-Gonzalez, S., Lambo, S., Hanna, B., Harim, Y., Jansen, M., Neuerburg, A., Friesen, O., Zuckermann, M., Rajendran, V., Gronych, J., Ayrault, O., Korshunov, A., Jones, D., Kool, M., Northcott, P., Lichter, P., Cortes-Ledesma, F., Pfister, S., and Liu, H. (2017). Chd7 is indispensable for mammalian brain development through activation of a neuronal differentiation programme. *Nat Commun.*, 20;8:14758.

[Feng et al., 2016] Feng, X., Juan, A. H., Wang, H. A., Ko, K. D., Zare, H., and Sartorelli, V. (2016). Polycomb Ezh2 controls the fate of GABAergic neurons in the embryonic cerebellum. *Development*, 143:1971–80.

[Fischer et al., 2011] Fischer, J., Beckervordersanforth, R., Tripathi, P., Steiner-Mezzadri, A., Ninkovic, J., and Goetz, M. (2011). Prospective isolation of adult neural stem cells from the mouse subependymal zone. *Nature Protocol*, 6:1981–89.

[Franke et al., 1992] Franke, A., DeCamillis, M., Zink, D., Cheng, N., Brock, H., and Paro, R. (1992). Polycomb and polyhomeotic are constituents of a multimeric protein complex in chromatin of drosophila melanogaster. *EMBO J*, 8:2941–50.

[Fuhrmann, 2010] Fuhrmann, S. (2010). Eye morphogenesis and patterning of the optic vesicle. *Curr. Top. Dev. Biol.*, 93:61–84.

[Fuhrmann et al., 2014] Fuhrmann, S., Zou, C., and Levine, E. (2014). Retinal pigment epithelium development, plasticity, and tissue homeostasis. *Exp. Eye Res.*, 123:141–150.

[Gage et al., 2015] Gage, P. J., Hurd, E. A., and Martin, D. M. (2015). Mouse models for the dissection of CHD7 functions in eye development and the molecular basis for ocular defects in CHARGE syndrome. *Invest Ophthalmol Vis Sci.*, 56 (13):7923–7930.

[Gaspar-Maia et al., 2009] Gaspar-Maia, A., Alajem, A., Polesso, F., Sridharan, R., Mason, M., Heidersbach, A., Ramalho-Santos, J., McManus, M., Plath, K., Meshorer, E., and Ramalho-Santos, M. (2009). Chd1 regulates open chromatin and pluripotency of embryonic stem cells. *Nature*, 460:863–868.

[Gibson et al., 2012] Gibson, W. T., Hood, R. L., Zhan, S. H., Bulman, D. E., Fejes, A. P., Moore, R., Mungall, A. J., Eydoux, P., Babul-Hirji, R., an, J., Marra, M. A., Consortium, F. C., Chitayat, D., Boycott, K. M., Weaver, D. D., and Jones, S. J. (2012). Mutations in EZH2 cause weaver syndrome. *The American Journal of Human Genetics*, 90:110–118.

[Gil et al., 2005] Gil, J., Bernard, D., and Peters, G. (2005). Role of polycomb group proteins in stem cell self-renewal and cancer. *DNA Cell Biol.*, 2:117–25.

[Graham et al., 2005] Graham, J. J., Rosner, B., Dykens, E., and Visootsak, J. (2005). Behavioral features of CHARGE syndrome (hall-hittner syndrome) comparison with down syndrome, prader-willi syndrome, and williams syndrome. *Am J Med Genet. A.*, 3:240–7.

[Gregory-Evansa et al., 2013] Gregory-Evansa, C. Y., Wallace, V. A., and Gregory-Evans, K. (2013). Gene networks: Dissecting pathways in retinal development and disease. *Progress in Retinal and Eye Research*, 33:40–66.

[Griffin et al., 2009] Griffin, E. W., Bechara, R. G., Birch, A. M., and Kelly, A. M. (2009). Exercise enhances hippocampal-dependent learning in the rat: Evidence for a BDNF-related mechanism. *Hippocampus*, 19:973–980.

[Guil et al., 2012] Guil, S., Soler, M., Portela, A., Carrere, J., Fonalleras, E., Gomez, A., Villanueva, A., and Esteller, M. (2012). Intronic RNA mediates EZH2 regulation of epigenetic targets. *Nature Structural and Molecular Biology*, 19 (7):664–670.

[Hall, 1979] Hall (1979). Familial congenital bowing with short bones. *Radiology*, 3:611–4.

[Hall and Georgel, 2007] Hall, J. and Georgel, P. (2007). CHD proteins: a diverse family with strong ties. *Biochem Cell Biol*, 4:463–76.

[Hanson et al., 1999] Hanson, R. D., Hess, J. L., Yu, B. D., Ernst, P., van Lohuizen, M., Berns, A., van der Lugt, N. M. T., Shashikant, C. S., Ruddle, F. H., Seto, M., and Korsmeyer, S. J. (1999). Mammalian *Trithorax* and *Polycomb*-group homologues are antagonistic regulators of homeotic development. *PNAS*, 96:14372–14377.

[Hartshorne et al., 2016] Hartshorne, N., Hudson, A., MacCuspie, J., Kennert, B., Nacarato, T., Hartshorne, T., and Blake, K. (2016). Quality of life in adolescents and adults with CHARGE syndrome. *Am J Med Genet A.*, 8:2012–21.

[He et al., 2016] He, D., Marie, C., Zhao, C., Kim, B., Wang, J., Deng, Y., Clavarioly, A., Frah, M., Wang, H., He, X., Hmidan, H., Jones, B. V., Witte, D., Zalc, B., Zhou, X., Choo, D. I., Martin, D. M., Parras, C., and Lu, Q. R. (2016). Chd7 cooperates with Sox10 and regulates the onset of CNS myelination and remyelination. *Nature Neuroscience*, pages 1–12.

[Hekimoglu and Ringrose, 2009] Hekimoglu, B. and Ringrose, L. (2009). Non-coding RNAs in polycomb/trithorax regulation. *RNA Biology*, 6 (2):129–137.

[Herzog et al., 2014] Herzog, V. A., Lempradl, A., Trupke, J., Okulski, H., Altmutter, C., Ruge, F., Boidol, B., Kubicek, S., Schmauss, G., Aumayr, K., Ruf, M., Pospisilik, A., Diamond, A., Senergin, H. B., Vargas, M. L., Simon, J. A., and Ringrose, L. (2014). A strand-specific switch in noncoding transcription switches the function of Polycomb/Trithorax response elements. *Nature Genetics*, pages 1–9.

[Hirabayashi et al., 2013] Hirabayashi, Y., Suzki, N., Tsuboi, M., Endo, T., Toyoda, T., Shinga, J., Koseki, H., Vidal, M., and Gotoh, Y. (2013). Polycomb limits the neurogenic competence of neural precursor cells to promote astrogenic fate transition. *Neuron*, 5:600–13.

[Hitchler and Domann, 2013] Hitchler, M. and Domann, F. (2013). Metabolic defects provide a spark for the epigenetic switch in cancer. *Free Radic Biol Med.*, 2:115–27.

[Hittner et al., 1979] Hittner, H., Hirsch, N., Kreh, G., and Rudolph, A. (1979). Colobomatous microphthalmia, heart disease, hearing loss, and mental retardation–a syndrome. *J Pediatr Ophthalmol Stabinusmus*, 2:122–8.

[Humphrey, 1967a] Humphrey, N. (1967a). The receptive fields of visual units in the superior colliculus of the rat. *J Physiol.*, 2:86–88.

[Humphrey, 1967b] Humphrey, T. (1967b). The development of the human hippocampal fissure. *J Anat.*, 101 (Pt 4):655–76.

[Hurd et al., 2007] Hurd, E., Capers, P., Blauwkamp, M., Adams, M., Raphael, Y., Poucher, H., and Martin, D. (2007). Loss of Chd7 function in gene-trapped reporter mice is embryonic lethal and associated with severe defects in multiple developing tissues. *Mamm Genome*, 2:94–104.

[Hyun et al., 2017] Hyun, K., Jeon, J., Park, K., and Kim, J. (2017). Writing, erasing and reading histone lysine methylations. *Experimental and Molecular Medicine*, 49:e324.

[Ihrie et al., 2011] Ihrie, R., Shah, J., Harwell, C., Levine, J., Guinto, C., Lezameta, M., Kriegstein, A., and Alvarez-Buylla, A. (2011). Persistent *sonic hedgehog* signaling in adult brain determines neural stem cell positional identity. *Neuron*, 2:250–62.

[Ingham, 1985] Ingham, P. (1985). A clonal analysis of the requirement for the *trithorax* gene in the diversification of segments in *Drosophila*. *Journal of Embryol. exp. Morph.*, 89:349–365.

[Jacobs et al., 2008] Jacobs, S., Harp, J., Devarakonda, S., Kim, Y., Rastinejad, F., and Khorasanizadeh, S. (2008). The active site of the SET domain is constructed on a knot. *Nat Struct Biol.*, 11:833–8.

[Janssen et al., 2012] Janssen, N., Bergman, J., Swertz, M., Tranebjaerg, L., Lodahl, M., Schoots, J., Hofstra, R., van Ravenswaaij-Arts, C., and Hoefsloot, L. (2012). Mutation update on the CHD7 gene involved in CHARGE syndrome. *Hum Mutat.*, 8:1149–60.

[Jones et al., 2015] Jones, K., Saric, N., Russell, J., Andoniadou, C., Scambler, P., and Basson, M. (2015). CHD7 maintains neural stem, cell quiescence and prevents premature stem cell depletion in adult hippocampus. *Stem Cells*, 33:196–210.

[Jongmans et al., 2006] Jongmans, M., Admiraal, R., van der Donk, K., Vissers, L., Baas, A., Kapusta, L., van Hagen, J., Donnai, D., de Ravel, T., Veltman, J., van Kessel, A., Vries, B. D., Brunner, H., Hoefsloot, L., and van Ravenswaaij, C. (2006). CHARGE syndrome: the phenotypic spectrum of mutations in the CHD7 gene. *J Med Genet.*, 4:306–14.

[Jongmans et al., 2008] Jongmans, M., Hoefsloot, L. H., van der Donk, K. P., Admiraal, R. J., Mangee, A., van de Laar, I., Hendriks, Y., Verheij, J. B., Walpole, I., Brunner, H. G., and van Ravenswaaij, C. M. (2008). Familial CHARGE syndrome and the CHD7 gene: A recurrent missense mutation. *American Journal of Medical Genetics Part A*, 146A:43–50.

[Kandaje et al., 2015] Kandaje, A., Meuleman, W., Ernst, J., Bilenky, A., Yen, A., Heravi-Moussavi, A., Kherapour, P., Zhang, Z., Wang, J., Ziller, M. J., Amin, V., Whitaker, J. W., Schulz, M. D., Ward, L. D., Sarkar, A., Quon, G., Sandstrom, R. S., Eaton, M. L., Wu, Y.-C., Pfenning, A. R., Wang, X., Claussnitzer, M., Liu, Y., Coarfa, C., Harris, R. A., Shoresh, N., Epstein, C. B., Gjoneska, E., Leung, D., Xie, W., Hawkins, R. D., Lister, R., Hong, C., Gascard, P., Mungall, A. J., Moore, R., Chuah, E., Tam, A., Canfield, T. K., Hansen, R. S., Kaul, R., Sabo, P. J., Bansal, M. S., Carles, A., Dixon, J. R., Farh, K.-H., Feizi, S., Karlic, R., Kim, A.-R., Kulkarni, A., Li, D., Lowdon, R., a d Tim R. Mercer, G. E., Neph, S. J., Onuchic, V., Polak, P., Rajagopal, N., Ray, P., Sallari, R. C., Siebenthall, K. T., Sinnott-Amstrong, N. A., Stevens, M., thurman abd Jie Wu, R. E., Zhang, B., Zhou, X., e. Beaudet, A., Boyer, L. A., DeJager, P. L., Farnham, P. J., Fisher, S. J., Haussler, D., Jones, S. J. M., Li, W., Marra, M. A., McManus, M. T., Sunyaev, S., Thomson, J. A., Tlsty, T. D., Tsai, L.-H., Wang, W., Waterland, R. A., Zhang, M. Q., Chadwick, L. H., Bernstein, B. E., Costello, J. F., Ecker, J. R., Hirst, M., Meissner, A., Milosavljevic, A., Ren, B., Stamatoyannopoulos, J. A., Wang, T., and Kellis, M. (2015). Integrative analysis of 111 reference human epigenomes. *Nature*, 518:317–328.

[Kaneko et al., 2014] Kaneko, S., Bonasio, R., Saldana-Meyer, R., Yoshida, T., Son, J., Nishino, K., Umezawa, A., and Reinberg, D. (2014). Interactions between JARID2 and noncoding RNAs regulate PRC2 recruitment to chromatin. *Molecular Cell*, 53:1–11.

[Kaneko et al., 2010] Kaneko, S., Li, G., Son, J., Xu, C.-F., Margueron, R., Neubert, T. A., and Reinberg, D. (2010). Phosphorylation of the PRC2 component EZH2 is cell cycle-regulared and up-regulates its binding to ncRNA. *Gene and Development*, 24:2615–2620.

[Kaneko et al., 2013] Kaneko, S., Son, J., Shen, S. S., Reinberg, D., and Bonasio, R. (2013). PRC2 binds active promotors and contacts nascent RNAs in embryonic stem cells. *Nature Structure and molecular Biology*, 20:1258–1264.

[Kim et al., 2013] Kim, E., Kim, M., Woo, D., Shin, Y., Shin, J., Chang, N., Oh, Y., Kim, H., Rheey, J., Nakano, I., Lee, C., Joo, K., Rich, J., Nam, D., and Lee, J. (2013). Phosphorylation of EZH2 activates STAT3 signaling via STAT3 methylation and promotes tumorigenicity of glioblastoma stem-like cells. *Cancer Cell*, 6:839–52.

[Kim et al., 2007] Kim, E., Leung, C., and Johnson, R. R. J. (2007). In vivo analysis of Ascl1 defined progenitors reveals distinct developmental dynamics during adult neurogenesis and gliogenesis. *J Neuroscience*, 47:12764–74.

[Kim et al., 2011] Kim, M., Chung, N., Kang, M., Yoo, N., and Lee, S. (2011). Genetic and expressional alterations of CHD genes in gastric and colorectal cancers. *Histopathology*, 58(5):660–8.

[Klymenko and Mueller, 2004] Klymenko, T. and Mueller, J. (2004). The histone methyltransferase Trithorax and Ash1 prevent transcriptional silencing by polycomb group proteins. *EMBO reports*, 5:373–377.

[Klymenko et al., 2006] Klymenko, T., Papp, B., Fischle, W., Koecher, T., Schelder, M., Fritsch, C., Wild, B., Wilm, M., and Mueller, J. (2006). A polycomb group protein complex with sequence-specific DNA-binding and selective methyl-lysine-binding activities. *Genes Dev.*, 9:1110–22.

[Knoth et al., 2010] Knoth, R., Singec, I., Ditter, M., Pantazis, G., Capetian, P., Meyer, R. P., Horvat, V., Volk, B., and Kempermann, G. (2010). Murine features of neurogenesis in the human hippocampus across the lifespan from 0 to 100 years. *PLoS One*, 1::e8809. doi: 10.1371/journal.pone.0008809.

[Kohli and Zhang, 2013] Kohli, R. and Zhang, Y. (2013). TET enzymes, TDG and the dynamics of DNA demethylation. *Nature*, 502(7472):472–9.

[Kolybaba and Classen, 2014] Kolybaba, A. and Classen, A.-K. (2014). Sensing cellular states-signaling to chromatin pathways targeting polycomb and trithorax group function. *Cell Tissue Res*, 356:477–493.

[Koster et al., 2015] Koster, M., Snel, B., and Timmers, H. (2015). Genesis of chromatin and transcription dynamics in the origin of species. *Cell*, 161:724–731.

[Kuzmichev et al., 2004] Kuzmichev, A., Jenuwein, T., Tempst, P., and Reinberg, D. (2004). Different EZH2-containing complexes target methylation of histone H1 or nucleosomal histone H3. *Mol Cell*, 2:183–93.

[Kuzmichev et al., 2005] Kuzmichev, A., Margueron, R., Vaquero, A., Preissner, T. S., Scher, M., Kirmizis, A., Ouyang, X., Brockdorff, N., Abate-Shen, C., Farnham, P., and Reinberg, D. (2005). Composition and histone substrates of polycomb repressive group complexes change during cellular differentiation. *PNAS*, 102:1859–1864.

[Kuzmichev et al., 2002] Kuzmichev, A., Nishioka, K., Erdjument-Bromage, H., Tempst, P., and Reinberg, D. (2002). Histone methyltransferase activity associated with a human multiprotein complex containing the enhancer of zeste protein. *Genes Dev.*, 22:2893–905.

[Lalani et al., 2005] Lalani, S. R., Safiullah, A. M., Fernbach, S. D., Harutyunyan, K. G., Thaller, C., Peterson, L. E., McPherson, J. D., Gibbs, R. A., White, L. D., Hefner, M., l.H. Davenport, S., Jr., J. M. G., Bacino, C. A., Glass, N. L., Towbin, J. A., Craigen, W. J., Neish, S. R., Lin, A. E., and Belmont, J. W. (2005). Spectrum of CHD7 mutations in 110 individuals with CHARGE syndrome and genotype-phenotype correlation. *The American Journal of Human Genetics*, 78:303–314.

[Layman et al., 2010] Layman, W., Hurd, E., and Martin, D. (2010). Chromodomain proteins in development: lessons from CHARGE syndrome. *Clin Genet.*, 1:11–20.

[Lee et al., 2014] Lee, W., Teckie, S., Wiesner, T., Ran, L., Granada, C. N. P., Lin, M., Zhu, S., Cao, Z., Liang, Y., Sboner, A., Tap, W. D., Fletcher, J. A., Hubermann, K. H., Qin, L.-X., Viale, A., Singer, S., Zheng, D., Berger, M., Chen, Y., Antonescu, C. R., and Chi, P. (2014). PRC2 is recurrent inactivated through EED or SUZ12 loss in malignant peripheral nerve sheath tumors. *Nature Genetics Letter*, pages 1–6.

[Leung et al., 0015] Leung, D., Jung, I., Rajagopal, N., Schmitt, A., Selvarja, S., Lee, A. Y., Yen, C.-A., Lin, S., Lin, Y., Qiu, Y., Xie, W., Yue, F., Hariharan, M., Ray, P., Kuan, S., Edsall, L., Yang, H., Chi, N. C., Zhang, M. Q., Ecker, J. R., and Ren, B. (20015). Integrative analysis of haplotype-resolved epigenomes across human tissues. *Letter to Nature*, 518:350–354.

[Liao et al., 2012] Liao, G.-Y., An, J. J., Gharami, K., Waterhouse, E. G., and Vanevski, F. (2012). Dendritically targeted BDNF is essential for energy balance and response to leptin. *Nature Medicine*, 18 (4):564–571.

[Liu et al., 2016] Liu, J., Zhu, Y., Luo, G., Wang, X., Yue, Y., Wang, X., Zong, X., Chen, K., Yin, H., Fu, Y., Han, D., Wang, Y., Chen, D., and He, C. (2016). Abundant DNA 6ma methylation during early embryogenesis of zebrafish and pig. *Nat Commun.*, 7:13052.

[Liu et al., 2014] Liu, L., Yu, T., Wang, L., Mo, X., and Yu, Y. (2014). A novel CHD7 mutation in a chinese patient with CHARGE syndrome. *Meta Gene*, pages 469–478.

[Liu et al., 2013] Liu, Y., Harmelink, C., Peng, Y., Chen, Y., Wang, Q., and Jiao, K. (2013). CHD7 interacts with BMP R-SMADs to epigenetically regulate cardiogenesis in mice. *HMG*, pages 1–36.

[Lledo et al., 2008] Lledo, P., Merkle, F., and Alvarez-Buylla, A. (2008). Origin and function of olfactory bulb interneuron diversity. *Trends Neuroscience*, 8:392–400.

[Luger et al., 1997] Luger, K., Rechsteiner, T., Flaus, A., Waye, M., and Richmond, T. (1997). Characterization of nucleosome core particles containing histone proteins made in bacteria. *J Mol Biol*, 3:301–11.

[Ma et al., 2010] Ma, D., Marchetto, M., Guo, J., Ming, G., Gage, F., and Song, H. (2010). Epigenetic choreographers of neurogenesis in the adult mammalian brain. *Nat Neurosci*, 11:1338–44.

[Machado et al., 2019] Machado, R., Schneider, H., DeOcesano-Pereira, C., Lichtenstein, F., Andrade, F., Fujita, A., Trombetta-Lima, M., Weller, M., Bowman-Colin, C., and Sogayar, M. (2019). CHD7 promotes glioblastoma cell motility and invasiveness through transcriptional modulation of an invasion signature. *Sci Rep.*, 9:3952.

[Maletic-Savatic and Malinow, 1999] Maletic-Savatic, M. and Malinow, R. (1999). Rapid dendritic morphogenesis in CA1 hippocampal dendrites induced by synaptic activity. *Science*, 283 (5409):1923–1927.

[Manning and Yusufzai, 2017] Manning, B. and Yusufzai, T. (2017). The ATP-dependent chromatin remodeling enzymes CHD6, CHD7, and CHD8 exhibit distinct nucleosome binding and remodeling activities. *J Biol Chem*, 28:11927–11936.

[Marfella and Imbalzano, 2007] Marfella, C. and Imbalzano, A. (2007). The Chd family of chromatin remodelers. *Mutat Res*, 1-2:30–40.

[Marfella et al., 2006] Marfella, C., Ohkawa, Y., Coles, A., Garlick, D., Jones, S., and Imbalzano, A. (2006). Mutation of the SNF2 family member Chd2 affects mouse development and survival. *J Cell Physiol.*, 1:162–71.

[Margueron et al., 2008] Margueron, R., Li, G., Sarma, K., Blais, A., Zavadil, J., Woodcock, C., Dynlacht, B., and Reinberg, D. (2008). Ezh1 and Ezh2 maintain repressive chromatin through different mechanisms. *Mol Cell*, 4:503–18.

[Marie et al., 2018] Marie, C., Clavairoly, A., Frah, M., Hmidan, H., Yan, J., Zhao, C., Steenwinckel, J. V., Daveau, R., Zalc, B., Hassan, B., Thomas, J.-L., Gressens, P., Ravassard, P., Mozer, I., Martin, D. M., Lu, Q. R., and Parras, C. (2018). Oligodendrocyte precursor survival and differentiation requires chromatin remodeling by Chd7 and Chd8. *PNAS*, 115(35):E8246–E8255.

[Marigere et al., 2003] Marigere, F., Givalois, L., Rage, F., Arancibia, S., and Tapia-Arancibia, L. (2003). Rapid induction of BNDF expression in the hippocampus during immobilization stress challenge in adult rats. *Hippocampus*, 13:646–655.

[Marosi and Mattson, 2014] Marosi, K. and Mattson, M. P. (2014). BDNF mediates adaptive brain and body responses to energetic challenges. *Cell Press Review*, 25:89–98.

[Martin et al., 2005] Martin, C., Cao, R., and Zhang, Y. (2005). Substance preferences of the EZH2 histone methyltransferase complex. *The Journal of Biological Chemistry*, 281:8365–8370.

[McCabe et al., 2012] McCabe, M. T., Ott, H. M., Ganji, G., Korenchuk, S., Thompson, C., Aller, G. S. V., Liu, Y., Graves, A. P., III, A. D. P., Diaz, E., LaFrance, L. V., Mellinger, M., Duqenne, C., Tian, X., Kruger, R. G., McHugh, C. F., Brandt, M., Miller, W. H., Dhanak, D., Verma, S. K., and Tummino, P. J. (2012). EZH2 inhibition as a therapeutic strategy. *Nature Letter*, 492:108–112.

[Micucci et al., 2013] Micucci, J. A., Layman, W. S., Hurd, E. A., Sperry, E. A., Frank, S. F., Durham, M. A., Swiderski, D. L., Skidmore, J. M., Scacheri, P. C., Raphael, Y., and Martin, D. M. (2013). CHD7 and retinoic acid signaling cooperate to regulate neural stem cell and inner ear development in mouse models of CHARGE syndrome. *Human Molecular Genetics*, pages 1–15.

[Min et al., 2002] Min, J., Zhang, X., Cheng, X., Grewal, S., and Xu, R. (2002). Structure of the SET domain histone lysine methyltransferase Clr4. *Nat Struct Biol.*, 11:828–32.

[Min et al., 2003] Min, J., Zhang, Y., and Xu, R.-M. (2003). Structural basis of specific binding of Polycomb chromodomain to histone H3 methylated at Lys 27. *Genes and Development*, 17:1823–1828.

[Modarresi et al., 2012] Modarresi, F., Faghihi, M. A., Lopez-Toledano, M. A., Fatemi, R. P., Magistri, M., Brothers, S. P., van der Brug, M. P., and Wahlestedt, C. (2012). Inhibition of natural antisense transcripts *in vivo* results in gene-specific transcriptional upregulation. *Nature Biotechnology*, 30 (5):453–459.

[Moore et al., 2019] Moore, S., Berger, N., Luijsterburg, M., Piett, C., Stanley, F., Schraeder, C., Fang, S., Chan, J., Schriemer, D., Nagel, Z., van Attikum, H., and Goodarzi, A. (2019). The CHD6 chromatin remodeler is an oxidative DNA damage response factor. *Nat Commun.*, 10(1):241.

[Morin-Kensicki et al., 2001] Morin-Kensicki, E., Faust, C., LaMantia, C., and Magnuson, T. (2001). Cell and tissue requirements for the gene eed during mouse gastrulation and organogenesis. *Genesis*, 4:142–6.

[Moshkin et al., 2007] Moshkin, Y., Mohrmann, L., van Ljcken, W., and Verrijzer, C. (2007). Functional differentiation of SWI/SNF remodelers in transcription and cell cycle control. *Mol Cell Biol.*, 27(2):651–61.

[Mucci et al., 2015] Mucci, J. A., Sperry, E. D., and Martin, D. M. (2015). Chromodomain helicase DNA-binding proteins in stem cells and human development. *Stem Cell and Development*, 24:917–925.

[Neylon et al., 2012] Neylon, O. M., Werther, G. A., and Sabin, M. A. (2012). Overgrowth syndromes. *Current Opinion Review*, 24:505–511.

[Ng et al., 2000] Ng, J., Hart, C., Morgan, K., and Simon, J. (2000). A drosophila ESC-E(Z) protein complex is distinct from other polycomb group complexes and contains covalently modified ESC. *Mol Cell Biol.*, 9:3069–78.

[Nishina et al., 2012] Nishina, S., Kosaki, R., Yagihashi, T., Azuma, N., Okamoto, N., Hatsukawa, Y., Kurosawa, K., Yamane, T., Mizuno, S., Tsuzuki, K., and Kosaki, K. (2012). Ophthalmic features of CHARGE syndrome with CHD7 mutations. *Am J Med Genet A.*, 3:514–8.

[Ogier et al., 2013] Ogier, J. M., Carpinelli, M., Arhatari, B., Symons, R. A., Kile, B., and Burt, R. A. (2013). CHD7 deficiency in "looper", a new mouse model of CHARGE syndrome, results in ossicle malformation, otosclerosis and hearing impairment. *PLOS*, 9(5):1–11.

[Ohta et al., 1999] Ohta, Y., Suzuki, N., Nakamura, S., Hartwig, J., and Stossel, T. (1999). The small GTPase RalA targets filamin to induce filopodia. *Proc. Natl. Acad. Sci. U.S.A.*, 96(5):2122?8.

[Pagon et al., 1981] Pagon, R., Graham, J. J., Zonana, J., and Yong, S. (1981). Coloboma, congenital heart disease, and choanal atresia with multiple anomalies: CHARGE association. *J Pediatr*, 2:223–7.

[Parras et al., 2004] Parras, C., Galli, R., ans S Soares, O. B., Galichet, C., Battiste, J., Johnson, J., Nakafuku, M., Vescovi, A., and Guillemot, F. (2004). Mash1 specifies neurons and oligodendrocytes in the postnatal brain. *EMBO J*, 22:4495–505.

[Pasini et al., 2007] Pasini, D., Bracken, A., Hansen, J., Capillo, M., and Helin, K. (2007). The polycomb group protein Suz12 is required for embryonic stem cell differentiation. *Mol Cell Biol.*, 10:3769–79.

[Pasini et al., 2004] Pasini, D., Bracken, A., Jensen, M., Denchi, E. L., and Helin, K. (2004). Suz12 is essential for mouse development and for EZH2 histone methyltransferase activity. *EMBO J*, 20:4061–71.

[Pauli et al., 2009] Pauli, S., Pieper, L., Haeberle, J., Grzmil, P., Burfeind, P., Steckel, M., Lenz, U., and Michelmann, H. (2009). Proven germline mosaicism in a father of two children with CHARGE syndrome. *Clin Genet.*, 75(5):473–9.

[Pearce et al., 1992] Pearce, J., Singh, P., and Gaunt, S. (1992). The mouse has a polycomb-like chromobox gene. *Development*, 114:921–9.

[Pereira et al., 2010] Pereira, J. D., Sansom, S. N., Smith, J., Dobenecker, M.-W., Tarakhovsky, A., and Livesey, F. J. (2010). Ezh2, the histone methyltransferase of PRC2, regulates the balance between self-renewal and differentiation in the cerebral cortex. *PNAS*, 36:15957–15962.

[Prancknien et al., 2019] Prancknien, L., Preiksaitien, E., Gueneau, L., Reymond, A., and Kuinskas, V. (2019). *De Novo* duplication in the chd7 gene associated with severe CHARGE syndrome. *Genomics Insights.*, page doi: 10.1177/1178631019839010.

[Pray-Grant et al., 2005] Pray-Grant, M., Daniel, J., Schieltz, D., 3rd Yates, J., and Grant, P. (2005). Chd1 chromodomain links histone H3 methylation with SAGA- and SLIK-dependent acetylation. *Nature*, 7024:434–8.

[Qi et al., 2014] Qi, C., Liu, S., Qin, R., Zhang, Y., Wang, G., Shang, Y., Wang, Y., and Liang, J. (2014). Coordinated regulation of dendrite aborization by epigenetic factor CDYL and EZH2. *The Journal of Neuroscience*, 34 (13):4494–4508.

[Qian et al., 2016] Qian, X., Nguyen, H. N., Song, M. M., Hadiomo, C., Ogden, S. C., Hammack, C., Yao, B., Hamersky, G. R., Jacob, F., Zhong, C., jin Yoon, K., Jeang, W., Lin, L., Li, Y., Thakor, J., Berg, D. A., Zhang, C.,

Kang, E., Chickering, M., Nauen, D., Ho, C.-Y., Wen, Z., M-christian, K., Shi, P.-Y., Maher, B. J., Wu, H., Jin, P., Tang, H., Song, H., and li Ming, G. (2016). Brain-region-specific organoids using mini-bioreactor for modeling ZIKV exposure. *Cell*, 165:1–17.

[Radecki et al., 2005] Radecki, D. T., Brown, L. M., Martinez, J., and Teyler, T. J. (2005). BDNF protects against stress-induced impairments in spatial learning and memory LTP. *Hippocampus*, 15:246–253.

[Raedt et al., 2014] Raedt, T. D., Beert, E., Pamant, E., Luscan, A., Brems, H., Ortonne, N., Helin, K., Hornick, J. L., Mautner, V., Kehrer-Swatzki, H., Clapp, W., Brandner, J., Vidaud, M., Legius, M. U. E., and Cichowski, K. (2014). PRC2 loss amplifies ras-driven transcription and confers sensitive to BRD4-based therapies. *Nature Letter*, 514:1–12.

[Randall et al., 2009] Randall, V., McCue, K., Roberts, C., Kyriakopoulou, V., Beddow, S., Barrett, A., Vitelli, F., Prescott, K., Shaw-Smith, C., Devriendt, K., Bosman, E., Steffes, G., Steel, K., Simrick, S., Basson, M., Illingworth, E., and Scambler, P. (2009). Great vessel development requires biallelic expression of Chd7 and Tbx1 in pharyngeal ectoderm in mice. *J Clin Inv*, 11:3301–10.

[Rhodes et al., 2018] Rhodes, C. T., Zunino, G., Huang, S.-W. A., Cardona, S. M., Cardona, A. E., Berger, M. S., Lemmon, V. P., and Lina, C.-H. A. (2018). Region specific knock-out reveals distinct roles of chromatin modifiers in adult neurogenic niches. *Cell Cycle*, 17(3):377–389.

[Ribak et al., 1985] Ribak, C., Seress, L., and Amaral, D. (1985). The development, ultrastructure and synaptic connections of the mossy cells of the dentate gyrus. *J Neurocytol.*, 355:277–81.

[Riising et al., 2008] Riising, E., Boggio, R., Chiocca, S., Helin, K., and Pasini, D. (2008). The PRC2 is a potential target of SUMO modifications. *PLoS One*, 7:e2704.

[Ronan et al., 2013] Ronan, J., Wu, W., and Crabtree, G. (2013). From neural development to cognition: unexpected roles for chromatin. *Nat Rev Genet*, 5:347–59.

[Scheuermann et al., 2010] Scheuermann, J., de Ayala Alonso, A., Oktaba, K., Ly-Hartig, N., McGinty, R., Fraterman, S., Wilm, M., TW, T. M., and Mueller, J. (2010). Histone H2A deubiquitinase activity of the polycomb repressive complex PR-DUB. *Nature*, 7295:243–7.

[Schmitt et al., 2005] Schmitt, S., Prestel, M., and Paro, R. (2005). Intergenic transcription through a polycomb group response element counteracts silencing. *Genes and Development*, 19:697–708.

[Schnetz et al., 2009] Schnetz, M., Bartels, C., Shastri, K., Balasubramanian, D., Zentner, G., Balaji, R., Zhang, X., Song, L., Wang, Z., Laframboise, T., Crawford, G., and Scacheri, P. (2009). Genomic distribution of CHD7 on chromatin tracks h3k4 methylation patterns. *Genome Res.*, 19(4):590–601.

[Schoberleitner et al., 2019] Schoberleitner, I., Mutti, A., Sah, A., Wille, A., Gimeno-Valiente, F., Piatti, P., Kharitonova, M., Torres, L., Lopez-Rodas, G., Liu, J., Singewald, N., Schwarzer, C., and Lusser, A. (2019). Role for chromatin remodeling factor Chd1 in learning and memory. *Front Mol Neuroscience*, 23:12:3.

[Schuettengruber et al., 2007] Schuettengruber, B., Chourrout, D., Vervoort, M., Leblanc, B., and Cavalli, G. (2007). Genome regulation by polycomb and trithorax proteins. *Cell*, 4:735–45.

[Schulz et al., 2014] Schulz, Y., Freese, L., Maenz, J., Zoll, B., Voelter, C., Brockmann, K., Boegershausen, N., Becker, J., Wollnik, B., and Pauli, S. (2014). CHARGE and Kabuki syndromes: A phenotipic and molecular link. *HMG*, pages 1–22.

[Schuster and Stoeger, 2002] Schuster, E. and Stoeger, R. (2002). CHD5 defines a new subfamily of chromodomain-SWI2/SNF2-like helicases. *Mamm Genome*, 2:117–9.

[Schwartz and Pirrotta, 2013] Schwartz, Y. and Pirrotta, V. (2013). A new world of polycomb: unexpected partnerships and emerging functions. *Nat Rev Genet*, 12:853–64.

[Shim et al., 2012] Shim, S., Kwan, K. Y., Li, M., Lefebvre, V., and Sestan, N. (2012). *Cis*-regulatory control of corticospinal system development and evolution. *Nature*, 486:74–79.

[Shur and d Benayahu, 2005] Shur, I. and d Benayahu (2005). Characterization and functional analysis of CReMM, a novel chromodomain helicase DNA-binding protein. *J Mol Biol.*, 3:646–55.

[Shur et al., 2006a] Shur, I., Socher, R., and Benayahu, D. (2006a). *In vivo* association of CReMM/CHD9 with promoters in osteogenic cells. *J Cell Physiol.*, 2:374–8.

[Shur et al., 2006b] Shur, I., Solomon, R., and Benayahu, D. (2006b). Dynamic interactions of chromatin-related mesenchymal modulator, a chromodomain helicase-dna-binding protein, with promoters in osteoprogenitors. *Stem Cells*, 5:1288–93.

[Simon and Tamkun, 2002] Simon, J. A. and Tamkun, J. W. (2002). Programming off and on states in chromatin: mechanism of Polycomb and

Trithorax group complexes. *Current Opinion in Genetics and Development*, 12:210–218.

[Smith and Peterson, 2005a] Smith and Peterson (2005a). ATP-dependent chromatin remodeling. *Curr Top Dev Biol.*, 65:115–48.

[Smith and Peterson, 2005b] Smith, C. and Peterson, C. (2005b). A conserved Swi2/Snf2 atpase motif couples ATP hydrolysis to chromatin remodeling. *Mol Cell Biol.*, 14:5880–92.

[Song et al., 2011] Song, M. H., Cho, H.-J., Kee, H. K., Kwon, T. J., Lee, W.-S., Oh, S., Bok, J., Choi, J. Y., and Kim, U.-K. (2011). CHD7 mutational analysis and clinical considerations for auditory rehabilitation in deaf patients with CHARGE syndrome. *PLOS One*, 6:1–9.

[Sparmann and van Lohuizen, 2006] Sparmann, A. and van Lohuizen, M. (2006). Polycomb silencer control cell fate, development and cancer. *Nature reviews*, pages 846–856.

[Sperry et al., 2014] Sperry, E., Hurd, E., Durham, M., Reamer, E., Stein, A., and Martin, D. (2014). The chromatin remodeling protein CHD7, mutated in CHARGE syndrome, is necessary for proper craniofacial and tracheal development. *Developmental Dynamics*, 9:1055–66.

[Srinivasan et al., 2008] Srinivasan, S., Dorighi, K. M., and Tamkun, J. W. (2008). *Drosophila* Kismet regulates histone H3 lysine 27 methylation and early elongation by RNA polymerase II. *PLOS*, 10:1–14.

[Steffen et al., 2013] Steffen, P. A., Fonseca, J. P., Gaenger, C., Dworschak, E., Kockmann, T., Beisel, C., and Ringrose, L. (2013). Quantitative *in vivo* analysis of chromatin binding of Polycomb and Trithorax group proteins reveals retention of ASH1 on mitotic chromatin. *Nucleic Acids Research*, pages 1–16.

[Steffen and Ringrose, 2014] Steffen, P. A. and Ringrose, L. (2014). What are memories made of? How polycomb and trithorax proteins mediate epigenetic memory. *Nature Reviews Molecular Cell Biology*, 15:340–356.

[Stenkamp, 2015] Stenkamp, D. (2015). Development of the vertebrate eye and retina. *Prog Mol Biol Transl Sci.*, 134:397–414.

[Stokes and Perry, 1995] Stokes, D. and Perry, R. (1995). DNA-binding and chromatin localization properties of CHD1. *Mol Cell Biol.*, 5:2745–53.

[Tai et al., 2003] Tai, H., Geisterfer, M., Bell, J., Moniwa, M., Davie, J., Boucher, L., and McBurney, M. (2003). CHD1 associates with NCoR and histone deacetylase as well as with RNA splicing proteins. *Biochem Biophys Res Commun*, 1:170–6.

[Takada et al., 2007] Takada, I., Mihara, M., Suzawa, M., Ohtake, F., Kobayashi, S., Igarashi, M., Youn, M., Takeyama, K., Nakamura, T., Mezaki, Y., Takezawa, S., Yogiashi, Y., Kitagawa, H., Yamada, G., Takada, S., Minami, Y., Shibuya, H., Matsumoto, K., and Kato, S. (2007). A histone lysine methyltransferase activated by non-canonical Wnt signalling suppresses PPAR-gamma transactivation. *Nat Cell Biol.*, 11:1273–85.

[Tang et al., 2004] Tang, X., Milyavsky, M., Shats, I., Erez, N., Goldfinger, N., and Rotter, V. (2004). Activated p53 suppresses the histone methyltransferase EZH2 gene. *Oncogene*, 34:5759–69.

[Tatton-Brown et al., 2013] Tatton-Brown, K., Murray, A., Hanks, S., Douglas, J., Armstrong, R., Banka, S., brid, L. M., Clericuzio, C. L., Cormier-Daire, V., Cuching, T., Flinter, F., Jacquemont, M.-L., Joss, S., Kinning, E., Lynch, S. A., Magee, A., McConnell, V., Medeira, A., Ozono, K., Patton, M., Rankin, J., Shears, D., Simon, M., Splitt, M., Strenger, V., Stuurmann, K., Taylor, C., Titheradge, H., Maldergem, L. V., Temple, I. K., Cole, T., Seal, S., Consortium, C. O., and Rahman, N. (2013). Weaver syndrome and EZH2 mutations: clarifying the clinical phenotype. *American Journal of Medical Genetics*, pages 1–9.

[Tatton-Brown et al., 2014] Tatton-Brown, K., Seal, S., Ruakr, E., Harmer, J., Ramsay, E., del Vecchio Durate, S., Zachariou, A., Hanks, S., O'Brien, E., Aksglaede, L., Bralle, D., Dabir, T., Gener, B., Goudie, D., Homfray, T., Kumar, A., Pilz, D. T., Selicorni, A., Temple, K., Maldergem, L. V., Yachelevich, N., Consortium, C. O., van Montfort, R., and Rahman, N. (2014). Mutations in the DNA methyltransferase gene DNMT3A cause an overgrowth syndrome with intellectual disability. *Nature Genetics Letters*, pages 1–4.

[Tie et al., 2009] Tie, F., Banerjee, R., Jayashree, C. A. S., Prasad-Sinha, Stepanik, V., Zlobin, A., Diaz, M. O., Scacheri, P. C., and Harte, P. J. (2009). CBP-mediated acetylation of histone H3 lysine 27 antagonizes *Drosophila* Polycomb silencing. *Development*, 136:3131–3141.

[Tie et al., 2014] Tie, F., Banjerjee, R., Saiakhova, A. R., Howard, B., Monteith, K. E., Scacheri, P. C., Cosgrove, M. S., and Harte, P. J. (2014). Trithorax monomethylates histone H3K4 and interacts directly with CBP to promote H3K27 acetylation and antagonize Polycomb silencing. *The Company of Biologists*, 141:1129–1139.

[Tong et al., 1998] Tong, J., Hassig, C., Schnitzler, G., Kingston, R., and Schreiber, S. (1998). Chromatin deacetylation by an ATP-dependent nucleosome remodelling complex. *Nature*, 6705:917–21.

[Trievel et al., 2004] Trievel, R., Beach, B., Dirk, L., Houtz, R., and Hurley, J. (2004). Structure and catalytic mechanism of a SET domain protein methyltransferase. *Cell*, 1:91–103.

[Tsankov et al., 2015] Tsankov, A. M., Gu, H., Akopian, V., Ziller, M., Donaghey, J., Amit, I., Gnirke, A., and Meissner, A. (2015). Transcription factor binding dynamics during human ES cell differentiation. *Nature*, 518:344–349.

[Tsankova et al., 2006] Tsankova, N. M., Berton, O., Renthal, W., Kumar, A., Neve, R. L., and Nestler, E. J. (2006). Sustained hippocampal chromatin regulation in a mouse model of depression and antidepressant action. *Nature Neuroscience*, 9 (4):519–525.

[Tsukiyama, 2002] Tsukiyama, T. (2002). The *in vivo* functions of ATP-dependent chromatin-remodelling factors. *Nat Rev Mol Cell Biol.*, 3(6):422–9.

[Tsukiyama and Wu, 1995] Tsukiyama, T. and Wu, C. (1995). Purification and properties of an atp-dependent nucleosome remodeling factor. *Cell*, 83:1011–1020.

[van Nostrada et al., 2014] van Nostrada, J. L., Brady, C. A., Jung, H., Fuentes, D. R., Kozak, M. M., Johnson, T. M., Lin, C.-J., Swiderski, D. L., Vogel, H., Bernstein, J. A., Attie-Bitach, T., Chang, C.-P., Wysocka, J., Martin, D. M., and Attardi, L. D. (2014). Inappropiate p53 activation during development induces features of CHARGE syndrome. *Nature Letter*, pages 1–16.

[Vesseur et al., 2016] Vesseur, A., Langereis, M., Free, R., van Ravenswaaij-Arts, A. S. C., and Mylanus, E. (2016). Influence of hearing loss and cognitive abilities on language development in CHARGE syndrome. *Am J Med Genet.*, 8:2022–30.

[Villate et al., 2018] Villate, O., Ibarluzea, N., Fraile-Bethencourt, E., Valenzuela, A., Velasco, E., Grozeva, D., Raymond, F., Botella, M., and Tejada, M. (2018). Functional analyses of a novel splice variant in the CHD7 gene, found by next generation sequencing, confirm its pathogenicity in a spanish patient and diagnose him with CHARGE syndrome. *Front Genet.*, 9:7.

[Vissers et al., 2004] Vissers, L., van Ravenswaaij, C., Admiraal, R., Hurst, J., de Vries, B., van der Vliet, I. J. W., Huys, E., de Jong, P., Hamel, B., Schoenmakers, E., Brunner, H., Veltman, J., and van Kessel, A. (2004). Mutations in a new member of the chromodomain gene family cause CHARGE syndrome. *Nat Genet.*, 9:955–7.

[Wei et al., 2010] Wei, Y., Chen, Y., Li, L., Lang, J., Yeh, S., Shi, B., Yang, C., Yang, J., Lin, C., Lai, C., and Hung, M. (2010). CDK1-dependent phosphorylation of EZH2 suppresses methylation of H3K27 and promotes osteogenic differentiation of human mesenchymal stem cells. *Nat Cell Biol.*, 1:87–94.

[Weiss et al., 2012] Weiss, O., Kaufman, R., Michaeli, N., and Inbal, A. (2012). Abnormal vasculature interferes with optic fissure closure in lmo2 mutant zebrafish embryos. *Developmental Biology*, 369:191–198.

[Whittaker et al., 2017] Whittaker, D., Kasah, S., Donovan, A., Ellegood, J., Riegman, K., Volk, H., McGonnell, I., Lerch, J., and Basson, M. (2017). Distinct cerebellar foliation anomalies in a CHD7 haploinsufficient mouse model of CHARGE syndrome. *Am J Med Genet C Semin Med Genet.*, 4:doi: 10.1002/ajmg.c.31595.

[Wilson et al., 2002] Wilson, J., Jing, C., Walker, P., Howell, S. M. S., Blackburn, G., Gamblin, S., and Xiao, B. (2002). Crystal structure and functional analysis of the histone methyltransferase SET7/9. *Cell*, 1:105–15.

[Winston and Carlson, 1992] Winston, F. and Carlson, M. (1992). Yeast SNF/SWI transcriptional activators and the spt/sin chromatin connection. *Trends Genet.*, 8:387–391.

[Wood and Shilatifard, 2002] Wood, A. and Shilatifard (2002). Posttranslational modifications of histones by methylation. *Adv Protein Chem.*, 67:201–22.

[Wreggett et al., 1994] Wreggett, K., Hill, F., James, P., Hutchings, A., Butcher, G., and Singh, P. (1994). A mammalian homologue of drosophila heterochromatin protein 1 (HP1) is a component of constitutive heterochromatin. *Cytogenet Cell Genet.*, 66:99–103.

[Wu and Zhang, 2011] Wu, S. and Zhang, Y. (2011). Cyclin-dependent kinase 1 (CDK1)-mediated phosphorylation of enhancer of zeste 2 (Ezh2) regulates its stability. *j Biol Chem.*, 32:28511–9.

[Xiao et al., 2003] Xiao, B., Jing, C., Wilson, J. R., Walker, P. A., Vasisht, N., Kelly, G., Howell, S., Taylor, I. A., Blackburn, G. M., and Gamblin, S. J. (2003). Structure and catalytic mechanism of the human histone methyltransferase SET7/9. *Letters to Nature*, 421:652–656.

[Xue et al., 1998] Xue, Y., Wong, J., Moreno, G., Young, M., Cote, J., and Wang, W. (1998). NURD, a novel complex with both ATP-dependent chromatin-remodeling and histone deacetylase activities. *Mol Cell*, 6:851–61.

[Yang et al., 2017] Yang, P., Oldfield, A., Kim, T., Yang, A., Yang, J., and Ho, J. (2017). Integrative analysis identifies co-dependent gene expression regulation of BRG1 and CHD7 at distal regulatory sites in embryonic stem cells. *Bioinformatics*, 13:1916–1920.

[Yang et al., 2013] Yang, Y. W., Flynn, R. A., Chen, Y., Qu, K., Wan, B., Wang, K. C., Lei, M., and Chang, H. Y. (2013). Essential role of lncRN-Abinding for WDR5 maintenance of active chromatin and embryonic stem cell pluripotency. *eLife Research Article*, pages 1–19.

[Yu et al., 2013] Yu, T., Meiners, L., Danielsen, K., Wong, M., Bowler, T., Reinberg, D., Scambler, P., van Ravenswaaij-Arts CM, C., and Basson, M. (2013). Deregulated FGF and homeotic gene expression underlies cerebellar vermis hypoplasia in CHARGE syndrome. *Elife*, page doi: 10.7554/eLife.01305.

[Zentner et al., 2011] Zentner, G., Tesar, P., and Scacheri, P. (2011). Epigenetic signatures distinguish multiple classes of enhancers with distinct cellular functions. *Genome Res*, 21:1273–1283.

[Zhang et al., 2014] Zhang, J., Ji, F., Liu, Y., Lei, X., Li, H., Ji, G., Yuan, Z., and Jiao, J. (2014). Ezh2 regulates adult hippocampal neurogenesis and memory. *J Neuroscience*, 15:5184–99.

[Zhang and Bruice, 2006] Zhang, X. and Bruice, T. C. (2006). Reaction mechanism of guanidinoacetate methyltransferase, concerted or step wise. *PNAS*, 103 (44):16141–16146.

[Zhang et al., 2002] Zhang, X., Tamaru, H., Khan, S., Horton, J., Keefe, L., Selker, E., and Cheng, X. (2002). Structure of the neurospora SET domain protein DIM-5, a histone H3 lysine methyltransferase. *Cell*, 1:117–27.

[Zhang et al., 1999] Zhang, Y., Ng, H., Erdjument-Bromage, H., Tempst, P., Bird, A., and Reinberg, D. (1999). Analysis of the NuRD subunits reveals a histone deacetylase core complex and a connection with DNA methylation. *Genes Dev*, 15:1924–35.

[Zhao et al., 2008] Zhao, C., Deng, W., and Gage, F. H. (2008). Mechanisms and functional implications of adult neurogenesis. *Cell*, 132:645–660.

[Zhou et al., 2013] Zhou, J. X., Dhawan, S., Fu, H., Snyder, E., Bottino, R., Kundu, S., Kim, S. K., and Bhushan, A. (2013). Combined modulation of Polycomb and Trithorax genes rejuvenate ß-cell replication. *The Journal of Clinical Inverstigation*, 123:4849–4858.

[Ziller et al., 2015] Ziller, M. J., Edri, R., Yaffe, Y., donaghey, J., Pop, R., Mallard, W., Issner, R., Gifford, C. A., Goren, A., Xing, J., Gu, H., Cacchiarelli, D., Tsankov, A. M., Epstein, C., Rinn, J. L., Mikkelsen, T. S.,

Kohlbacher, O., Gnirke, A., Bernstein, B. E., Elkabetz, Y., and Meissner, A. (2015). Dissecting neural differentiation regulatory networks through epigenetic footprinting. *Letter to Nature*, 518:355–359.

[Zink and Paro, 1989] Zink, B. and Paro, R. (1989). In vivo binding pattern of a trans-regulator of homoeotic genes in *Drosophila melanogaster*. *Nature*, 6206:468–71.

5 Appendix

5.1 List of Abbreviations

in vivo Experiments in the living organism

in vitro Experiments in the lab

kDa kilodalton

EDTA Ethylenediaminetetraacetate

BSA Bovine serum albumin

BrdU 5-bromo-2-deoxyuridine

IdU 5-Iodo-2-deoxyuridine

CldU 5-chloro-2-deoxyuridine

Cre DNA recombinase

DKFZ *Deutsches Krebsforschungs Zentrum*

EtOH Ethanol

PBS Phosphat buffer saline

DAPI 4,6-diamidino-2-phenylindole

RNA Ribonucleic acid

DNA Deoxyribonucleic acid

CHIP Chromatin Immunoprecipitation

SFM Serum free medium

FBS Fetal Bovine Serum

NSC Neural stem cells

SVZ Subventricular zone

DG Dentate gyrus

OB Olfactory bulbs

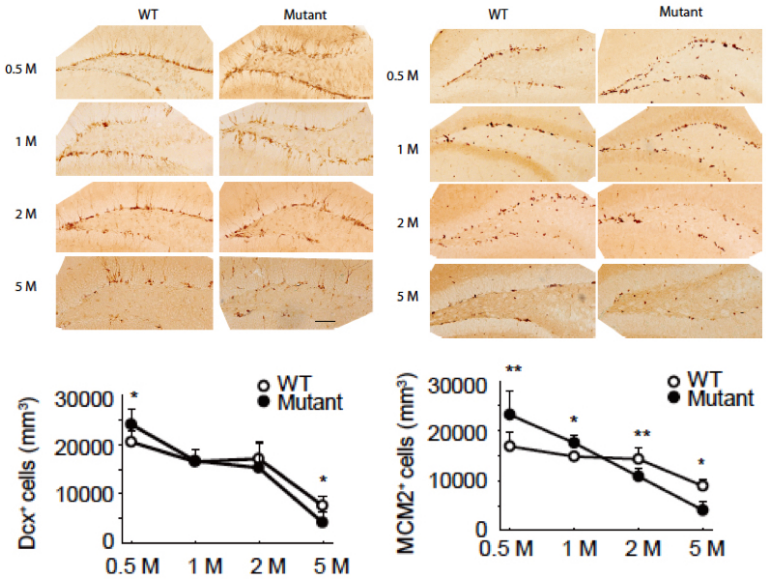

Figure 44: **Y. Li unpublished, staining and quantification of Doublecortin and MCM2 (Nestin Cre EZH2$^{fl/fl}$)**The knock-out was induced in ten week old mice. After the knock-out induction mutant and Control litter mates were analyzed 0.5, 1, 2, and 5 month later. After staining the positive cells were count manually.

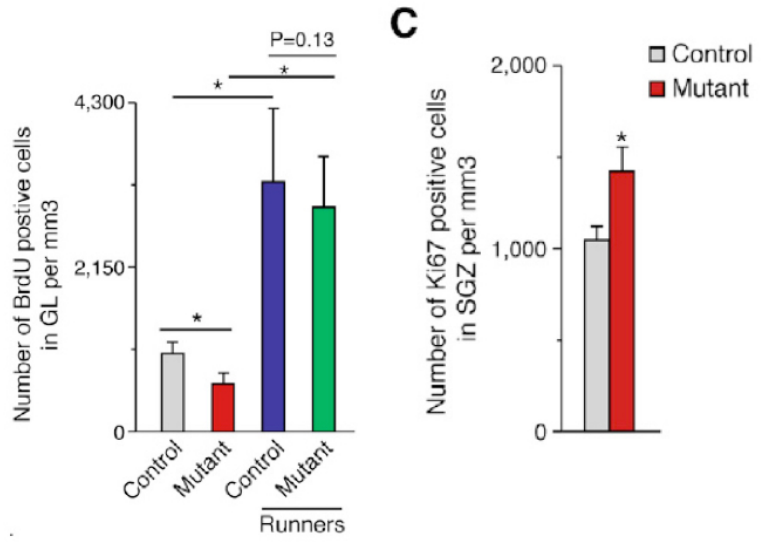

Figure 45: **From W. Feng et al. 2013, quantification of BrdU positive and Ki67 positive cells (NesCre;CHD7$^{fl/fl}$)** The knock-out was induced in eight week old mice. After the knock-out induction mutant and Control litter mates were analyzed after four weeks voluntary running (BrdU) and directly after the induction (Ki67). Stained cells were count manually.

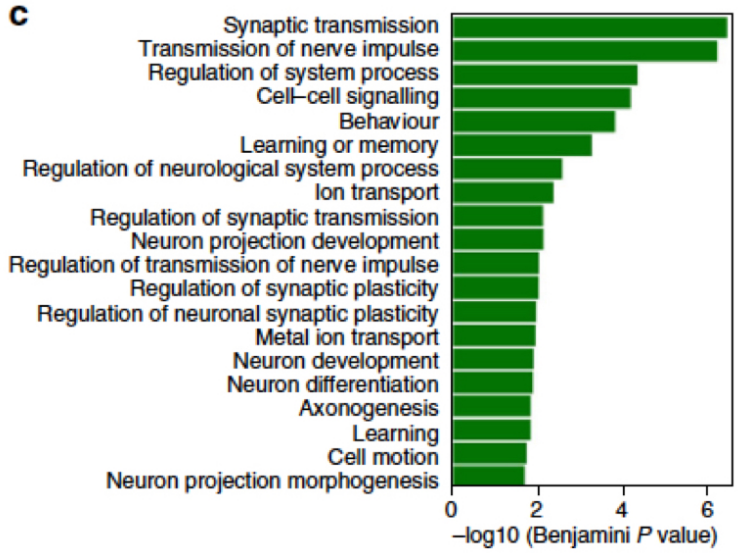

Figure 46: **From W. Feng et al. 2017, p7 Fig. 4c** DAVID Gene Ontology Biological Process analysis of genes downregulated in Chd7 homozygous mutant GNPs compared to WT. GO terms with Benjamini adjusted P-value 0.05 are shown (Atho1::Cre CHD7$^{fl/fl}$).

5.2 Supplement Data

5.2.1 Published Data - W. Feng et al., 2013 and 2017

5.2.2 Reelin on CHARGE cerebellum tissue

Shown in Feng et al., 2017, Reelin is regulated by CHD7 in cerebella granular neurons. This finding initiated a small scale analysis of Reelin in the CHARGE mouse. Figure 48 depicts immunofluorescence pictures of Control and CHARGE mouse cerebellum (A) and qPCR results for CHD7 and Reelin with two mice per genotype in graph B and C respectively. Reelin is secreted by granular neurons and taken up by purkinje cells, thus the staining shows a cytosolic signal for Reelin in the Purkinje cells of Control mice. The signal for CHARGE mouse purkinje cells looks less cytosolic and is hinting towards a nuclear signal distribution (A, CMVCre;CHD7$^{+/fl}$). The preliminary qPCR results show a reduced CHD7 signal and a reduction in the relative expression of Reelin both in the CHARGE mouse cerebellum (graph B and C). Three animals were tested via qPCR, one animal was excluded as outliner.

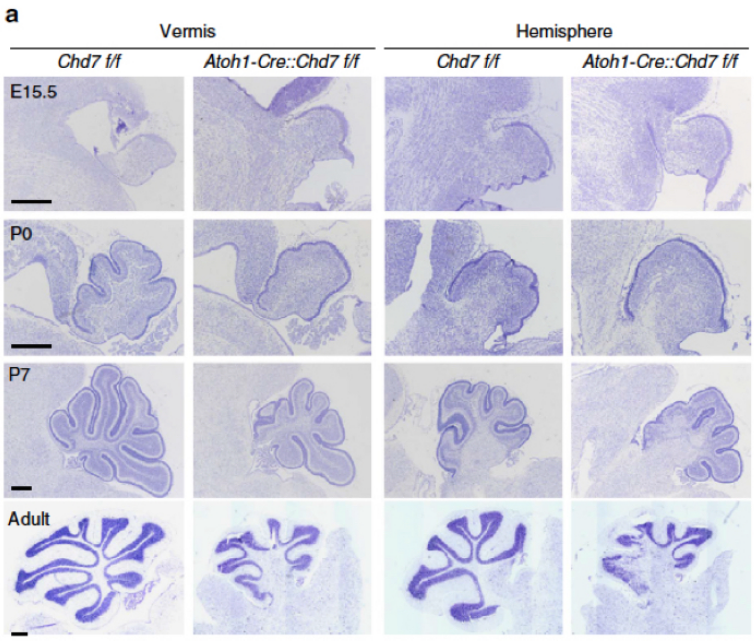

Figure 47: **From W. Feng et al. 2017, p.4 Fig. 2 a, deformations under CHD7 deficiency** Nissl staining of E15.5, P0, P7 and adult cerebella including vermis and hemisphere from [Chd7$^{fl/fl}$] and [Atoh1-Cre::Chd7$^{fl/fl}$] mice. Left side in each panel is the anterior part of cerebella. Scale bars, 100 mm.

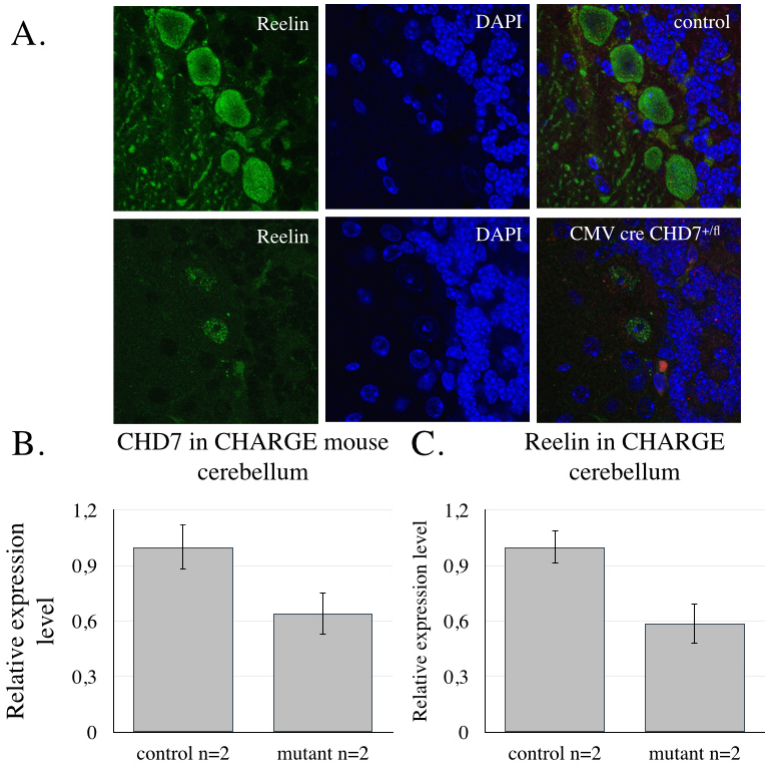

Figure 48: **Immunofluorescence picture and qPCR graph for reelin in the cerebellum (Control and CHARGE mouse)** A: Stained cerebellum slices of the ten week old Control (CMV Cre-) and CHARGE mouse (CMVCre;CHD7$^{+/fl}$) cerebellum were treated with antibodies against reelin (1:200, Merck Millipore, 488) and DAPI (1:10000) and pictures were taken with a laser microscope (LSM780, Zeiss). B: qPCR of CHARGE mouse analyzing the relative expression level of CHD7 in Control (CMV Cre-) and mutant (CMVCre;CHD7$^{+/fl}$) mice cerebellum tissue. C: qPCR of CHARGE mouse analyzing the relative expression level of reelin in Control (CMV Cre-) and mutant (CMVCre;CHD7$^{+/fl}$) mice cerebellum tissue. N-values represent animal numbers.

In CHARGE mouse vs. Control, gene annotation on significant genes

Sublist	Category	Term	RT	Genes	Count	%	P-Value	Benjamini
	GOTERM_BP_DIRECT	DNA methylation on cytosine	RT		20	2.4	1.9E-19	4.4E-16
	GOTERM_BP_DIRECT	DNA replication-dependent nucleosome assembly	RT		20	2.4	4.3E-19	5.0E-16
	GOTERM_BP_DIRECT	positive regulation of gene expression, epigenetic	RT		20	2.4	4.3E-19	5.0E-16
	GOTERM_BP_DIRECT	nucleosome assembly	RT		31	3.7	1.1E-18	8.7E-16
	GOTERM_BP_DIRECT	protein heterotetramerization	RT		21	2.5	1.2E-16	6.5E-14
	GOTERM_BP_DIRECT	chromatin silencing at rDNA	RT		20	2.4	6.8E-14	3.2E-11
	GOTERM_BP_DIRECT	negative regulation of megakaryocyte differentiation	RT		12	1.4	2.3E-12	9.0E-10
	GOTERM_BP_DIRECT	DNA replication-independent nucleosome assembly	RT		12	1.4	6.3E-10	2.1E-7
	GOTERM_BP_DIRECT	DNA-templated transcription, initiation	RT		13	1.5	6.7E-9	1.9E-6
	GOTERM_BP_DIRECT	regulation of gene silencing	RT		8	1.0	1.6E-7	4.2E-5
	GOTERM_BP_DIRECT	cell projection organization	RT		16	1.9	6.7E-4	1.5E-1
	GOTERM_BP_DIRECT	regulation of ion transmembrane transport	RT		14	1.7	2.0E-3	3.4E-1
	GOTERM_BP_DIRECT	cell-cell adhesion	RT		17	2.0	2.5E-3	3.8E-1
	GOTERM_BP_DIRECT	histone H3-K27 trimethylation	RT		4	0.5	2.7E-3	3.8E-1
	GOTERM_BP_DIRECT	response to cAMP	RT		8	1.0	3.1E-3	4.0E-1
	GOTERM_BP_DIRECT	regulation of transcription, DNA-templated	RT		111	13.2	5.1E-3	5.5E-1
	GOTERM_BP_DIRECT	skin development	RT		8	1.0	6.3E-3	6.0E-1
	GOTERM_BP_DIRECT	chromatin silencing	RT		8	1.0	9.9E-3	7.5E-1

Figure 49: **List of significantly regulated genes (CHARGE vs Control)** This list has been kindly provided by C. Shao

In CHARGE mouse vs. Control, gene annotation on significantly up regulated genes

	GOTERM_BP_DIRECT	nucleosome assembly	RT		29	8.8	4.9E-28	4.0E-25
	GOTERM_BP_DIRECT	DNA methylation on cytosine	RT		20	6.1	1.7E-27	7.1E-25
	GOTERM_BP_DIRECT	positive regulation of gene expression, epigenetic	RT		20	6.1	4.0E-27	1.1E-24
	GOTERM_BP_DIRECT	DNA replication-dependent nucleosome assembly	RT		20	6.1	4.0E-27	1.1E-24
	GOTERM_BP_DIRECT	protein heterotetramerization	RT		20	6.1	2.8E-23	5.8E-21
	GOTERM_BP_DIRECT	chromatin silencing at rDNA	RT		20	6.1	1.0E-21	1.7E-19
	GOTERM_BP_DIRECT	negative regulation of megakaryocyte differentiation	RT		12	3.6	5.5E-17	7.5E-15
	GOTERM_BP_DIRECT	DNA replication-independent nucleosome assembly	RT		12	3.6	1.8E-14	2.1E-12
	GOTERM_BP_DIRECT	DNA-templated transcription, initiation	RT		12	3.6	2.9E-12	3.0E-10
	GOTERM_BP_DIRECT	regulation of gene silencing	RT		8	2.4	2.0E-10	1.8E-8
	GOTERM_BP_DIRECT	regulation of transcription, DNA-templated	RT		60	18.2	5.3E-6	4.3E-4
	GOTERM_BP_DIRECT	chromatin silencing	RT		8	2.4	3.4E-5	2.6E-3
	GOTERM_BP_DIRECT	xenophagy	RT		9	2.7	1.3E-4	8.6E-3
	GOTERM_BP_DIRECT	cell projection organization	RT		10	3.0	3.6E-4	2.3E-2
	GOTERM_BP_DIRECT	positive regulation of defense response to virus by host	RT		9	2.7	4.1E-4	2.3E-2
	GOTERM_BP_DIRECT	cilium morphogenesis	RT		9	2.7	3.4E-3	1.7E-1
	GOTERM_BP_DIRECT	axoneme assembly	RT		4	1.2	3.8E-3	1.8E-1
	GOTERM_BP_DIRECT	cell-cell adhesion	RT		9	2.7	6.4E-3	2.7E-1

Figure 50: **List of significantly regulated genes (CHARGE vs Control)** This list has been kindly provided by C. Shao

In CHARGE mouse vs. Control, gene annotation on significantly down regulated genes

Sublist	Category	Term	RT	Genes	Count	%	P-Value	Benjamini
	GOTERM_BP_DIRECT	regulation of ion transmembrane transport	RT		13	2.6	8.7E-5	1.5E-1
	GOTERM_BP_DIRECT	cell adhesion	RT		27	5.3	9.3E-5	8.6E-2
	GOTERM_BP_DIRECT	potassium ion transmembrane transport	RT		9	1.8	1.3E-3	5.6E-1
	GOTERM_BP_DIRECT	cell differentiation	RT		33	6.5	1.8E-3	5.8E-1
	GOTERM_BP_DIRECT	regulation of neuronal synaptic plasticity	RT		5	1.0	2.6E-3	6.3E-1
	GOTERM_BP_DIRECT	transport	RT		62	12.2	3.3E-3	6.5E-1
	GOTERM_BP_DIRECT	angiogenesis	RT		14	2.8	4.6E-3	7.2E-1
	GOTERM_BP_DIRECT	filopodium assembly	RT		4	0.8	4.8E-3	6.9E-1
	GOTERM_BP_DIRECT	actin cytoskeleton organization	RT		10	2.0	6.6E-3	7.6E-1
	GOTERM_BP_DIRECT	response to cAMP	RT		6	1.2	6.9E-3	7.4E-1
	GOTERM_BP_DIRECT	protein homooligomerization	RT		12	2.4	7.3E-3	7.2E-1
	GOTERM_BP_DIRECT	long-term memory	RT		5	1.0	8.1E-3	7.3E-1
	GOTERM_BP_DIRECT	regulation of Rho protein signal transduction	RT		7	1.4	9.7E-3	7.6E-1
	GOTERM_BP_DIRECT	mRNA processing	RT		16	3.1	9.9E-3	7.4E-1

Figure 51: **List of significantly regulated genes (CHARGE vs Control)** This list has been kindly provided by C. Shao

5.2.3 RNA Sequencing - Lists of significantly changed Processes

5.2.4 An *in vitro* double knock-out hints towards no reduction in key transcription factors

To further investigate the characteristics of neural stem cells with floxed *ezh2* and *chd7* genes (CHD7$^{fl/fl}$;EZH2$^{fl/fl}$), the neural stem cells of three animals were isolated, cultured and transfected either with a CAG-Cre-IRES-GFP (inducing the knock-out), or a CAG-IRES-GFP virus (not inducing the knock-out).

The virus was produced in HEK293T cells, and subsequently the neural stem cells were transfected with this virus (Fig. 52A). After another four weeks of expanding the transfected neural stem cells, these cells were FAC sorted for GFP. Out of six induced/ not induced cell line combinations, four cell lines could be sorted, ranging from a transfection rate between 30 and 50% (Fig. 52 example in B).

In a qPCR analysis the expression of the not-Cre-induced cell line (CAG-IRES-GFP) was taken as 100% while the three cell lines treated with the Cre recombinase virus are shown together. Both CHD7 and EZH2 range around a relative expression level of 30% and 50% respectively, while the key regulators SOX4, SOX11 and PTEN are not altered in comparison to the Control cell line (Fig. 52C). This is especially intriguing because a *chd7* single knock-out in neural stem cells showed a reduction in the SoxC transcription factors SOX4 and SOX11.

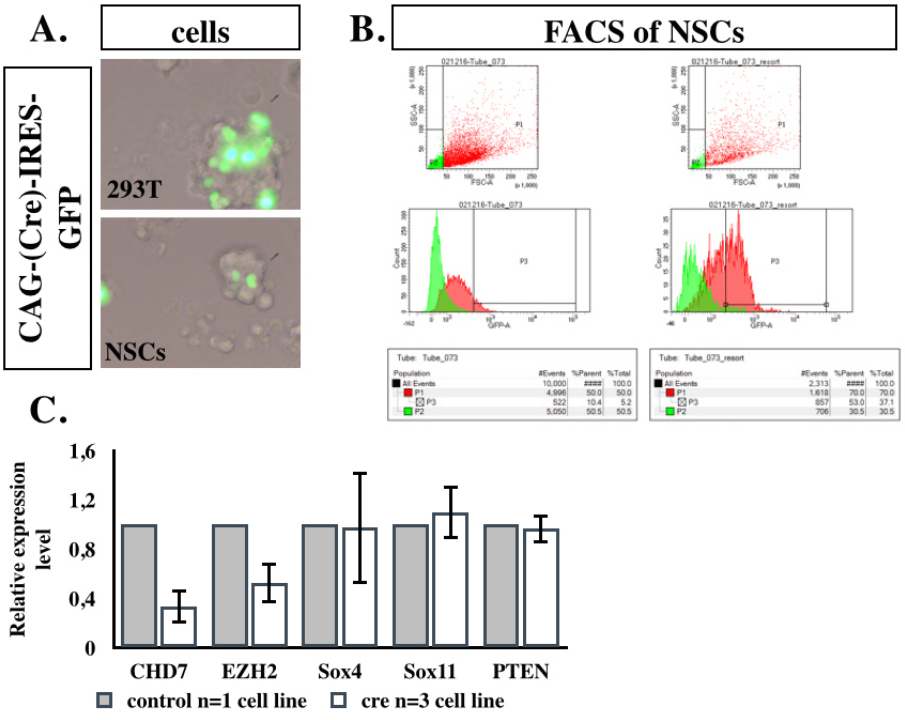

Figure 52: **Neural stem cells carrying the double knock-out (CHD7 fl/fl and EZH2$^{fl/fl}$) show no reduction in the expression level of key transcription factors (cell lines with and without knock-out)** A: Through-light and GFP fluorescent pictures of viral transfected HEK293T cells and neural stem cells (NSC) treated treated with/ without Cre-IRES-GFP virus and IRES-GFP virus, respectively. B: Example results of the FAC sorting for GFP. Shown is a Control (CAG-IRES-GFP). C: qPCR for the relative expression level of CHD7, EZH2, SOX4, SOX11, and PTEN in the sorted NSC cells. The sample size n=1 Control NSC cells, and n=3 knock-out NSC cells. The cell lines originate from three animals.

5.2.5 Cell Treatment with Chemically altered EZH2 Inhibitors

The EZH2 inhibitor GSK126 does not cross the blood-brain-barrier thus in theory neural stem cells could react to a possible treatment. Therefor, neural stem cells were incubated with the EZH2 inhibitor, and the H3K27me3 protein level was analyzed.

To maybe overcome the blood-brain-barrier in the future the inhibitor was chemically altered (by Dr. Aubry Miller) to enable an efficient crossing. The different versions of this inhibitor were first tested on HEK293T cells to determines the working concentration, and then tested on neural stem cells to check whether the chemical alteration had an influence on the inhibitor function.

Different concentrations of the EZH2 inhibitor were tested, and showed a downregulation of H3K27me3 already with a concentration of 100 nM in comparison to the Control cells with no treatment, while BDNF and EZH2 protein level remained unchanged (Fig. 53A). Further, different versions of the EZH2 inhibitor were tested on neural stem cells. Since 3 and 10 mM gave good results, these concentrations were further used. After 72h of incubation with the different EZH2 inhibitors and chemical altered versions, the neural stem cells were harvested and 20 μl protein per sample was blotted for EZH2, beta-tubulin and H3K27me3. A reduced H3K27me3 signal for the inhibitor-treated cells could be observed, in comparison to the Control cells treated with DMSO (Fig. 53B)[25].

5.2.6 BrdU Distribution in the Dentate Gyrus - non significant Data

A single knock out of EZH2 was analyzed by Yuting Li and the preliminary data hinted toward a different distribution of DCX positive cells in the dentate gyrus.

Therefore, ten week oly mice of the double knock out (NesCreERT2;CHD7$^{fl/fl}$;EZH2$^{fl/fl}$) and Control litter mates were analyzed according to their cell distribution of BrdU positive cells in regions of the dentate gyrus.

First, dentate gyrus sizes were compared by using a volume measurement tool (ImageJ) and the BrdU positive cells were counted manually. To count the cells per region, the dentate gyrus was separated into three regions of the same width using a line drawing tool (ImageJ). The positive cells were counted in a blind analysis of knock out and Control animals. The distribution of BrdU positive cells in the subgranular zone (SGZ), the

[25] Beyond the scope of this project these chemically altered inhibitors were further tested on blood-brain-barrier models

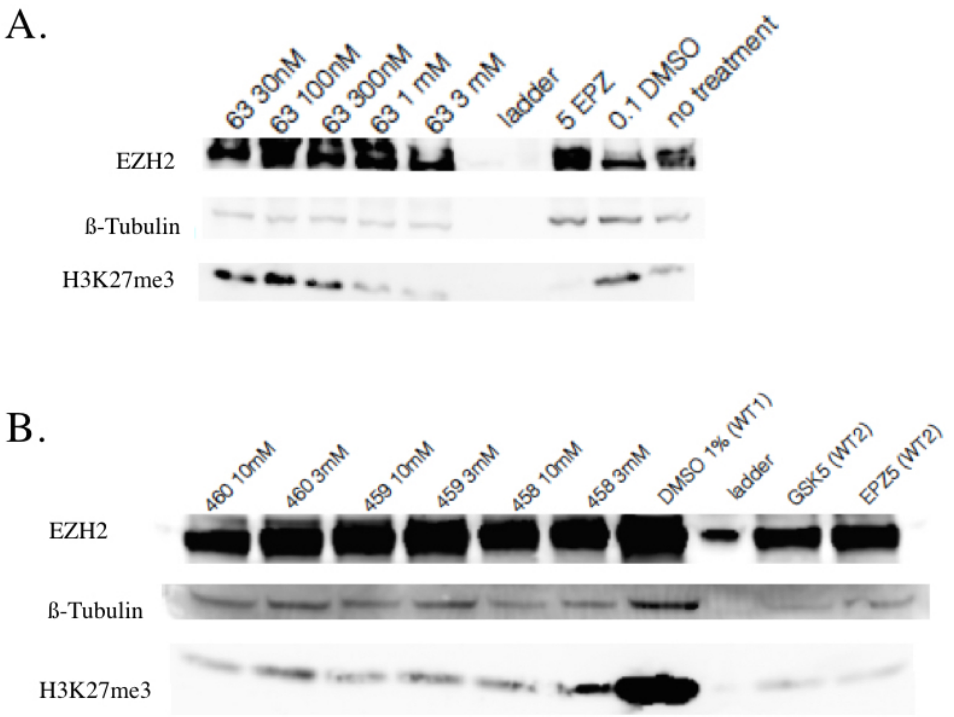

Figure 53: **Chemical altered EZH2 inhibitors are still capable of H3K27me3 downregulation in neural stem cells** A: HEK293T cells were incubated with a chemical variation of the EZH2 inhibitor GSK126 (64) with the concentration of 30 nM, 100 nM, 300 nM, 1 mM, 3 mM, and 10 mM. The cells were treated for 72h, then harvested and 20 μl protein per sample was blotted for EZH2, beta-tubulin, BDNF and H3K27me3. B: Neural stem cells were treated a chemical variation of the EZH2 inhibitor GSK126 (460, 459, 458) with the concentration of 3 mM, and 10 mM. The cells were treated for 72 h, then harvested and 20 μl protein per sample was blotted for EZH2, beta-tubulin, BDNF and H3K27me3.

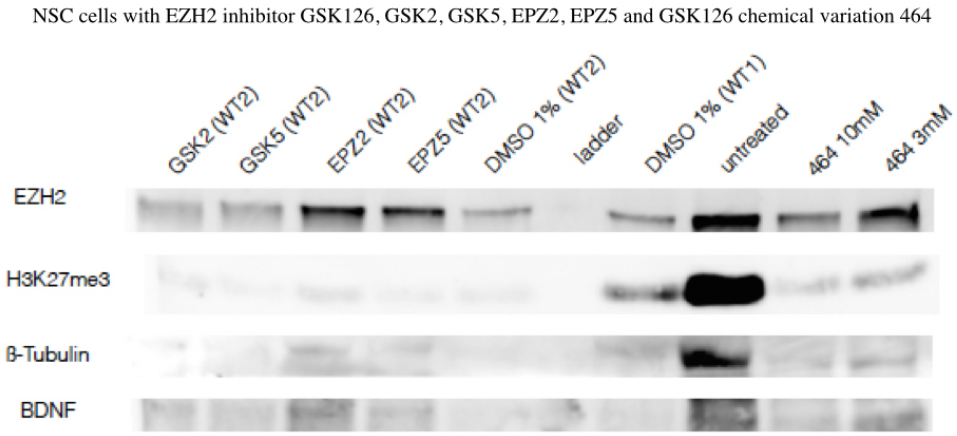

Figure 54: **Neural stem cells treated with GSK2, GSK5, EPZ2, EPZ5, DMSO. DMSO and the chemical GSK126 variation 464** The cells were treated for 72 h, then harvested and 20 μl protein per sample was blotted for EZH2, beta-tubulin, BDNF and H3K27me3.

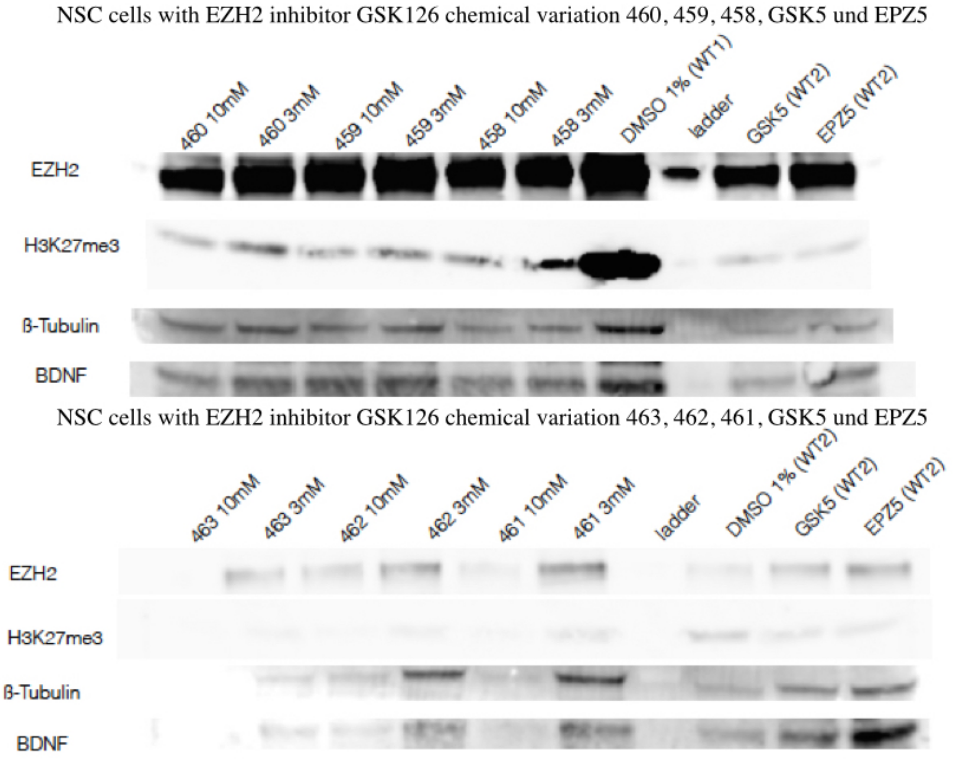

Figure 55: **Neural stem cells treated with chemical GSK126 variation 463 to 458, DMSO, GSK5 and EPZ5** The cells were treated for 72 h, then harvested and 20 μl protein per sample was blotted for EZH2, beta-tubulin, BDNF and H3K27me3.

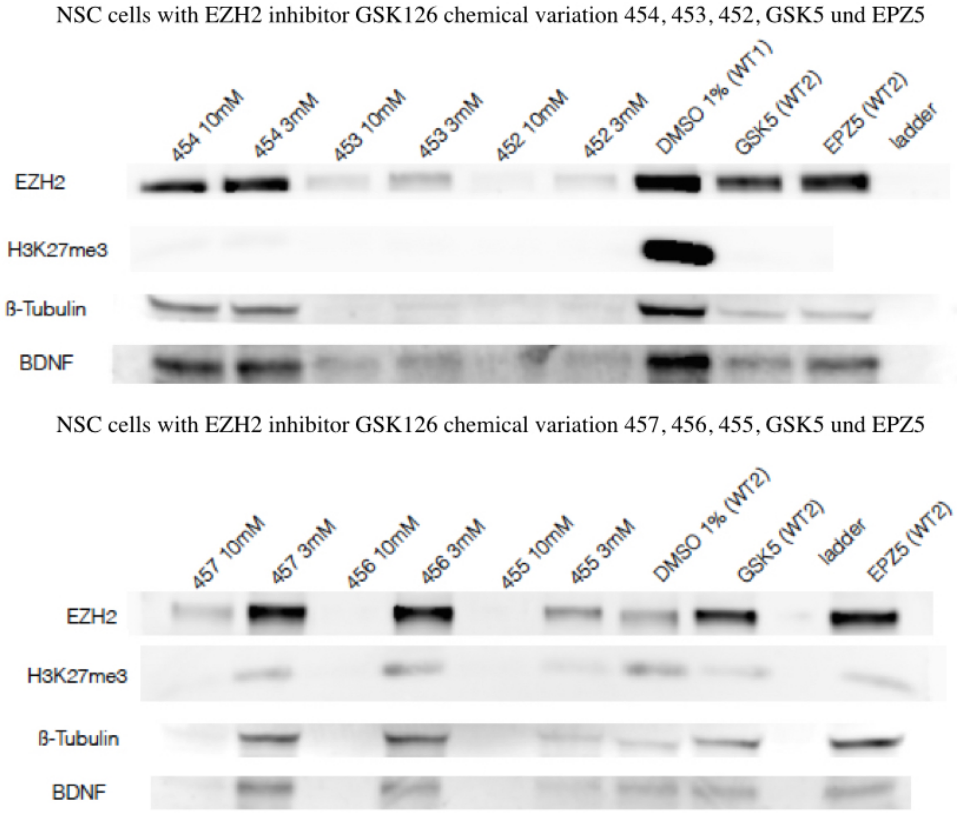

Figure 56: **Neural stem cells treated with chemical GSK126 variation 454, 453, 453, 457, 456, 455. DMSO, GSK5 and EPZ5 are Controls** The cells were treated for 72 h, then harvested and 20 μl protein per sample was blotted for EZH2, beta-tubulin, BDNF and H3K27me3.

middle and upper granular layer (GL) were counted.

The only observed difference concerned running and non running animals. No significant differnce has been observed between the mutant and Control group (Fig. 57).

5.2.7 DCX in the Dentate Gyrus - non significant Data

Dentate gyrus sizes were compared by using a volume measurement. DCX positive cells were counted manually (Fig.58, 2).

To count the cells per region, the dentate gyrus was separated into three regions of the same width using a line drawing tool (ImageJ). After a blind analysis the distribution of doublecortin positive cells in the subgranular zone (SGZ), the middle and upper granular layer (GL) were not significantly different between the mutant and Control group (Fig. 58, 3).

In the single knock-out of EZH2, Yuting Li saw that the neurons develop more processes than their Control litter mates. This has not been observed in the double knock-out. The length of the primary process was analyzed (Fig. 59, 1).

Only the knock-out mouse group that was sacrificed two weeks after the tamoxifen injection had significantly shorter primary processes (Fig. 59, 2).

To answer the question whether the neurons of the double knock-out are bigger or shorter than the Control neurons, the longest visible neuronal branch was measured using a tool. Seventy cells of Control mice and 40 cells of mutant mice dentate gyrus were measured and compared. There was no significant difference between the neuronal length of the mutant and the Control mice group (Fig. 58, 3).

To exclude that only neurons of a certain length were considered all measured dendritic lengths of 70 Control and 40 knock-out neurons were plotted together. The distribution lays in between 100 and 300 μm, Control and knock-out neurons are quite equal distributed (Fig. 58, 4).

During the blind analysis of the doublecortin stainings some of the cells were attracting attention. Against the normal direction of growth their primary processes were growing in a ninety degree angle left or right into the granular layer (Fig. 60, 1).

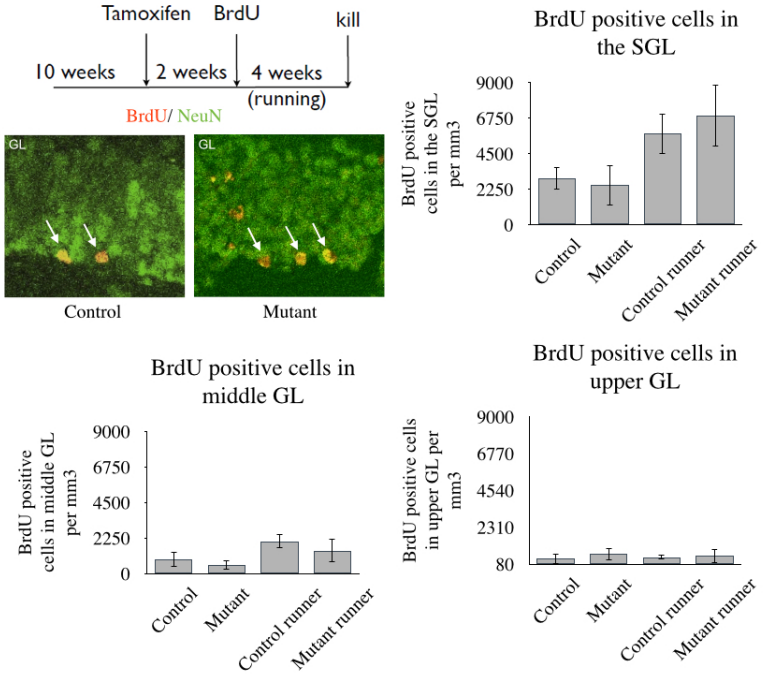

Figure 57: **Immunofluorescence picture and regional cell number quantification of BrdU positive cells in the dentate gyrus (NesCreERT2;CHD7$^{fl/fl}$;EZH2$^{fl/fl}$)** The ten week old litter mates were treated with Tamoxifen for 5 days and after another two weeks BrdU was injected and the mice were placed into a running cage. Subsequently 40μm brain vibratom slices of the dentate gyrus were stained with Doublecortin (santa cruz, goat 1:100). The quantification was done manually and 4 to 6 dentate gyrus pictures were count per animal. Control n=5, double KO n=6, Control runner n=5,double KO runner n=7.Before counting the dentate gyrus was separated into subgranular zone (SGZ), middle and upper granular layer (GL), cells were counted per region.

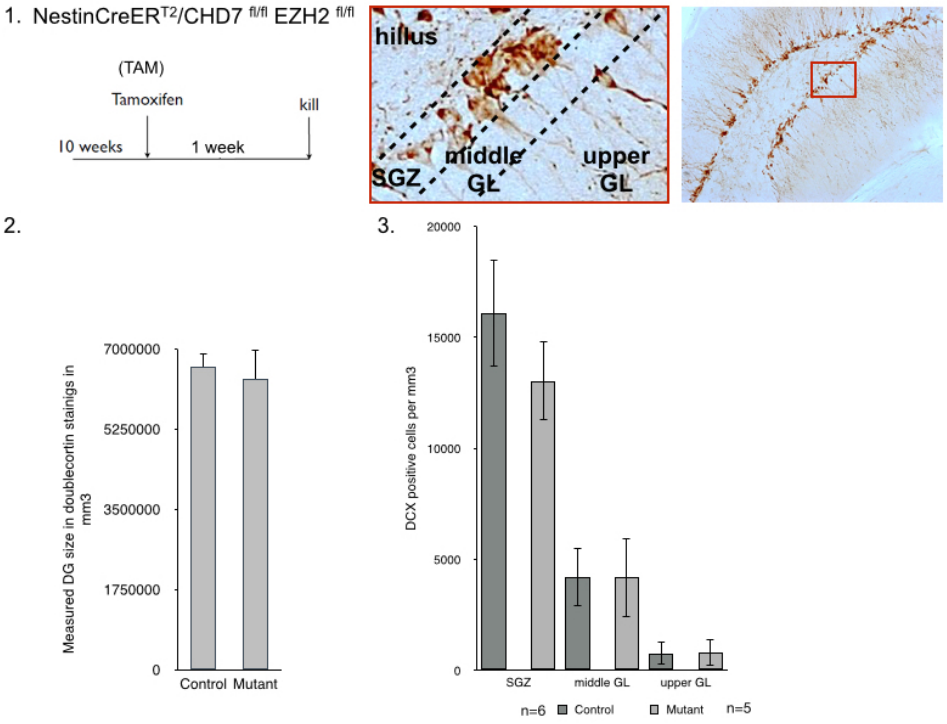

Figure 58: **Histology picture and regional cell number quantification of Doublecortin positive cells in the dentate gyrus (NesCreERT2;CHD7$^{fl/fl}$;EZH2$^{fl/fl}$).** 1: The ten week old litter mates were treated with Tamoxifen for 5 days and after another two weeks and the mice were placed into a running cage. Brain slices were stained with Doublecortin. 2: Control of the dentate gyrus size. The dentate gyrus was measured entirely with a polygon tool of the microscope software and compared between mutant and Control. 3: The quantification was done manually and 4 to 6 dentate gyrus pictures were count per animal. Before counting the dentate gyrus was separated into subgranular zone (SGZ), middle and upper granular layer (GL), cells were counted per region; n= 5 mutant and n=6 Control mice.

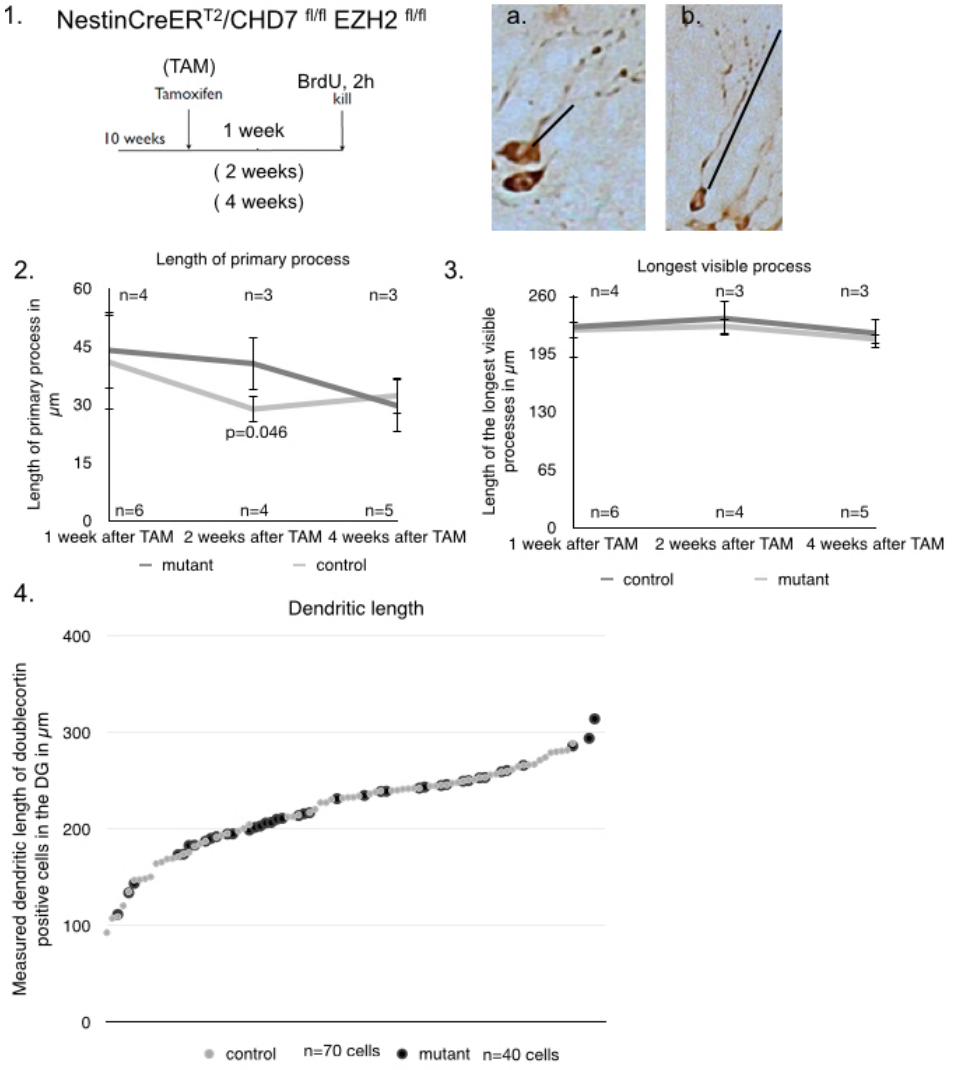

Figure 59: **Histology picture and quantifications of the cell process length for Doublecortin positive cells in the dentate gyrus (NesCreERT2;CHD7$^{fl/fl}$;EZH2$^{fl/fl}$).** 1: The ten week old litter mates were treated with Tamoxifen for 5 days and after another two weeks and the mice were placed into a running cage. Brain slices were stained with Doublecortin. Example pictures show the measured length of the primary processes and the visible dendritic length. 2 and 3: The quantification was done with a measuring tool of the microscope software, 4 to 6 dentate gyrus pictures per animal were screened. N-values stand for animals per time point and genotype. 2: Used were only primary processes where the first branching was visible. 3: Only the longest visible continuous dendrites were measured. 4: Graph of the over all distribution of all considered dendrite length, only separated into Control and mutant group. Statistical analysis t-test p=0.046.

(The used animals and staining procedure were the same as mentioned for Fig. 32). All wrong orientated cells in the subgranular zone (SGZ) were counted and plotted for the Control and the mutant mouse group. They were not significantly different (Fig. 60, 2).

For the hillus region these cells were counted too and did not show a difference in the groups (Fig. 60, 3).

In the following it was analyzed whether cells without visible process occur more often in the subgranular zone (SGZ) of knock-out mice as this could be a hint towards not integrated cells. (The used animals and staining procedure were the same as mentioned in Fig. 32).

For seven animals four to six dentate gyrus were counted for these cells but no significant difference was found Fig. 60, 2.

5.2.8 NestinCre Survival Study

As the homozygous knock-out of both CHD7 and EZH2 is lethal, the knock-out was combined with a Nestin promotor to limit the knock-out to brain stem cells. From the time point nestin is expressed the knock-out is active and therefore influencing the embryonic development. With this genetic system (NesCre;CHD7$^{fl/fl}$) Weijun could show that a homozygous knock-out is already seldom with 4% of the total number of born pups and interestingly all surviving animals were female (W. Feng unpublished).

To analyze whether a reduces EZH2 expression could increase the survival of NesCre;CHD7$^{fl/fl}$ mice we used a mating strategy giving us the variety of genetic combinations restricted to neural stem cells (namely NesCre;CHD7$^{fl/fl}$;EZH2$^{fl/fl}$, NesCreCHD7$^{+/fl}$;EZH2$^{+/fl}$, NesCre;CHD7$^{fl/fl}$;EZH2$^{+/fl}$, NesCre;CHD7$^{fl/fl}$;EZH2$^{+/fl}$).

The double homozygous combination of CHD7 and EZH2 was lethal, the pups seemed fully developed but were born dead. A combination of CHD7 homozygous and EZH2 heterozygous survived birth, but died shortly after. Interestingly, a heterozygous expression of CHD7 could prolong the survival of a homozygous EZH2 knock-out. Instead of 12 days for a homozygous EZH2 knock-out, these pups survived 3 weeks. They were severely underfeed and died with their eyes still closed. Further remarkable seems that a double heterozygous combination of CHD7 and EZH2 equalizing CHARGE and Weaver syndrome together in the neural stem cells, was indistinguishable from the Control mice. All of these double heterozygous mice were killed with 10 weeks of age and showed no abnormalities. All these observations were made together with Weijun Feng (Fig. 62).

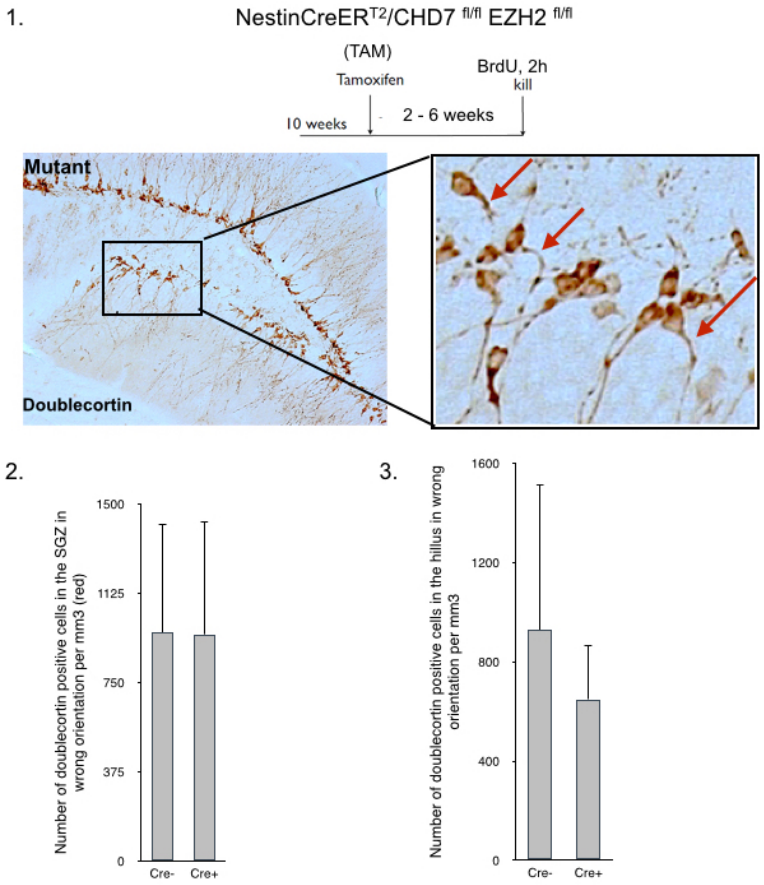

Figure 60: **Histology picture and quantification of disorientated Doublecortin positive cells in the dentate gyrus (NesCreERT2;CHD7$^{fl/fl}$;EZH2$^{fl/fl}$).** 1. The ten week old litter mates were treated with Tamoxifen for 5 days and after another two weeks and the mice were placed into a running cage. Subsequently 40μm brain vibratom slices of the dentate gyrus were stained with Doublecortin. Only cells with a clear left or right orientation agains the hillus-granular layer axis were considered. The quantification was done manually and 4 to 6 dentate gyrus pictures were count per animal. For each group Control (cre-) and mutant (cre+) n=7. 2: Number of cells with a wrong orientation in the granular layer. 3: Number of cells with a wrong orientation in the hillus.

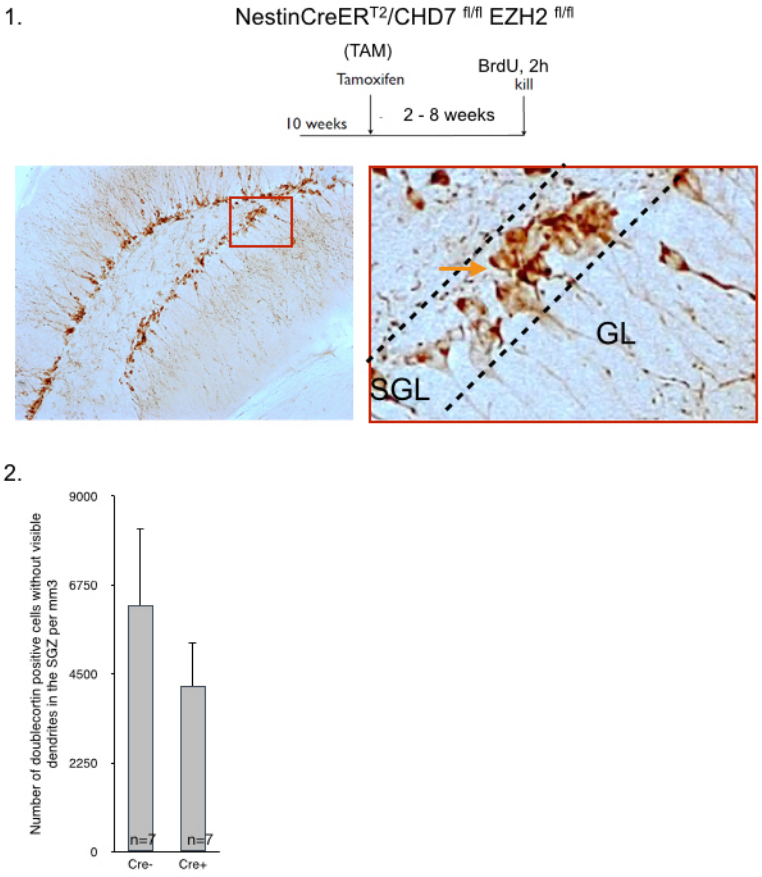

Figure 61: **Histology picture and quantification Doublecortin positive cells in the dentate gyrus (NesCreERT2;CHD7$^{fl/fl}$;EZH2$^{fl/fl}$).** 1: The ten week old litter mates were treated with Tamoxifen for 5 days and after another two weeks and the mice were placed into a running cage. Subsequently 40μm brain vibratom slices of the dentate gyrus were stained with Doublecortin. The quantification was done manually and 4 to 6 dentate gyrus pictures were count per animal. 2: Number of cells without visible dendrite in the subgranular layer (SGL).

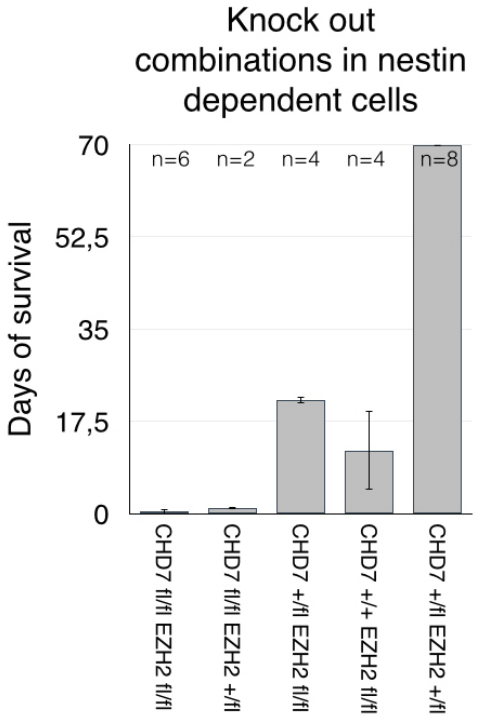

Figure 62: **The survival days of different knock-out combinations (NesCre;CHD7flox;EZH2flox)** A double heterozygous combination was indistinguishable from the Control litter mates. These mice were sacrificed 70 days after birth.

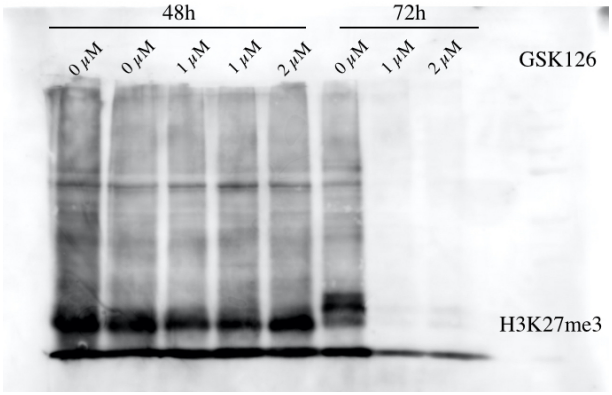

Figure 63: Complete western blot for H3K27me3 (17 kDa) using the harvested HEK293T cells with *chd7* knock-down after 48h and 72 h of GSK126 incubation.

Erklärung

Hiermit bestätige ich, dass ich diese Arbeit eigenständig erstellt habe und alle Quellen genannt werden.

Heidelberg, June 21, 2020

Einverständnisserklärung

Hiermit erkläre ich mich damit einverstanden, dass diese Arbeit in der Fachbereichsbibliothek Biologie der Karl Ruprecht Universität ausgestellt werden darf.

Heidelberg, June 21, 2020